

# Exploring the Foundation of Quantum Information in Quantum Optics

by

Xian Ma

A thesis  
presented to the University of Waterloo  
in fulfillment of the  
thesis requirement for the degree of  
Doctor of Philosophy  
in  
Physics

Waterloo, Ontario, Canada, 2016

© Xian Ma 2016

I hereby declare that I am the sole author of this thesis. This is a true copy of the thesis, including any required final revisions, as accepted by my examiners.

I understand that my thesis may be made electronically available to the public.

## Abstract

Quantum information is promising in solving certain computational problems and information security. The power of its speed up and privacy is based on one of the most tested physical theory: quantum mechanics. Many of the promises of quantum information has already been demonstrated in different implementations, which could also be viewed as witness of quantum mechanics. As we progress further in quantum information, we find that some of the aspects of quantum mechanics could be tested in a novel way. Performing those tests may lead to new physical theory or at least reinforce our belief of the accuracy of quantum mechanics. In this thesis, I report a few different approaches in testing the foundation of quantum mechanics using results obtained from quantum optics. While developing such test, quantum state tomography is heavily used to characterize our system. I also report a simplified way of performing quantum state tomography for quantum state that is close to pure state.

## **Acknowledgements**

I am deeply indebted to my parents Jianlin Zhang and Jianhua Ma for everything. I want to thank my wife Xue Rui and my daughter Reyna Ma for their love and support. I must thank Dr. Raymond Laflamme, for giving me the opportunity to be part of his research group, for his constant support and guidance. I must thank the members of my advisory committee; Dr. Jonathan Baugh, Dr. Joseph Emerson, and Dr. Frank Wilhelm for their interest in my research and for their support. I am thankful to everyone at the IQC.

# Table of Contents

List of Tables	vii
List of Figures	viii
<b>1 Introduction</b>	<b>1</b>
<b>2 Background: quantum optics and quantum information</b>	<b>3</b>
2.1 Quantum optics . . . . .	3
2.1.1 Photon modes and evolution . . . . .	3
2.1.2 Parametric down converted photons . . . . .	4
2.1.3 Dual-rail qubits and its relation to polarization qubits . . . . .	8
2.1.4 Unitary gates for photon-polarization qubits . . . . .	9
2.2 Quantum information . . . . .	10
2.2.1 Quantum state tomography and Maximum Likelihood Estimation . . . . .	10
<b>3 Testing quantum foundations in space using artificial satellite</b>	<b>13</b>
3.1 Introduction . . . . .	13
3.2 T. Ralph and G. Milburn’s alternative quantum optics theory . . . . .	14
3.3 Testing quantum mechanics with artificial satellites . . . . .	16

<b>4</b>	<b>Testing envariance</b>	<b>20</b>
4.1	Introduction . . . . .	20
4.2	Deriving Born rule from envariance . . . . .	21
4.3	Experimental testing envariance . . . . .	25
4.4	Bounds to Born rule . . . . .	32
4.5	Conclusion . . . . .	35
<b>5</b>	<b>Pure State Tomography using Pauli Observables</b>	<b>38</b>
5.1	Introduction . . . . .	38
5.2	Historical results on UDP and UDA . . . . .	40
5.3	2 qubit pure state tomography using Paulis measurements . . . . .	41
5.4	3 qubit pure state tomography using Paulis measurements . . . . .	43
5.5	Pure state tomography in NMR system . . . . .	45
5.5.1	Pure state tomography for a 2-qubit state . . . . .	46
5.5.2	Pure state tomography for 3-qubit state . . . . .	47
5.6	Pure state tomography for polarized photon qubits . . . . .	49
<b>6</b>	<b>Conclusion</b>	<b>55</b>
	<b>References</b>	<b>57</b>
	<b>APPENDICES</b>	<b>63</b>
<b>A</b>	<b>Testing of envariance to Born rule continued</b>	<b>64</b>
<b>B</b>	<b>Proof of UDA using selected Paulis for 3 qubits</b>	<b>70</b>

# List of Tables

4.1	Wave plate setting used to implement polarization rotations. . . . .	27
4.2	Summary of the results for comparing stages <b>I</b> and <b>III</b> . . . . .	31

# List of Figures

2.1	Generation of polarization entangled photons via parametric down conversion	7
3.1	Proposed scheme testing gravitationally induced decorrelation	17
3.2	Coincidence rate prediction for testing gravitationally induced decorrelation	18
4.1	Experimental setup for testing envariance	26
4.2	Experimental measurement procedure of testing envariance	28
4.3	Reconstructed density matrix of the initial state from the source, after implement the first rotation and final state	29
4.4	Analysis of the experimental results for testing envariance.	30
4.5	Generalized correlations for the singlet state as a function of $n$ using Son's theory [1].	34
4.6	Correlation functions versus the rotation angle $\phi$ .	36
5.1	NMR experiment substance	46
5.2	Pure state tomography for 2 qubits	48
5.3	Performance of 2-qubit protocol using selected Pauli measurements against randomly Pauli measurements.	49
5.4	scheme to create the GHZ state via global controls in NMR	50
5.5	Pure state tomography for GHZ state.	51
5.6	Performance of 3-qubit protocol using selected Pauli measurements against randomly Pauli measurements.	52
5.7	Measurement scheme for a polarization-encoded $n$ -photon state.	53

A.1 Testing “Fine graining” . . . . .	67
A.2 Preparation of entangled state $\alpha 00\rangle + \beta 11\rangle$ . . . . .	68

# Chapter 1

## Introduction

Quantum Mechanics is arguably the most tested physical theory in human history. It has been directly and indirectly tested in numerous experiments since its discovery in the early 20th century. Many promises of quantum mechanics has been realized such as transistor and atomic clock, and those discovery are verification of quantum mechanics themselves. Moreover, with the help of those technology, one was able to design more precise experiments testing quantum mechanics. In the past few decades, quantum information was developed to help us understand unique advantages of quantum mechanics over classical counter parts such as computational power and information security. It has been realized in many systems such as NMR, optics, superconducting electrode and ion trap. It is another piece of evidence that quantum mechanics as we known is accurate. A natural question arises: could one use quantum information as a tool to further test quantum mechanics?

The key to above question is knowing what to test. As many existing proposal of testing quantum mechanics pointed out, to test a theory, one should find some generalized theory that reduce to the original one when certain parameters become negligible. The development of quantum information gave us many different angles to look at quantum mechanics, which gave birth to a few theories which one could use to test the foundation of quantum mechanics.

Many predecessors have proposed and performed tests to quantum mechanics. Like Steven Weinberg in the 80s who proposed a family of generalization to quantum mechanics which could be tested using spinning particles in external fields. In that work, he points out the inconsistency of many other attempts to generalize the quantum mechanics by introducing non-linear terms in the Schrodinger equation. From a mathematician's perspective, Andrew M. Gleason proved that for a system whose state lives in a separable

Hilbert space of complex dimension at least 3, a unique trace class operator exist for any quantum probability measurement with Hermitian observables. In other words, Born rule of probability naturally follows when we describe our state in the complex Hilbert space, and require probability measurement to be non-negative and always normalized under different basis. More recently, a 3-slit photon interference experiment is done which put bounds on deviations from the Born rule. The success of quantum mechanics in various test and the incompatibility with general relativity motivate us to seek different angle in the test of quantum foundations.

In this thesis, I am going focus on two separate proposal testing quantum mechanics. First is to look at gravitationally induced entanglement de-correlation[2]. A generalized theory proposed by Ralph and Milburn in a sequences of papers gives entangled photons traveling in curved space time some additional de-correlation due to an additional degree of freedom from the said theory. This theory is adopted to develop potential experiment proposal for a satellite with only quantum uplink capacity. Second, we turn our attention to environmental induced invariance(envariance), and its application to test quantum mechanics. The symmetry of envariance could be used to explain decoherence and therefore bypass the need of introducing Born rule as an axiom of quantum mechanics. In an optics experiment, we tested this symmetry and used the result to bound the Born rule using certain extended theory of quantum mechanics[3]. At last, we discuss something we discover along the line while we are investigating the above tests: the tomography of quantum state that is close to a pure state using Pauli observables. When dealing with state that is close to pure state, we discovered that much less quantum operation are needed to reconstruct our quantum state compared to the general case. For two and three qubits system, we listed the minimum number of Pauli operation required to perform tomography on a pure quantum state, and tested the robustness in experiments[4].

My contribution of the thesis have already been published in the following papers:

[1] D Rideout, T Jennewein, G Amelino-Camelia, T F Demarie, B L Higgins, A Kempf, A Kent, R Lalamme, X Ma, R B Mann, et al. Fundamental quantum optics experiments conceivable with satellitesreaching relativistic distances and velocities. *Classical and Quantum Gravity*, 29(22):224011, 2012.

[2] L Vermeyden, X Ma, J Lavoie, M Bonsma, Urbasi Sinha, R Laflamme, and KJ Resch. Experimental test of environment-assisted invariance. *Physical Review A*, 91(1):012120, 2015.

[3] X Ma, T Jackson, H Zhou, J Chen, D Lu, M D Mazurek, K AG Fisher, X Peng, D Kribs, K J Resch, Z Ji, B Zeng, and R Laflamme Pure-state tomography with the expectation value of Pauli operators.*Physical Review A*, 93(3):032140, 2016.

# Chapter 2

## Background: quantum optics and quantum information

In this chapter, we are going to introduce some basic background material in quantum optics and quantum information, which would be useful to understand the subsequent chapters. It will also serve to establish the notation and terminology used in this work. The background material is separated into two sections: Section 2.1, Quantum optics and Section 2.2, Quantum information. Both will give the basic information that is required and direct to more resources if interested.

### 2.1 Quantum optics

#### 2.1.1 Photon modes and evolution

First, we would like to expand the optical fields over a set of modes  $\{\hat{a}_1, \hat{a}_1^\dagger, \hat{a}_2, \hat{a}_2^\dagger, \dots\}$ . For convenience, we pick  $\hat{a}_{k_i}$  and  $\hat{a}_{k_j}$  to be orthogonal modes when  $k_i \neq k_j$ . Therefore, operators  $\hat{a}_{k_i}$  and  $\hat{a}_{k_j}$  have boson commutation relations

$$[\hat{a}_{k_i}, \hat{a}_{k_j}] = [\hat{a}_{k_i}^\dagger, \hat{a}_{k_j}^\dagger] = 0 \quad (2.1)$$

$$[\hat{a}_{k_i}, \hat{a}_{k_j}^\dagger] = \delta_{k_i k_j} \quad (2.2)$$

In Heisenberg picture, the quantum modes of the output state could be write as rearrangement of the modes and their conjugates. Without losing generality, we define the evolution

to be

$$\hat{b}_k = f_k(\hat{a}_1, \hat{a}_1^\dagger, \hat{a}_2, \hat{a}_2^\dagger \dots) \quad (2.3)$$

where  $\hat{b}_k$  is the output mode  $k$ . In other word, if we have a detector designed to measure mode  $k$  at the output, the mode arrived at the detector would be  $\hat{b}_k$ . The form of  $f_k$  depends on the unitary(or sometimes non-unitary) evolution  $U(\hat{a}_1, \hat{a}_1^\dagger, \hat{a}_2, \hat{a}_2^\dagger \dots)$  we are interested in. Here, we assume this initial state is the vacuum state, where  $\hat{a}_k|0\rangle = 0$  for any mode  $k$ . We can consider the expectation value for a photon number at detector  $k$  of the form

$$n = \langle 0 | \hat{b}_k^\dagger \hat{b}_k | 0 \rangle. \quad (2.4)$$

Moreover, if we measure the correlation between modes  $k_i$  and  $k_j$ , the coincidence is given by

$$C_{k_i k_j} = \langle 0 | \hat{b}_{k_i}^\dagger \hat{b}_{k_i} \hat{b}_{k_j}^\dagger \hat{b}_{k_j} | 0 \rangle. \quad (2.5)$$

## 2.1.2 Parametric down converted photons

To create entangled photons, one would require nonlinear interaction between photons. One of the most common nonlinear interaction is the parametric down conversion. It happens when photon modes enters a medium with nonlinear susceptibility tensor  $\tilde{\chi}$ , where the dielectric polarization density could be expressed as

$$P(t) = \epsilon_0(\chi^{(1)}E(t) + \chi^{(2)}E^2(t) + \chi^{(3)}E^3(t) + \dots), \quad (2.6)$$

where  $\epsilon_0$  is the vacuum permittivity and  $E(t)$  is the electrical field. The coefficients  $\chi^{(n)}$  are the n-th order susceptibility, and we are interested in the nonlinear effects due to the  $\chi^{(2)}$  term. The interaction Hamiltonian of the parametric down conversion has the form of an integral over the volume of the crystal [5]

$$H_I(t) = \frac{\epsilon_0 \chi^{(2)}}{2} \int_V dV \hat{E}_p^{(+)} \hat{E}_s^{(-)} \hat{E}_i^{(-)} + h.c., \quad (2.7)$$

where  $\hat{E}_p^{(+)}$  is the positive frequency part of the pump optical field,  $\hat{E}_s^{(-)}$  and  $\hat{E}_i^{(-)}$  are the negative frequency part of the signal and idler optical field, respectively. Using this Hamiltonian, it is possible to generate pairs of entangled photons. In this section we are going to consider a simple case where all pump, signal and idler modes are single mode plane waves traveling in the  $\hat{z}$  direction. For a more general derivation, please see Ref. [5] and [6].

Under our plane wave assumption, the field operators could be expressed as

$$\hat{E}_p^{(+)} = i\sqrt{\frac{\hbar\omega_p}{2\epsilon_0 V}}\hat{a}_p \exp[i(k_p z - \omega_p t)], \quad (2.8)$$

$$\hat{E}_s^{(-)} = -i\sqrt{\frac{\hbar\omega_s}{2\epsilon_0 V}}\hat{a}_s^\dagger \exp[-i(k_s z - \omega_s t)], \quad (2.9)$$

$$\hat{E}_i^{(-)} = -i\sqrt{\frac{\hbar\omega_i}{2\epsilon_0 V}}\hat{a}_i^\dagger \exp[-i(k_i z - \omega_i t)]. \quad (2.10)$$

where  $\hat{a}_p$  is the annihilation operator for the pump,  $\hat{a}_s^\dagger$  and  $\hat{a}_i^\dagger$  are creation operators for the signal and the idler respectively.

If the signal and the idler are initialize as vacuum state and the pump initialized in a coherent state, where the wave function at  $t = 0$  is  $|\phi(0)\rangle = |\alpha\rangle_p |0\rangle_s |0\rangle_i$ . The wave function of the three modes in the first-order perturbation theory takes the form

$$\begin{aligned} |\phi(t)\rangle &= |\phi(0)\rangle + \frac{1}{i\hbar} \int_0^t dt' H_I(t') |\phi(0)\rangle \\ &= |\phi(0)\rangle + \frac{1}{i\hbar} \int_0^t dt' \frac{\epsilon_0 \chi^{(2)}}{2} \int_V dV \hat{E}_p^{(+)} \hat{E}_s^{(-)} \hat{E}_i^{(-)} |\phi(0)\rangle \\ &= |\phi(0)\rangle - \frac{\epsilon_0 \chi^{(2)}}{2\hbar} \left(\frac{\hbar}{2\epsilon_0 V}\right)^{\frac{3}{2}} \sqrt{\omega_s \omega_i \omega_p} \int_0^t dt' \int_V dV \hat{a}_p \exp[i(k_p z - \omega_p t')] \\ &\quad \times \hat{a}_s^\dagger \exp[-i(k_s z - \omega_s t')] \hat{a}_i^\dagger \exp[-i(k_i z - \omega_i t')] |\phi(0)\rangle \\ &= |\phi(0)\rangle - \frac{\epsilon_0 \chi^{(2)}}{2\hbar} \left(\frac{\hbar}{2\epsilon_0 V}\right)^{\frac{3}{2}} \sqrt{\omega_s \omega_i \omega_p} \int_0^t dt' \int_V dV \exp[i(k_p - k_s - k_i)z] \\ &\quad \times \exp[i(\omega_s + \omega_i - \omega_p)t'] \hat{a}_p \hat{a}_s^\dagger \hat{a}_i^\dagger |\phi(0)\rangle \end{aligned} \quad (2.11)$$

If we ignore the pump and output vacuum state, the second term in Eq 2.11 gives us wave function of a photon pair

$$|\psi(t)\rangle = -\frac{\alpha \epsilon_0 \chi^{(2)}}{2\hbar} \left(\frac{\hbar}{2\epsilon_0 V}\right)^{\frac{3}{2}} \sqrt{\omega_s \omega_i \omega_p} \int_0^t dt' \int_V dV \exp[i(k_p - k_s - k_i)z] \exp[i(\omega_s + \omega_i - \omega_p)t'] |1\rangle_s |1\rangle_i. \quad (2.12)$$

We could make a few observations by looking at this wave function. First, since the interaction time  $t$  is usually much longer than the optical frequency. We have

$$\int_0^t dt' \exp[i(\omega_s + \omega_i - \omega_p)t'] \approx \int_0^\infty dt' \exp[i(\omega_s + \omega_i - \omega_p)t'] = 2\pi \delta(\omega_s + \omega_i - \omega_p), \quad (2.13)$$

so the frequencies of the two photon should satisfy

$$\omega_s + \omega_i = \omega_p. \quad (2.14)$$

This is the energy conservation of the process. Moreover, if we assume the interaction happen in a area with length and  $L$ , we have

$$\int_0^L dz \exp[i(k_p - k_s - k_i)z] = \exp[i(k_p - k_s - k_i)\frac{L}{2}] \text{sinc}[(k_p - k_s - k_i)\frac{L}{2}]. \quad (2.15)$$

In order to maximize the entangled photon output, the function  $\text{sinc}[(k_p - k_s - k_i)\frac{L}{2}]$  needs to be maximized. This is called phase matching. Note that we used the first-order perturbation theory in Eq 2.11. The higher order terms in the series of expansion would lead to terms describing multiple photons generated in each mode. It is worth pointing out that those multiple photon output are not simply product of entangle pairs[7].

### Energy-time entangled photons

As described in Eq 2.14, the two photons generated by parametric down conversion have natural correlation in energy. This could be used to produce energy-time entangled photons [8][9] that we use later in Chapter 3.

To verify the idler and the signal photon are indeed entangled, one could measure both photons in distant detectors. If the difference of arrival time  $t_i$  and  $t_s$  violates  $\Delta(t_i - t_s)\Delta(\omega_i + \omega_s) > 1$ , it is sufficient to show bipartite entanglement between the two photons[10]. With the energy conservation  $\omega_s + \omega_i = \omega_p$ , the inequality could be simplified as  $\Delta(t_i - t_s)\Delta(\omega_p) > 1$ .

### Polarization entangled photons

To discuss the polarization entangled photon, it is important to review the polarization states of photon pairs generated by parametric down conversion. There are two types correlated polarizations. When the signal and idler photons have parallel polarization, it is called type I correlation. When the signal and idler photons have perpendicular polarizations, it is called type II correlation. In this section, we are going to introduce one method to generate polarization entangled photons using type II parametric down conversion, which we use later in Chapter 4. For other interesting methods to generate polarization entangled photons please refer to Ref [11].

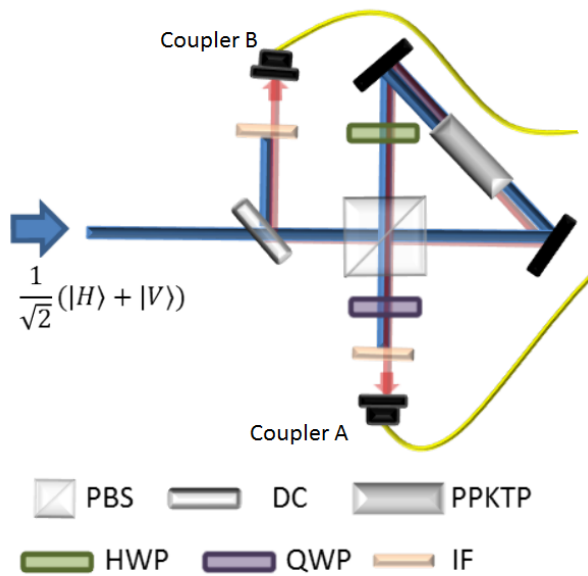


Figure 2.1: Preparation of polarization entangled photons. The blue line represents the pump beam, which gets removed at filter(IF). The pink and purple lines represent the signal and idler. The pump light is a 45 degree polarized beam. The horizontal photons from the pump beam travels counterclockwise after the polarizing beam splitter, and generate pairs of horizontal idler and vertical signal photons through type II PDC at PPKTP. The vertical photons from the pump beam travels clockwise, and generate pairs of vertical idler and horizontal signal photons. The half wave plate is put in for phase matching purpose. As two path are indistinguishable, we create polarization entangled photons at the couplers.

As shown in Fig 2.1, we input a 45 degree polarized pump beam:

$$|\psi\rangle = \frac{1}{\sqrt{2}}(|H\rangle + |V\rangle). \quad (2.16)$$

The horizontal photons from the pump beam gets transmitted at the polarizing beam splitter, and generating horizontal idler and vertical signal photons at the nonlinear crystal PPKTP. The horizontal idler gets transmitted by the polarized beam splitter to the coupler A, while the vertical signal gets reflected to the coupler B. Therefore, the setup produces the transformation  $|H\rangle \rightarrow |H\rangle_A|V\rangle_B$ . The vertical photons from the pump beam gets reflected at the polarizing beam splitter, and generating vertical idler and horizontal signal photons. The vertical idler gets reflected by the polarized beam splitter to the coupler A, while the horizontal signal gets transmitted to the coupler B. Therefore, the setup produces the transformation  $|V\rangle \rightarrow |V\rangle_A|H\rangle_B$ . Since two paths are indistinguishable, we arrived at polarization entangled state:

$$|\phi\rangle = \frac{1}{\sqrt{2}}(|H\rangle_A|V\rangle_B + |V\rangle_A|H\rangle_B). \quad (2.17)$$

By adjusting the angle of the QWP at the coupler A, we could produce

$$|\phi\rangle = \frac{1}{\sqrt{2}}(|H\rangle_A|V\rangle_B + e^{i\theta}|V\rangle_A|H\rangle_B). \quad (2.18)$$

By tilting the quarter wave plate, this source generates two of the four Bell states.

### 2.1.3 Dual-rail qubits and its relation to polarization qubits

In the original linear optics quantum computing scheme [12], dual-rail qubits are used to build an ideal quantum computer. The location of a photon in two possible paths are used to encode a qubit. If we name the two spatial mode  $a$  and  $b$ , the logic 0 is given by a photon traveling in spatial mode  $a$ ,  $|0\rangle_L = |10\rangle_{ab}$ , while logic 1 is given by a photon traveling in spatial mode  $b$ ,  $|1\rangle_L = |01\rangle_{ab}$ . The single qubit unitaries for dual-rail qubits could be implemented with beam splitters and phase shifters. To show that using both phase shifters and beam splitters are sufficient for any single qubit gates, we first observe that phase shifter on mode  $a$  would give us arbitrary rotation about the Z axis up to a global phase. The unitary for a phase shifter placed on the path of mode is given by

$$U_{PS}(\phi) = \begin{pmatrix} e^{i\phi} & 0 \\ 0 & 1 \end{pmatrix} \quad (2.19)$$

A beam splitter with transmittance  $\sin \theta$  could be described by

$$U_{PS}(\theta) = \begin{pmatrix} \cos \theta & -\sin \theta \\ \sin \theta & \cos \theta \end{pmatrix} \quad (2.20)$$

If one put a phase shifter  $U_{PS}(\phi_1)$  after a beam splitter  $U_{PS}(\theta)$  after a phase shifter  $U_{PS}(\phi_1)$ , one could have universal single qubit gate for dual-rail qubits.

$$U_{PS}(\phi_2)U_{PS}(\theta)U_{PS}(\phi_1) = \begin{pmatrix} e^{i(\phi_1+\phi_2)} \cos \theta & -e^{i\phi_2} \sin \theta \\ e^{i\phi_1} \sin \theta & \cos \theta \end{pmatrix} \quad (2.21)$$

The two polarization degree of freedom for photons, the horizontally and vertically polarization  $|H\rangle, |V\rangle$ , could also be used as basis for implementing qubits. The polarization qubits can be converted to the dual-rail qubits by introducing a piece of polarized beam splitter(PBS), which transmits  $|H\rangle$  and reflects  $|V\rangle$ . If we name the transmitted spatial mode, mode  $a$ , and the reflected mode, mode  $b$ . PBS transforms input state  $\alpha|H\rangle + \beta|V\rangle$  as a polarization qubit to  $\alpha|10\rangle_{ab} + \beta|01\rangle_{ab}$  as a dual rail qubit. It is worth noting, one could easily reverse the setting to convert a dual-rail qubit into a polarization qubit.

### 2.1.4 Unitary gates for photon-polarization qubits

In order to perform universal one qubit unitary on a photon-polarization qubits, one uses sets of waveplates to alter the polarization state of photons traveling through it. Waveplates are made of birefringent material, whose index of refraction varies depending on the polarization and propagation direction light. By controlling the thickness of such crystal, one could build half wave plate(HWP) and quarter wave plate(QWP). By rotating the major axis of HWP or QWP, the waveplates' unitary changes. For an HWP with its major axis at an angle  $\theta$ , we have

$$\begin{aligned} U_{HWP}(\theta) &= e^{-i\theta Y} e^{-i\frac{\pi}{2}Z} e^{i\theta Y} \\ &= -i \begin{pmatrix} \cos 2\theta & \sin 2\theta \\ \sin 2\theta & -\cos 2\theta \end{pmatrix} \\ &= -i (Z \cos 2\theta + X \sin 2\theta) \end{aligned} \quad (2.22)$$

where  $X$ ,  $Y$  and  $Z$  are Pauli Matrices,

$$X = \begin{pmatrix} 0 & 1 \\ 1 & 0 \end{pmatrix} \quad (2.23)$$

$$Y = \begin{pmatrix} 0 & -i \\ i & 0 \end{pmatrix} \quad (2.24)$$

$$Z = \begin{pmatrix} 1 & 0 \\ 0 & -1 \end{pmatrix} \quad (2.25)$$

similarly, for a QWP with its major axis at an angle  $\theta$ , we have

$$\begin{aligned} U_{QWP}(\theta) &= e^{-i\theta Y} e^{-i\frac{\pi}{4}Z} e^{i\theta Y} \\ &= \frac{1}{\sqrt{2}} \begin{pmatrix} 1 - i \cos(2\theta) & -i \sin 2\theta \\ -i \sin 2\theta & 1 + i \cos(2\theta) \end{pmatrix} \\ &= \frac{1}{\sqrt{2}} (\mathbf{1} - iX \sin 2\theta - iZ \cos 2\theta) \end{aligned} \quad (2.26)$$

Note that using either a single QWP or a HWP will not give us all universal single qubit unitaries by rotating the crystal. Therefore, we stack a few waveplates together to get universal single qubit rotations. One of the simplest way to implement it would be to stack a QWP after an HWP and finally after a QWP.

$$\begin{aligned} &U_{QWP}(\theta_1) U_{HWP}(\theta_2) U_{QWP}(\theta_3) \\ &= Z (\cos 2\theta_2 - \cos 2\theta_3 \cos(2\theta_2 - 2\theta_1) - \sin 2\theta_3 \sin(2\theta_2 - 2\theta_1)) \\ &\quad Y (\sin(2\theta_3 - 2\theta_2) + \sin(2\theta_2 - 2\theta_1)) \\ &\quad X (\sin 2\theta_2 - \sin 2\theta_3 \cos(2\theta_2 - 2\theta_1) + \cos 2\theta_3 \sin(2\theta_2 - 2\theta_1)) \\ &\quad -iI (\cos(2\theta_3 - 2\theta_2) + \cos(2\theta_2 - 2\theta_1)) \end{aligned} \quad (2.27)$$

By rotating the major axis of the three crystal, any single qubit gate could be realized by this set up.

## 2.2 Quantum information

### 2.2.1 Quantum state tomography and Maximum Likelihood Estimation

One key task in quantum information is quantum state tomography, where the density matrix representing our quantum state is determined via a number of measurements. With

many identically prepared copies of a quantum system, one perform a series of measurements on the system. If the measurements are chosen carefully, one could infer the quantum state of such system with good precision. For example, say we have a one qubit quantum state  $\rho$ . We could always write  $\rho$  in Pauli basis, where

$$\rho = \alpha_0 \mathbf{I} + \alpha_1 X + \alpha_2 Y + \alpha_3 Z. \quad (2.28)$$

We could prepare multiple copies of  $\rho$  and measure them with Pauli observables  $X$ ,  $Y$  and  $Z$ . The expected value of measurement could be written as  $\text{Tr}(\rho X) = e_1$ ,  $\text{Tr}(\rho Y) = e_2$ , and  $\text{Tr}(\rho Z) = e_3$ . Combined with the normalization, we get  $\text{Tr}(\rho \mathbf{I}) = 1$ , where  $\alpha_0 = \frac{1}{2}$ . Therefore, we can reconstruct our state as

$$\rho = \frac{1}{2} \mathbf{I} + e_1 X + e_2 Y + e_3 Z. \quad (2.29)$$

This naive method of using linear combination of experiment data to reconstruct density matrix works when we ignore any noise in the process. After we introduce experimental noise, it might give us a density matrix which does not fulfill the requirement of being positive semidefinite. This problem is more severe among low rank states, which are more likely to obtain a negative eigenvalue from random perturbation. In order to guarantee the reconstruction yield a positive semidefinite matrix, one could implement maximum likelihood method in the state reconstruction.

To use maximum likelihood method, one start by assuming certain noise model for the measurement results. Imagine we performed 4 sets of measurements to obtain the experimental values for  $\text{Tr}(\rho \mathbf{I}) = e_0$ ,  $\text{Tr}(\rho X) = e_1$ ,  $\text{Tr}(\rho Y) = e_2$ , and  $\text{Tr}(\rho Z) = e_3$ . Note that the observable of identity operator is counted here. In most implementation, this is done with calibration which is usually not noise free. One would assume the measurement outcomes  $\{e_0, e_1, e_2, e_3\}$  are normally distributed with some unknown mean and variance, which is reasonable given a large number of instance are measured to obtain the experimental expected values. It is fair to use central limit theorem to assume the experimental values are following normal distribution. Each measurement is assigned with an expectation value  $\bar{e}_i$  and a variance  $\sigma_i^2$ , where  $\sigma_i^2$  could be determined with further assumption of our error model. Therefore, the probability of getting the measured outcome  $\{e_0, e_1, e_2, e_3\}$  is given by

$$P(e_1, e_2, e_3, e_4 | \bar{e}_0, \bar{e}_1, \bar{e}_2, \bar{e}_3) = \frac{1}{N} \prod_{n=1}^4 \exp\left[-\frac{(e_i - \bar{e}_i)^2}{2\sigma_i^2}\right], \quad (2.30)$$

where  $N$  is the normalization constant.

Instead of directly use the experimentally measured value in our state reconstruction, maximum likelihood estimation tries to find the set of values of the model parameters that maximizes the probability of getting the experimentally measured value given such model parameters. Our optimization task becomes to find such expectation value  $\{\bar{e}_0, \bar{e}_1, \bar{e}_2, \bar{e}_3\}$  which maximize the probability  $P(e_1, e_2, e_3, e_4|\bar{e}_0, \bar{e}_1, \bar{e}_2, \bar{e}_3)$ . To simplify the expression, we can take logarithm of Eq. 2.30:

$$\ln P(e_1, e_2, e_3, e_4|\bar{e}_0, \bar{e}_1, \bar{e}_2, \bar{e}_3) = -\ln N - \sum_{n=1}^4 \frac{(e_i - \bar{e}_i)^2}{2\sigma_i^2}. \quad (2.31)$$

To further simplify Eq. 2.31, we need to make assumptions on the variances  $\sigma_i^2$  according to our physical system. For example, when photon number is measured, we could assume the measurement outcome follows the Poisson distribution, where  $\sigma_i = \sqrt{\bar{e}_i}$ . Therefore, our optimization task could reduce to finding the minimum of following function:

$$L(e_1, e_2, e_3, e_4|\bar{e}_0, \bar{e}_1, \bar{e}_2, \bar{e}_3) = \sum_{n=1}^4 \frac{(e_i - \bar{e}_i)^2}{2\bar{e}_i}, \quad (2.32)$$

where  $L(e_1, e_2, e_3, e_4|\bar{e}_0, \bar{e}_1, \bar{e}_2, \bar{e}_3)$  is called the likelihood function. Some times the variance  $\sigma_i^2$  are the same for different measurements, where  $\sigma_i = \bar{\sigma}$ . The optimization is further reduced to finding the minimum of likelihood function

$$L(e_1, e_2, e_3, e_4|\bar{e}_0, \bar{e}_1, \bar{e}_2, \bar{e}_3) = \sum_{n=1}^4 (e_i - \bar{e}_i)^2, \quad (2.33)$$

which is also known as the least squares fitting.

# Chapter 3

## Testing quantum foundations in space using artificial satellite

### 3.1 Introduction

Quantum mechanics and general relativity are two of the most successful theories in the 20th century. Although both of them survived numerous tests with great accuracy, they are not compatible in certain area. Quantum theory exceptionally describes the behaviour of physical systems at small scales, while general relativity theory predicts systems at large scales. One expects that both theories are limiting cases of one set of unified laws of physics. However, the success of both theory makes it extremely difficult to find experimental evidence that points us towards such unifying laws of physics.

Going forward, we need more experimental guidance. We could observe and capture events that naturally occurs in the universe, such as the cosmic microwave background (CMB), which is so far the best potential for solid experimental evidence for quantum gravitational effects. However, the observation of CMB counts only a passive one-shot experiment since the big bang can not be repeated.

Therefore, it is important that we push our direct tests of quantum theory to scales where the curvature of spacetime is no longer negligible. Some experiments have been already performed up to hundreds of kilometers on the Earth[13]. Such tests still fall short to probe the potential important physics that arises at the intersection of quantum theory and general relativity. The next step would be looking at potential experiments in even larger scale, in the outer space. A test conceivable with artificial satellites in Earth orbit

or elsewhere in the solar system may be helpful to eliminate various alternative physical theories and place bounds on phenomenological models.

At time of this project was conducted, there was a scientific proposal, where an artificial satellite with uplink quantum channel capacity would be available. The task was to look at different alternative physical theories and find ones that have significant difference to the standard quantum fields theory that could be detected on the satellite.

In this Chapter, we look an alternative quantum optics theory proposed by T. Ralph and G. Milburn in a series of papers. By introducing a second time-like degree of freedom called event operator, entangled photon traveling in curved space time would gain additional de-correlation under this alternative quantum optics theory. My work in this chapter is described in Section 3.3, where we adopted this theory for our uplink satellite and determined the required photon detector resolution for the satellite.

## 3.2 T. Ralph and G. Milburn's alternative quantum optics theory

The standard quantum fields theory in curved spacetime [14] allows quantum entanglement to survive unchecked in a wide variety of gravitational environments. Ideally, entangled photons created locally and traveling through regions of different gravitational background will still possess all the entanglement they begin with. Local detectors can be carefully designed to reveal this. One would need to take into account other factors which may also alter the amount entanglement, such as redshift, time-of-arrival delay, phase locking, modification, mode shape, etc. Of course, there is always the possibility that the description of standard quantum field is not accurate, and an alternative theory is needed. An alternative theory of the behaviour of photons under different gravitational background was introduced by Ralph and Milburn in a series of papers [15, 16, 17, 18, 19] originally designed to explain the thought experiment of quantum information propagation in presence of closed timelike curves but later used to predict measurable decoherence induced by gravitation.

The motivation of this alternative theory is to allow photon modes to interact with its past. Under Deutsch model [20] for closed timelike curves, a quantum state is allowed to interact with a version of itself in the past as long as we enforce the density operator of the state to match. This can not be done with photon modes in standard quantum field theory, since the all point along the geodesic of the light ray commutes. This alternative theory attempts to localize the photon modes in the temporal degree of freedom, so that

photon mode of the present and the past no longer commute. This theory also provides some visible changes to entangled pairs traveling in curved spacetime, which could be used to test the theory.

The essence of this proposal is to supplement ordinary field theory with an additional degree of freedom called an *event operator*, which is associated with the detectors used to measure the field quanta in a given setup. In flat spacetime with detectors in the same reference frame, the event operator is of no visible consequence because time passes at the same rate for all detectors. But when two detectors are in curved spacetime, their local clocks run at different rates and fall out of sync gradually. When the amount by which they desynchronize during the photons' times of flight is longer than the timing resolution of the detectors, then, although the delay in the time of arrival can be accounted for in the detector design, the presence of the event operator (whose duration is associated to the detector's temporal resolution) ensures that the two photons lose coherence.

What is the event operator? Lets start by writing out the mode annihilation operator for a field traveling in the positive  $x$  direction:

$$\hat{a}(t, x) = \int dk G(k) e^{ik(x-t+\psi)} \hat{a}_k \quad (3.1)$$

where  $t$  is the time,  $k$  is the optical frequency and  $G(k)$  is a normalized spectral mode distribution and  $\psi$  is the phase shift. Note that we have chosen the speed of light to be  $c = 1$  so that the time  $t$  is in units of space. It is natural to assume  $G(k) = 0$  for  $k < 0$ , since optical modes with negative frequency would not be physical.

It is easy to verify that all points along the geodesic of the light ray are equivalent for this traveling field. In other word a translation of Eq. 3.1 by  $x \rightarrow x + \delta, t \rightarrow t + \delta$  produces no change in the mode operator:

$$\hat{a}(t + \delta, x + \delta) = \int dk G(k) e^{ik(x+\delta-t-\delta+\psi)} \hat{a}_k = \hat{a}(t, x). \quad (3.2)$$

The essence of this alternative quantum optics theory is the event operator. We introduce a second spectral degree of freedom,  $\Omega$ , and a distribution,  $J(\Omega)$ , over this degree of freedom to each of the input modes, such that Eq. 3.1 becomes

$$\bar{a}(x, t) = \int dk G(k) e^{ik(x-t+\psi)} \times \int d\Omega J(\Omega) e^{i\Omega t} \bar{a}_{k,\Omega} \quad (3.3)$$

where  $\bar{a}(x, t)$  is called the event operator. Note that

$$[\bar{a}_{k,\Omega}, \bar{a}_{k',\Omega'}^\dagger] = \delta(k - k')\delta(\Omega - \Omega'). \quad (3.4)$$

We can view  $\bar{a}_{k,\Omega}$  as a description of optical mode localized not only in the frequency  $k$  but also in the second spectral degree of freedom  $\Omega$ . By adding this independent, local temporal parametrization of the quantum optical modes, we aim to make observable at different points along the geodesic commute.

### 3.3 Testing quantum mechanics with artificial satellites

The scheme proposed in Ref. [19] involves preparing a pair of entangled photons via spontaneous parametric down-conversion (SPDC). One of the entangled photons is measured directly on the ground station after a time delay, while the other is sent to the satellite, traversing a varying gravitational potential. Figure 3.1 illustrates the process.

Using the localized event operator introduced in this alternative theory, the maximum coincidence detection rate of two photons should decline due to intrinsic decoherence by the curved spacetime. As described earlier in this chapter, the local clock of two detector experiencing different gravitational potential falls out of sync. The difference in proper time  $\Delta$  between the two detectors during the time of flight of the photons determine the timescale for the event operators in question, and therefore sets the timescale on which decoherence will take place. In our setting, one of the entangled photon is reflected at the surface of the Earth, and remained in the lab until measured. Therefore it is always at the distance  $x_l = r_e$  to the Earth center, where  $r_e = 6.38 \times 10^6 m$  is the radius of the Earth. The other photon is sent to the satellite, which is at distance  $x_s = r_e + h$  to the Earth center, where  $h$  is the height of the satellite. Therefore, in a Schwarzschild metric, the difference in proper time  $\Delta$  between the two detectors is given by

$$\begin{aligned} \Delta &= M \ln\left(\frac{x_s}{x_l}\right) \\ &\approx M \frac{h}{r_e} \end{aligned} \tag{3.5}$$

where  $2M = 8.87 \times 10^{-3} m$  is the Schwarzschild radius of the Earth. When the difference in proper time  $\Delta$  is larger than the detector temporal resolution  $d_t$ , decoherence occurs. In the model proposed by Ralph and Milburn in Ref. [19], the reduced correlation function is given by

$$C = C_{\max} \exp\left(-\frac{\Delta^2}{4d_t^2}\right), \tag{3.6}$$

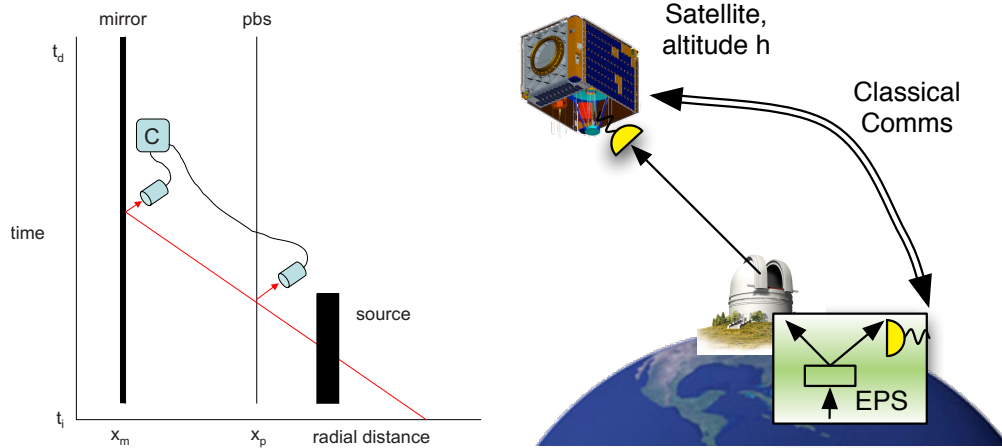


Figure 3.1: Left: The original proposed scheme to test gravitationally induced decorrelation. A source prepares a pair of orthogonal polarization modes with entangled photons. Two modes initially propagate towards the surface of the Earth. Using the polarizing beamsplitter (pbs), two modes are separated at height  $x_p$ . The detectors located at height  $x_p$  and  $x_m$  pick up the signals and feed the measurement result to the correlator via classical channels. Figure taken from Ref. [19]. Right: A possible implementation could employ an uplink of the quantum signals from the source on the ground to the receiver in the satellite, which inverts the signs of the gravitational potential difference, but should lead to the same effect. The entangled photons prepared using SPDC are initially perfectly correlated and spatially degenerate. Two single photon detectors capture the detection times of photons and stream the data to a computer. The detection data from the satellite is sent to the ground for analysis.

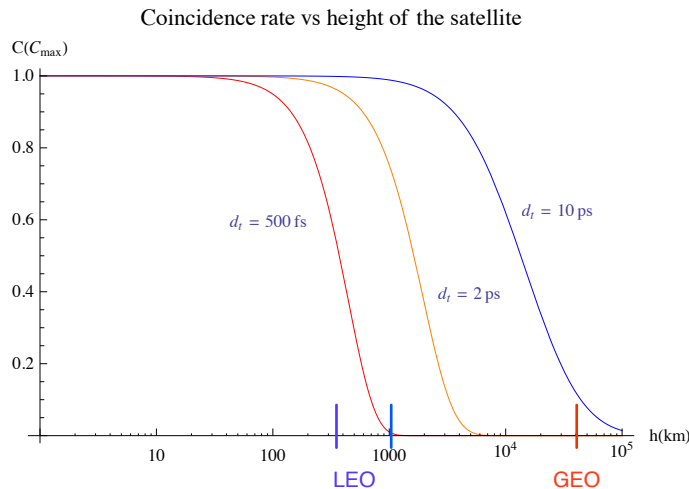


Figure 3.2: Coincidence predictions from the experiment proposed in Ref. [19]. The coincidence detection rate (i.e. detection events in both detectors) as a function of temporal difference of the detection  $t_{d2} - t_{d1}$  should be peaked around the light traveling time difference in the two “arms”. The maximum coincidence rate  $C$  describes the photon correlation upon detection, within the (intrinsic) detection time  $d_t$ .

where  $C_{\max}$  is the maximum correlation function we should observe in flat spacetime, and  $d_t$  is the temporal resolution of the photon detectors.

If the photodetector resolution time is 500 fs, then the decoherence should easily be observed for satellite altitudes above 400 km,<sup>1</sup> as illustrated in Figure 3.2. With a GEO satellite, which orbits at altitude 36,000 km, the effect would be more significant, and even with 10 ps response time (the response time of a typical contemporary photodetector), a visible decorrelation effect could occur.

Due to the careful timing required, this scheme is challenging but still possibly doable. It is interesting to note that the predicted decoherence induced by gravity under this alternative theory applies only to quantum entanglement, and is in addition to any spreading of classical correlations. Because there are many sources of decoherence for photons traveling between satellites and the ground, it will be much easier to refute the event-operator hypothesis than to confirm it — if we were able to generate entanglement beyond what is predicted by Eq. 3.6, the hypothesis as proposed would be contradicted. On the other

<sup>1</sup>This is a conservative estimate compared to the 200 fs quoted in Ref. [19], which would result in decoherence above 90 km.

hand, if decoherence were found, it would be difficult to rule out other source of decoherence, which we may overlooked. If that is the case, one could employ a satellite in an elliptical orbit to perform the test when the satellite is at different heights to see whether the decorrelation changes in accord with Eq. 3.6.

Note that an alternative approach to the setup of Figure 3.1 (right panel) is to equip a retroreflecting mirror on the satellite instead of a photon detector. However, one of the entangled photon pair would have to travel through the atmosphere twice instead of just once, which would cause further loss of photon. It would have the benefit that the requirement of satellite orbit height is halved at which an effect can be seen. The theory would predict the same curves as in Figure 3.2 but with each tick mark on the horizontal axis replaced with half its current value. As a trade off between photon loss and satellite height requirement, it might be advantageous in certain setups.

# Chapter 4

## Testing envariance

### 4.1 Introduction

Envariance, or environment - assisted invariance, is a quantum symmetry that discovered by Zurek in attempt to explain the origin of decoherence [21, 22, 23]. It applies in cases where a bipartite quantum state is present. The state consists of a system part, labeled S, and an environment part, labeled E. If some non-trivial action is applied to the system part only, described by some unitary evolution,  $U_S = u_S \otimes I_E$ , then the state is said to be envariant under  $U_S$  if another unitary applied to the environment,  $U_E = I_S \otimes u_E$ , can restore the initial state. Mathematically, it can be expressed,

$$U_S |\psi_{SE}\rangle = (u_S \otimes I_E) |\psi_{SE}\rangle = |\psi'_{SE}\rangle \quad (4.1)$$

$$U_E |\psi'_{SE}\rangle = (I_S \otimes u_E) |\psi'_{SE}\rangle = |\psi_{SE}\rangle. \quad (4.2)$$

Envariance is an example of an assisted symmetry [21] where once the system is transformed under some unitary  $U_S$ , it can be restored to its original state by another operation on a distinct system: the environment. It is hard to imagine such symmetry in a classical framework, since non-trivial changes applied to a classical system could be never be restored by action on a distant classical system.

Envariance is a uniquely quantum symmetry in the following sense. A pure state represents complete knowledge of the quantum system. In an pure entangled quantum state, however, complete knowledge of the whole system does not imply complete knowledge of its parts. It is therefore possible that an operation on one part of a quantum state can alter the global state, but its local effects are masked by incomplete knowledge of that

part; the effect on the global state can then be undone by an action on a different part. In contrast, complete knowledge of a composite classical system implies complete knowledge of each of its parts. Thus transforming one part of a classical system cannot be masked by incomplete knowledge and cannot be undone by a change on another part.

Envariance plays a prominent role in work related to fundamental issues of decoherence and quantum measurement [21, 22, 23]. Decoherence converts amplitudes in coherent superposition states to probabilities in mixtures and is central to the emergence of the classical world from quantum mechanics [24, 25]. Mathematically the mixture appears in the reduced density operator of the system which is extracted from the global wavefunction by a partial trace [26, 27]. This partial trace limits the approach for deriving, as opposed to separately postulating, the connection between the wavefunction and measurement probabilities known as Born rule [28], since the partial trace *assumes* Born rule is valid [22, 25]. Envariance was employed in a derivation of Born rule which sought to avoid circularity inherent to approaches which rely on partial trace [22]. For comments on this derivation, see for example [25].

In the present work, we subject envariance to experimental test in an optical system. We use the polarization of a single photon to encode the system,  $S$ , and the polarization of a second single photon to encode the environment,  $E$ . We subject the system photon to a wide range of polarization rotations with the goal of benchmarking the degree to which we can restore the initial state by applying a second transformation on the environment photon. My contribution for this work was designing the experiment described in section 4.3 and putting bounds on the Born rule in section 4.4.

## 4.2 Deriving Born rule from envariance

Before we go into the experiment, let's give the brief introduction of deriving Born rule from envariance. Like other derivation of the Born rule such as Gleason's theorem, this derivation follows a number of general assumptions behind quantum mechanics. One could argue that under the same set of assumptions, Gleason's theorem should also follow. It is worth pointing out that this derivation is aimed to provide a different perspective at the Born rule, which is more accessible for people from physics background. Moreover, one may argue that Gleason's theorem gives no insight into physical significance of quantum probabilities, in other word, it is not clear why the observer should assign probabilities in accord with the measure provided by the Gleason's approach. This derivation attempts to justify the quantum definition of probability. In this section, our final goal is to show the

Born rule for quantum state  $|\psi_{\mathcal{SE}}\rangle = \sum_{k=1}^N \alpha_k |\sigma_k\rangle |\epsilon_k\rangle$ . Mathematically, we would like to show that

**Theorem 1.** *For state in Schmidt form*

$$|\psi_{\mathcal{SE}}\rangle = \sum_{k=1}^N \alpha_k |\sigma_k\rangle |\epsilon_k\rangle \quad (4.3)$$

The probability of measuring  $|\sigma_k\rangle$  in system  $p_k \propto |\alpha_k|^2$ .<sup>1</sup>

The derivation could be divided into two parts.

First, prove that for  $|\alpha_i|^2 = \frac{1}{N}$ ,  $p_k = \frac{1}{N}$ . Then, generalize the result to any rational  $|\alpha_i|^2$ .

**Theorem 2.** *For state in Schmidt form*

$$|\psi_{\mathcal{SE}}\rangle = \sum_{k=1}^N \frac{1}{\sqrt{N}} e^{i\theta_k} |\sigma_k\rangle |\epsilon_k\rangle \quad (4.4)$$

The probability of measuring  $|\sigma_k\rangle$  in system is  $p_k = \frac{1}{N} \forall k \in \{1, 2, \dots, N\}$ .

Let's swap the  $i$ th and  $j$ th elements in the system. We could do this by swap the label of those 2 eigenstate without touching any experimental setup. The unitary for the swap could be written as:

$$u_{\mathcal{S}} = |\sigma_i\rangle \langle \sigma_j| + |\sigma_j\rangle \langle \sigma_i| + \sum_{k \neq i, j} |\sigma_k\rangle \langle \sigma_k| \quad (4.5)$$

The state after the swap operation becomes

$$\begin{aligned} (u_{\mathcal{S}} \otimes \mathbf{1}) |\psi_{\mathcal{SE}}\rangle &= \frac{1}{\sqrt{N}} e^{i\theta_j} |\sigma_i\rangle |\epsilon_j\rangle + \frac{1}{\sqrt{N}} e^{i\theta_i} |\sigma_j\rangle |\epsilon_i\rangle \\ &+ \sum_{k \neq i, j} \frac{1}{\sqrt{N}} e^{i\theta_k} |\sigma_k\rangle |\epsilon_k\rangle \end{aligned} \quad (4.6)$$

The initial state is envariant under unitary  $(u_{\mathcal{S}} \otimes \mathbf{1})$ . One may apply a unitary  $u_{\mathcal{E}}$  solely on the environment to recover the original state  $|\psi_{\mathcal{SE}}\rangle$ . The said unitary  $u_{\mathcal{E}}$  could be expressed as

$$u_{\mathcal{E}} = e^{i(\theta_j - \theta_i)} |\epsilon_i\rangle \langle \epsilon_j| + e^{i(\theta_i - \theta_j)} |\epsilon_j\rangle \langle \epsilon_i| + \sum_{k \neq i, j} |\epsilon_k\rangle \langle \epsilon_k| \quad (4.7)$$

---

<sup>1</sup>Born rule for bipartite entangled state

We could check that

$$(u_S \otimes u_E) |\psi_{SE}\rangle = \sum_{k \neq i, j} \frac{1}{\sqrt{N}} e^{i\theta_k} |\sigma_k\rangle |\epsilon_k\rangle + \frac{1}{\sqrt{N}} e^{i\theta_i} e^{i(\theta_j - \theta_i)} |\sigma_j\rangle |\epsilon_j\rangle + \frac{1}{\sqrt{N}} e^{i\theta_j} e^{i(\theta_i - \theta_j)} |\sigma_i\rangle |\epsilon_i\rangle \quad (4.8)$$

$$= \sum_k \frac{1}{\sqrt{N}} e^{i\theta_k} |\sigma_k\rangle |\epsilon_k\rangle \quad (4.9)$$

$$= |\psi_{SE}\rangle \quad (4.10)$$

Before we ask what is the probability of getting outcome  $|\sigma_i\rangle$  and  $|\sigma_j\rangle$  when we measure the system, we make the following three assumptions.

First, unitary transformations must act on the system to alter its state. Probabilities of getting outcome  $|\sigma_i\rangle$  or outcome  $|\sigma_j\rangle$  should not be affected by transformation  $u_E$ , which acts only on the environment.

Second, the state of the system  $S$  is all that is needed to predict measurement outcomes, including their probabilities.

Finally, the state of a larger composite system that includes  $S$  as a subsystem is all that is needed to determine the state of the system  $S$ .

Assume we have probability  $p_i$  of getting outcome  $|\sigma_i\rangle$  and probability  $p_j$  of getting outcome  $|\sigma_j\rangle$ . Since the swap operation only relabels eigenstate  $i$  and  $j$ , we have

$$p(i | |\psi_{SE}\rangle) = p(j | (u_S \otimes \mathbf{1}) |\psi_{SE}\rangle) \quad (4.11)$$

Since operations solely on the environment should not change the measurement outcome in the system, we have

$$p(j | (u_S \otimes \mathbf{1}) |\psi_{SE}\rangle) = p(j | (u_S \otimes u_E) |\psi_{SE}\rangle) \quad (4.12)$$

After the applying both unitary, we got the original state back, where  $(u_S \otimes u_E) |\psi_{SE}\rangle = |\psi_{SE}\rangle$ . Therefore,

$$p(j | (u_S \otimes u_E) |\psi_{SE}\rangle) = p(j | |\psi_{SE}\rangle) \quad (4.13)$$

Now, from Eq. 4.11, Eq. 4.12 and Eq. 4.13, we conclude that

$$p(j | |\psi_{SE}\rangle) = p(i | |\psi_{SE}\rangle) \quad (4.14)$$

Due to the freedom of choice of index  $i$  and  $j$ , the probabilities of measuring any state in this system are the same! Since there are  $N$  possible outcomes, and the probabilities should sum up to 1. Thus, the probability of measuring any eigenstate  $|\sigma_k\rangle$  in the system is  $p_k = \frac{1}{N}$ .

We could use the result in Theorem 2 to show Theorem 1. Consider the special example where  $N = 2$ .

$$|\psi_{S\mathcal{E}}\rangle = \frac{\sqrt{N-M}}{\sqrt{N}} |\sigma_l\rangle |\epsilon_l\rangle + \frac{\sqrt{M}}{\sqrt{N}} |\sigma_j\rangle |\epsilon_j\rangle \quad (4.15)$$

Now we put in a large enough ancillary pointer state, and entangle the state with the pointer state.

$$|\psi_{S\mathcal{E}}\rangle |e_0\rangle = \frac{\sqrt{N-M}}{\sqrt{N}} |\sigma_l\rangle_S |\epsilon_l\rangle_E |p_0\rangle_P + \frac{\sqrt{M}}{\sqrt{N}} |\sigma_j\rangle_S |\epsilon_j\rangle_E |p_1\rangle_P \quad (4.16)$$

The entangling operation  $U_p$  is done between the environment and pointer state.

$$\mathbf{1}_S \otimes U_p |\psi_{S\mathcal{E}}\rangle |e_0\rangle = \frac{\sqrt{N-M}}{\sqrt{N}} |\sigma_l\rangle_S |\epsilon_l\rangle_E |p_0\rangle_P + \frac{\sqrt{M}}{\sqrt{N}} |\sigma_j\rangle_S |\epsilon_j\rangle_E |p_1\rangle_P \quad (4.17)$$

Since the ancillary system is large enough, we could rewrite the pointer states in a different basis where

$$|p_0\rangle_P = \sum_{k=1}^{N-M} \frac{1}{\sqrt{N-M}} |\eta_k\rangle_P \quad (4.18)$$

$$|p_1\rangle_P = \sum_{k=N-M+1}^N \frac{1}{\sqrt{M}} |\eta_k\rangle_P \quad (4.19)$$

Thus, we could rewrite the state  $\mathbf{1}_S \otimes U_p |\psi_{S\mathcal{E}}\rangle |e_0\rangle$  as

$$\begin{aligned} \mathbf{1}_S \otimes U_p |\psi_{S\mathcal{E}}\rangle |e_0\rangle &= \frac{\sqrt{N-M}}{\sqrt{N}} |\sigma_l\rangle_S |\epsilon_l\rangle_E \sum_{k=1}^{N-M} \frac{1}{\sqrt{N-M}} |\eta_k\rangle_P \\ &\quad + \frac{\sqrt{M}}{\sqrt{N}} |\sigma_j\rangle_S |\epsilon_j\rangle_E \sum_{k=N-M+1}^N \frac{1}{\sqrt{M}} |\eta_k\rangle_P \\ &= \sum_{k=1}^{N-M} \frac{1}{\sqrt{N}} |\sigma_l\rangle_S |\epsilon_l\rangle_E |\eta_k\rangle_P \\ &\quad + \sum_{k=N-M+1}^N \frac{1}{\sqrt{N}} |\sigma_j\rangle_S |\epsilon_j\rangle_E |\eta_k\rangle_P \end{aligned} \quad (4.20)$$

Now we can use Theorem. 2, where the probability of measuring each  $|\eta_k\rangle_P$  should be the same. In other words,

$$P(|\eta_k\rangle_P | \mathbf{1}_S \otimes U_p |\psi_{S\mathcal{E}}\rangle |e_0\rangle) = \frac{1}{N}. \quad (4.21)$$

Thus, the probability of detect  $|\sigma_l\rangle_S$  in system and  $|\eta_k\rangle_P$  in the pointer where  $k \in [1, N-M]$  is  $\frac{N-M}{N}$ . The probability of detect  $|\sigma_j\rangle_S$  in system and  $|\eta_k\rangle_P$  in the pointer where  $k \in [N-M+1, N]$  is  $\frac{M}{N}$ .

The probability of measuring  $|\sigma_j\rangle_S$  in the system given state  $\mathbf{1}_S \otimes U_p |\psi_{S\mathcal{E}}\rangle |e_0\rangle$  should be  $\frac{M}{N}$ . Since the transformation  $U_p$  does not act on the system, the probability of measuring  $|\sigma_j\rangle_S$  in the system given state  $|\psi_{S\mathcal{E}}\rangle |e_0\rangle$  is  $\frac{M}{N}$ . This proof could be easily extended to any  $N > 2$ , which prove the Theorem 1. Therefore, we have shown that with a few assumptions, we could derive Born rule from envariance.

### 4.3 Experimental testing envariance

The derivation presented in Section. 4.2 could be divided into 2 parts. The first part is the core idea of the derivation, which relates the symmetry to probability of measurement outcomes. It also requires less resources, where only a two-qubit system is needed. Testing the second part is more difficult, and the proposal is listed in Appendix A, where a minimum of 4 qubits is needed. In this section, the first part of the derivation is tested.

Our test requires a source of high-quality two-photon polarization entanglement, an optical set-up to perform unitary operations on zero, one, or both of the photons, and polarization analyzers to characterize the final state of the light. Our experimental setup is shown in Fig. 4.1. We produce pairs of polarization-entangled photons using spontaneous parametric down-conversion (SPDC) in a Sagnac interferometer [29, 30, 31]. In the ideal case, this source produces pairs of photons in the singlet state,

$$|\psi_{SE}\rangle = \frac{1}{\sqrt{2}} (|H\rangle_S |V\rangle_E - |V\rangle_S |H\rangle_E), \quad (4.22)$$

where  $|H\rangle$  ( $|V\rangle$ ) represents horizontal (vertical) polarization, and **S** and **E** label the photons. This state is envariant under all unitary transformations and has the convenient symmetry that  $u_S = u_E$  for all  $u_S$ . This symmetry could also be understood by noticing that only one singlet state exist with 0 angular momentum. We pump a 10 mm periodically-poled Potassium titanyl phosphate crystal (PPKTP), phase-matched to produce photon pairs at 809.8 nm and 809.3 nm from type-II down-conversion using 6 mW from a CW diode

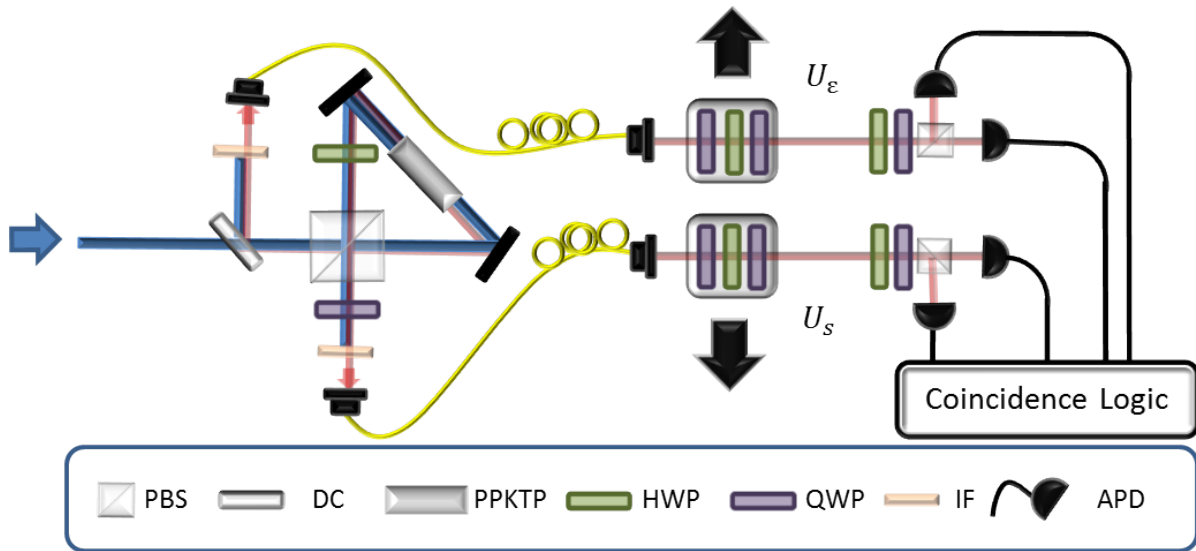


Figure 4.1: Experimental setup. The entangled photon pairs are created using type-II spontaneous parametric down-conversion. The pump laser is focused on a periodically-poled KTP crystal and pairs of entangled photons with anti-correlated polarizations are emitted. The pump is filtered using a band-pass filter, and polarization controls adjust for the alterations due to the coupling fibers. The entangled photon pairs are set so one photon is considered the system, and the other is considered the environment. After the source the unitary transformations are applied. A three wave plate combination is required to apply an arbitrary unitary transformation: quarter wave-plate (QWP), half wave-plate (HWP), QWP. A set of this combination of wave plates is mounted on each translation stage which can slide the wave plates in and out of the path of the incoming photons. The photons are then detected using polarizing beam splitters (PBS) and two wave plates to take projective measurements. The counts measured using avalanche photodiode (APD) are then analyzed using coincidence logic.

Rotation Axis	$\alpha(\theta)$	$\beta(\theta)$	$\gamma(\theta)$
$\hat{x}$	$\pi/2$	$-\theta/4$	$\pi/2$
$\hat{y}$	$\pi/2 + \theta/2$	$\theta/4$	$\pi/2$
$\hat{z}$	$\pi/4$	$-\pi/4 - \theta/4$	$\pi/4$

Table 4.1: Wave plate settings used to implement polarization rotations. The angles  $\alpha$ ,  $\beta$  and  $\gamma$  are the wave plate angles for the first QWP, the HWP and the second QWP respectively. The angle  $\theta$  is the rotation angle of the polarization about the specified axis on the Bloch sphere.

pump laser with center wavelength 404.8 nm. The output from the source is coupled into single-mode fibres, where polarization controllers correct unwanted polarization rotations in the fiber. The light is coupled out of the fibers and directed to two independent polarization analyzers. Each analyzer consists of a half-wave plate (HWP), quarter-wave plate (QWP), and a polarizing beam-splitter (PBS). Between the fiber and the analyzers are two sets of wave plates—a QWP, a HWP, then another QWP—which can be inserted as a group into the beam paths to implement controlled polarization transformations. Photons from both ports of each PBS are detected using single-photon counting modules (Perkin-Elmer SPCM-AQ4C) and analyzed using coincidence logic with a 1 ns coincidence window, counting for 5 s. We typically measured total coincidence rates of 5.4 kHz across the four detection possibilities for photons S and E.

For our experiment, we implemented rotations about the standard  $\hat{x}$ ,  $\hat{y}$ , and  $\hat{z}$  axes of the Bloch sphere; in addition we implemented rotations about an axis  $\hat{m} = (\hat{x} + \hat{y} + \hat{z})/\sqrt{3}$ . The wave plate angles used to implement rotations by an angle  $\theta$  about the  $\hat{x}$ ,  $\hat{y}$ , and  $\hat{z}$  axes are shown in Table 4.1; The angles to implement rotations about  $\hat{m}$  were determined numerically using MATHEMATICA.

Our experiment proceeds in three stages as depicted in Fig. 4.2: first characterizing the initial state (**I**), then characterizing the state after a transformation is applied to the system photon (**II**), and finally characterizing the state after that same transformation is applied to both system and environment (**III**). We record a tomographically-overcomplete set of measurements at each stage, performing the 36 combinations of the polarization measurements,  $|H\rangle$ ,  $|V\rangle$ ,  $|D\rangle = (|H\rangle + |V\rangle)/\sqrt{2}$ ,  $|A\rangle = (|H\rangle - |V\rangle)/\sqrt{2}$ ,  $|R\rangle = (|H\rangle + i|V\rangle)/\sqrt{2}$ , and  $|L\rangle = (|H\rangle - i|V\rangle)/\sqrt{2}$  on each photon and counting for 5 s for each setting. The 5 s time is chosen to give us enough photon counts to reduce short noise while minimize the changes in pump laser overtime. The states were then reconstructed using the maximum likelihood method from Ref. [32]. This procedure was repeated for a diverse range of

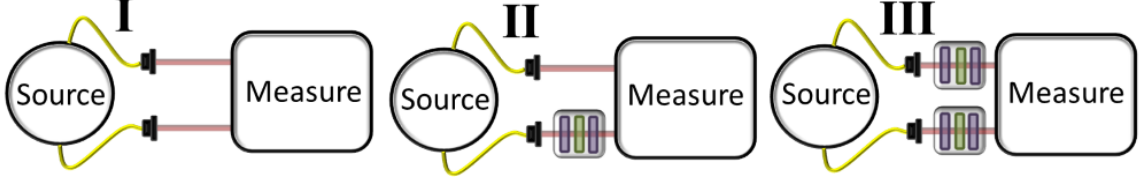


Figure 4.2: Experimental measurement procedure. We investigated the impact of each unitary transformation by performing quantum state tomography at three different stages: directly on the initial state with no unitary transformations (**I**), on the state with a transformation applied to the system photon (**II**), and on a state with the same transformation applied to both the system and environment photon (**III**).

transformations. We configured our setup to implement unitary rotations in multiples of  $30^\circ$  from  $0^\circ$  to  $360^\circ$  about each of the  $\hat{x}$ ,  $\hat{y}$ ,  $\hat{z}$ , and  $\hat{m}$  axes. The data acquisition time for this procedure over the set of 13 rotation angles about each axis was approximately six hours. The source was realigned before each set of rotations to achieve maximum fidelity with the singlet state from 0.985 to 0.990.

Figure 4.3a)–c) show the real and imaginary parts of the reconstructed density matrix of the quantum state at the three stages in the experiment, **I**, **II**, and **III** respectively. The fidelity [33] of the state with the ideal  $|\psi^-\rangle$  state during these samples of two of the stages are 0.987 for both **I**, and **III**, respectively, and is defined as [33]:

$$F(\rho, \sigma) = \{\text{Tr}[(\sqrt{\rho}\sigma\sqrt{\rho})^{1/2}]\}^2 \quad (4.23)$$

We can use this definition to calculate the fidelity between the state at stages **I** and **III**. Comparing between the states shown in Fig. 4.3 panels a) and c) the resulting fidelity is 0.995.

The summary of the results from our experiment is shown in Fig. 4.4. The coloured data points in Fig. 4.4a)–d) show the fidelity of the experimentally reconstructed state at stage **III** with the reconstructed state from the initial stage **I**, i.e.,  $F(\rho_{\text{expt}}^{\text{I}}, \rho_{\text{expt}}^{\text{III}})$ , as a function of the rotation angle for rotations about the  $\hat{x}$ ,  $\hat{y}$ ,  $\hat{z}$ , and  $\hat{m}$ , respectively. The open circles show the theoretical expectation for the fidelity between the measured state at stage **I** with the expected state in stage **III**, calculated by acting the unitaries on the measured state from stage **I**, i.e.,  $F(\rho_{\text{expt}}^{\text{I}}, \rho_{\text{th}}^{\text{III}})$ . The fidelities are very high, close to the limit of 1, in all cases and we see reasonable agreement with expectation.

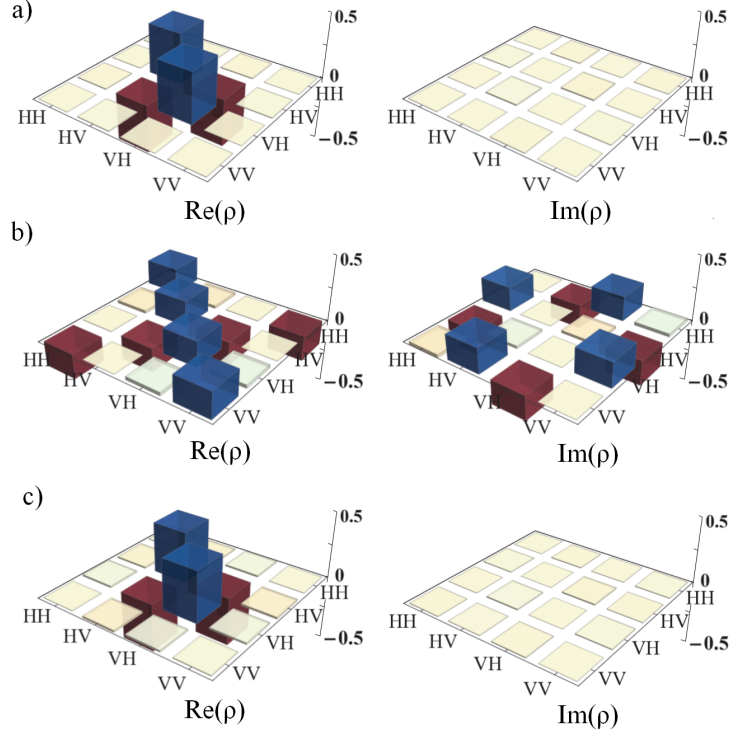


Figure 4.3: a) The real and imaginary parts of the reconstructed density matrix of the initial state from the source (stage **I** of the procedure). It has 0.987 fidelity [33] with the ideal. b) The system photon is transformed using wave plates set to implement the rotation of  $90^\circ$  about the  $\hat{x}$  axis, stage **II**. The resulting density matrix shown has 0.488 fidelity with the ideal initial state, 0.501 with the initial reconstructed state and 0.995 with the expected state, calculated by transforming the density matrix from a). c) The reconstructed density matrix after the same unitary from b) is applied to both photons, stage **III**. This state has a 0.987 fidelity with the ideal, 0.995 with the reconstructed state from a), and 0.997 with the expected state calculated by transforming the state from part a).

We considered the effects of Poissonian noise, which describes the fluctuations of the number of photons detected, and waveplate calibration on our results and found that these effects were too small to explain the deviation between  $F(\rho_{\text{expt}}^{\mathbf{I}}, \rho_{\text{expt}}^{\mathbf{III}})$  and  $F(\rho_{\text{expt}}^{\mathbf{I}}, \rho_{\text{th}}^{\mathbf{III}})$ . To account for this, we characterized the fluctuations in the state produced by the source itself by comparing the state produced in subsequent stage **I** states in the data collection; recall that stage **I** for each choice of unitary is always the same (no additional waveplates

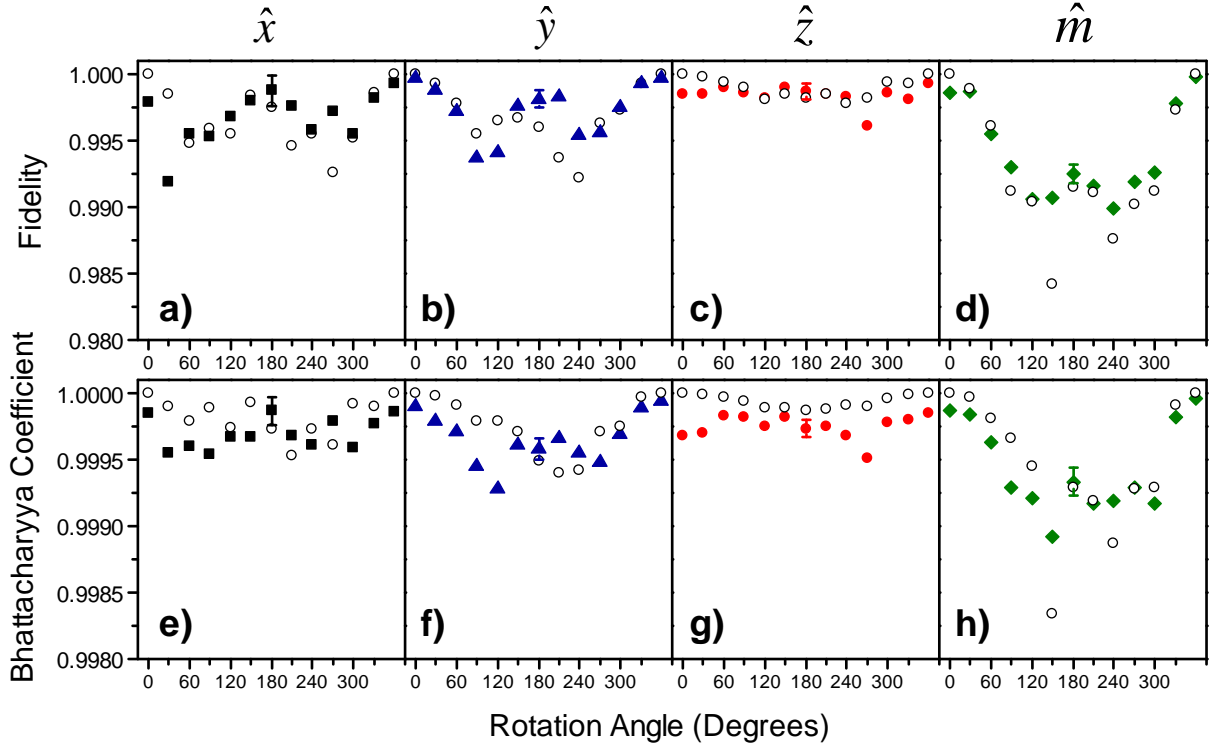


Figure 4.4: Analysis of the experimental results. Panels a)–d) show the fidelity analysis results for unitary rotations about  $\hat{x}$ ,  $\hat{y}$ ,  $\hat{z}$ , and  $\hat{m}$  axes as functions of rotation angle. The coloured data points are the comparison between stage **I** and stage **III** (comparing the source state and the state after the unitary has been applied to both qubits). The open circles show a theoretical comparison. Panels e)–h) show the quantum Bhattacharyya results comparing stage **I** and stage **III** in the coloured data points for each of the four axis, with the open circles being the theoretical comparison. For plots which include a comparison of stage **I** and **II** (applying the unitary to one qubit only) and theoretical comparisons, see the appendix. The error bar for each graph is the standard deviation of comparisons of source state measurements during the experiment.

Rotation Axis	Average Fidelity	Average $BC$
$\hat{x}$	$0.997 \pm 0.001$	$0.9997 \pm 0.0001$
$\hat{y}$	$0.9973 \pm 0.0007$	$0.99966 \pm 0.00008$
$\hat{z}$	$0.9984 \pm 0.0006$	$0.99975 \pm 0.00007$
$\hat{m}$	$0.9941 \pm 0.0007$	$0.9994 \pm 0.0001$
Overall average:	$0.9966 \pm 0.0004$	$0.99963 \pm 0.00005$

Table 4.2: Summary of the results for comparing stages **I** and **III** using fidelity and Bhattacharyya Coefficient ( $BC$ ) analysis and averaging over each unitary rotation. The overall average is representative of the overall envariance of our state.

inserted) and thus provides a good measure of the source stability. Specifically, we calculated the standard deviation in the fidelity of the state produced at a stage **I** in the  $i^{\text{th}}$  round of the experiment to that produced in the *next*,  $(i + 1)^{\text{th}}$ , stage **I**,  $F(\rho_{\text{expt}}^{\mathbf{I},i}, \rho_{\text{expt}}^{\mathbf{I},i+1})$ . The standard deviation in these fidelities calculated from the data taken within each set of rotation axes are shown as representative error bars on the plots in Figs. 4.4a)–d). The standard deviation of this quantity over all the experiments was 0.0008. We characterize the difference between the measured and expected fidelities by calculating the standard deviation in the quantity,  $F(\rho_{\text{expt}}^{\mathbf{I}}, \rho_{\text{expt}}^{\mathbf{III}}) - F(\rho_{\text{expt}}^{\mathbf{I}}, \rho_{\text{th}}^{\mathbf{III}})$ , for each experiment. (This is the difference between the coloured and open data points in Figs. 4.4a)–d).) over all experiments to be 0.002. This value is comparable to the error in the fidelity due to source fluctuations. Refer to the appendix to see the comparison between stage **I** and stage **II**, which would not fit on the scale of Fig. 4.4.

From our data, we extract the average fidelity  $F(\rho_{\text{expt}}^{\mathbf{I}}, \rho_{\text{expt}}^{\mathbf{III}})$  for the set of measurements made for each unitary axis and show the results in Table II. As measured by the average fidelity, our experiment benchmarks envariance to  $0.9966 \pm 0.0004$ ,  $((99.66 \pm 0.04)\%$  of the ideal) averaged over all rotations.

Fidelity has conceptual problems as a measure for testing quantum mechanics, since the density matrix we used to compute the fidelity is reconstructed using state tomography, which is under the assumption of Born rule. The Bhattacharyya Coefficient ( $BC$ ) is a measure of the overlap between two discrete distributions  $P$  and  $Q$ , where  $p_i$  and  $q_i$  are the probabilities of the  $i^{\text{th}}$  element for  $P$  and  $Q$  respectively. The  $BC$  is defined [34],

$$BC = \sum_i \sqrt{p_i q_i}. \quad (4.24)$$

If we normalize the measured tomographic data by dividing by the sum of the counts, we can treat this as a probability distribution. The  $BC$  then can be calculated using the

distribution of measurements at each stage in the experiment, directly analogous to the approach used with fidelity. It should be noted that the  $BC$  has some limitations when applied in this case. If two quantum states produce identical measurement outcomes, its value is 1. Unlike fidelity though, it is not the case that the  $BC$  goes to 0 for orthogonal quantum states. For example, the  $BC$  for two orthogonal Bell states measured with an overcomplete set of polarization measurements is  $7/9$ . Furthermore, the value of the  $BC$  is dependent on the particular choice of measurements taken. While we are employing a commonly-used measurement set for characterizing two qubits, other choices would produce different  $BC$ s. Nevertheless, this metric can be employed to quantify the envariance in our experiment without quantum assumptions, making it appropriate for testing quantum mechanics.

The Bhattacharyya Coefficients from our measured data are shown in Fig. 4.4e)–h). We normalize the measured counts from stages **I** and **III** to give us probability distributions  $p_{\text{expt}}^{\mathbf{I}}$  and  $p_{\text{expt}}^{\mathbf{III}}$ . The coloured data points in Figs. 4.4e)–h) show the  $BC$  between these distributions,  $BC(p_{\text{expt}}^{\mathbf{I}}, p_{\text{expt}}^{\mathbf{III}})$ . The open circles are a theoretical expectation of the  $BC$  given the tomographic measurements from stage **I**; for these theoretical values we used state tomography, and thus assumed quantum mechanics, to obtain the expected distribution  $p_{\text{th}}^{\mathbf{III}}$  and calculate the expected  $BC$ ,  $BC(p_{\text{expt}}^{\mathbf{I}}, p_{\text{th}}^{\mathbf{III}})$ .

Using an analogous procedure to that employed with the fidelity, we estimate the uncertainty in the  $BC$  by comparing subsequent measured distributions in stage **I** throughout the experiment, i.e.,  $BC(p_{\text{expt}}^{\mathbf{I},i}, p_{\text{expt}}^{\mathbf{I},i+1})$ . A representative error bar calculated from the data for a set of unitaries around the same axis are shown in Fig. 4.4e)–h). The standard deviation in this quantity over all the data is 0.00005. As before we characterize the difference between the measured and expected  $BC$ s as the standard deviation of the quantity  $BC(p_{\text{expt}}^{\mathbf{I}}, p_{\text{expt}}^{\mathbf{III}}) - BC(p_{\text{expt}}^{\mathbf{I}}, p_{\text{th}}^{\mathbf{III}})$  which is 0.00009 over all experiments. As before, this value is comparable to the error due to source fluctuations. Data showing the  $BC$  between stage **I** and **II** are shown in the appendix along with analogous theoretical comparison. A summary of the  $BC$  analysis results are in Table 4.2. The average measured  $BC$  is  $0.99963 \pm 0.00005$  ( $99.963 \pm 0.005\%$  of the ideal) across all tested unitaries.

## 4.4 Bounds to Born rule

In our experiment, we place a bound on the degree of envariance. It has been shown that envariance can be used to derive Born rule [23, 28]. However, the derivation does not relate bounds on Born rule to bound on envariance. In order to do so, we explore a recently proposed extension of quantum mechanics by Son [1]. Son’s theory generalizes Born rule,

replacing the familiar power of 2 which relates wavefunctions to probabilities with a power of  $n$ . In this section, we summarize Son's theory and use it to put a bound on  $n$  using our experimental data.

We first consider measurements on a pair of qubits in the maximally entangled singlet state using standard quantum mechanics. We define measurement observables  $\hat{a} = \vec{\alpha} \cdot \vec{\sigma}_1$  and  $\hat{b} = \vec{\beta} \cdot \vec{\sigma}_2$  where  $\vec{\alpha}, \vec{\beta}$  are unit vectors and  $\vec{\sigma}_1, \vec{\sigma}_2$  are the Pauli matrices for the two qubits. The result of measurements  $a$  and  $b$  for qubits 1 and 2 respectively can take on the values  $\pm 1$ . The correlation function is defined by

$$E = \langle ab \rangle = P_{a=b} - P_{a \neq b}, \quad (4.25)$$

where  $P_{a=b}$  and  $P_{a \neq b}$  are probabilities that  $a = b$  and  $a \neq b$  respectively. The correlation function only depends on the angle  $2\theta$  between  $\vec{\alpha}$  and  $\vec{\beta}$  for the singlet state. From Born rule, we have the probability amplitudes  $\psi_{a=b}$  and  $\psi_{a \neq b}$  satisfy  $P_{a=b} = |\psi_{a=b}|^2$  and  $P_{a \neq b} = |\psi_{a \neq b}|^2$ . Therefore, the correlation function in standard quantum mechanics is given by

$$E_{QM}(\theta) = |\psi_{a=b}|^2 - |\psi_{a \neq b}|^2 = -\cos 2\theta. \quad (4.26)$$

We now consider Son's theory, where Born rule is generalized to be  $P_{a=b} = |\psi_{a=b}|^n$  and  $P_{a \neq b} = |\psi_{a \neq b}|^n$ , and the correlation function is thus,

$$E(\theta, n) = |\psi_{a=b}|^n - |\psi_{a \neq b}|^n, \quad (4.27)$$

where standard quantum mechanics is the special case  $E(\theta, 2) = E_{QM}(\theta)$ . As in standard quantum mechanics, Son assumed that the correlation function depends only on the angle between measurement settings. Son showed that the constraints  $|\frac{\partial \psi_{a=b}}{\partial \theta}|^2 + |\frac{\partial \psi_{a \neq b}}{\partial \theta}|^2 \propto 1$  and  $|\psi_{a=b}|^n + |\psi_{a \neq b}|^n = 1$  and the boundary condition  $E(0, n) = -1$  and  $E(\frac{\pi}{2}, n) = 1$  are sufficient to solve for  $E(\theta, n)$ . See [1] for further details on the deviation. Figure 4.5 shows  $E(\theta, n)$  for different value  $n$ .

In the experiment, we rotated one qubit while leaving the other qubit unchanged during the stage **II** (See Figure 4.2). If we use the same measurement basis on both qubits for that rotated state, we are effectively measuring the singlet state input with two measurement basis with angle  $\theta$  apart. For example, we can choose the rotation axis and the measurement basis to be  $[Z, (D, A)]$ , where the first qubit is rotated around Z axis, while measurements on the qubits are done in (D, A) basis. Since the rotation axis Z is orthogonal to the measurement basis (D, A), we could view the rotation of qubit as a rotation of the measurement basis in the D-A plane. For a rotation angle  $\phi$ , the angle between two measurement basis is given by  $2\theta = \pi - |\pi - 2\phi|$ . We could derive prediction of  $E(\phi, n)$  from Son's theory, and test it with our data.

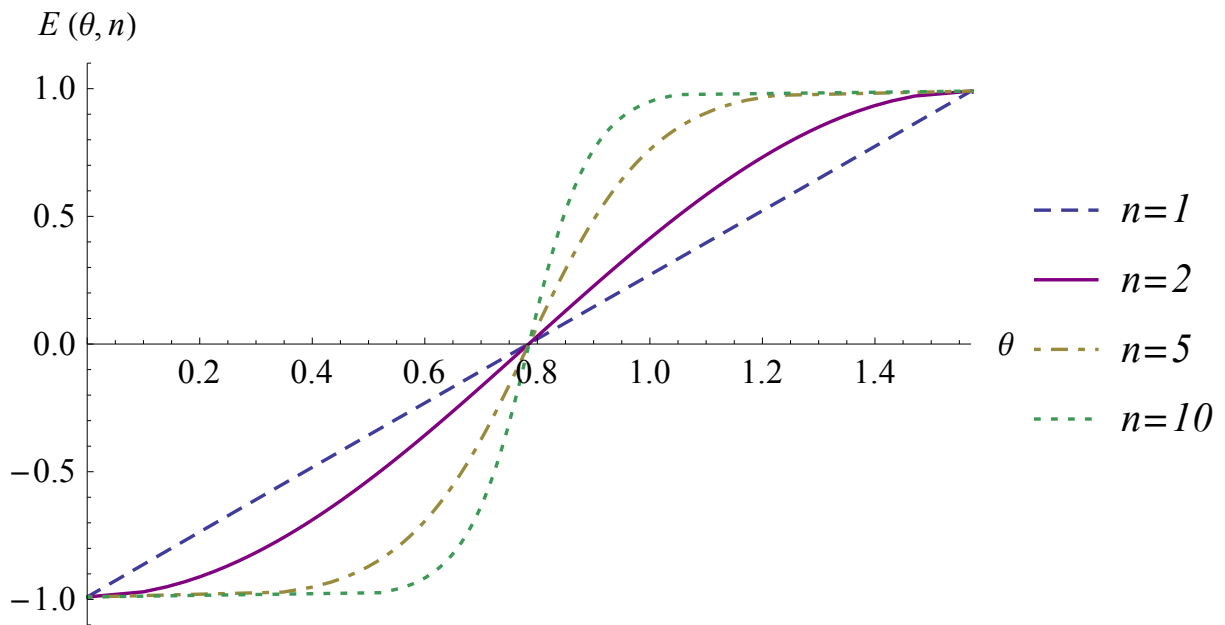


Figure 4.5: Generalized correlations for the singlet state as a function of  $n$  using Son's theory [1]. The correlation as a function of  $\theta$  is shown for  $n = 1$  (dashed blue line),  $n = 2$  (purple line),  $n = 5$  (dash-dotted brown line) and  $n = 10$  (dotted green line). The  $n = 2$  case corresponds to standard quantum mechanics.

Son's derivation assumes a perfect singlet state which must be relaxed to obtain a comparison with experiment. For a realistic state, the correlation function will not necessarily depend only on  $\theta$ . In his derivation, Son additionally assumed  $E(0, n) = -1$  and  $E(\pi/2, n) = 1$ , i.e., perfect correlations, which are not experimentally achievable. To relax these assumptions, we consider the difference between two correlation functions measured for a general state  $\rho$  and the ideal state  $|\psi^-\rangle$ ,  $E(\phi, n, \rho)$  and  $E(\phi, n, |\psi^-\rangle)$  where  $\phi$  is the rotation angle of one of the settings. For  $n \approx 2$ , we make the assumption that  $E(\phi, n, \rho) - E(\phi, n, |\psi^-\rangle) \approx E(\phi, 2, \rho) - E(\phi, 2, |\psi^-\rangle)$ . Thus for states close to the ideal singlet state and for  $n$  close to 2, we have the relation:

$$E(\phi, n, \rho) \approx E(\phi, n, |\psi^-\rangle) + E(\phi, 2, \rho) - E(\phi, 2, |\psi^-\rangle). \quad (4.28)$$

We calculated  $E(\phi, 2, \rho)$  and  $E(\phi, 2, |\psi^-\rangle)$  from standard quantum mechanics, and use Son's theory to calculate  $E(\phi, n, |\psi^-\rangle)$ . For a given set of data  $E_{exp}(\phi_i)$ , we find  $\rho$  and  $n$  to minimize the objective function  $L = \sum_i [E(\phi_i, n, \rho) - E_{exp}(\phi_i)]^2 / [\delta E_{exp}(\phi_i)]^2$ , where  $\delta E_{exp}(\phi_i)$  is the standard deviation of correlation function  $E_{exp}(\phi_i)$  predicted assuming Poissonian count statistics. Figure 4.6 shows the results of fitting the correlation functions for 6 sets of data. From this, we extracted  $n = 2.04, 2.01, 2.00, 2.01, 2.01, 2.00$ ; averaging these results and using their standard deviation to estimate the uncertainty yields  $n = 2.01 \pm 0.02$  in good agreement with Born rule where  $n = 2$ .

## 4.5 Conclusion

Our deviation from perfect envariance can be understood from our initial state fidelity. However, we also consider the magnitude of the violation of Born rule if one instead assumes all of the deviation stems from such a violation. One recently proposed extension of Born rule [1] determines probabilities by raising the wavefunction to the power of  $n$  rather than Born rule which raises the wavefunction to the power of 2. In this theory, the correlation between measurement outcomes as a function of measurement setting on a singlet state depends on the power of  $n$ , thus we can test this theory using our experimental data. Fitting our experimental data to this model, we find  $n = 2.01 \pm 0.02$  in good agreement with Born rule.

We have experimentally tested the property of envariance on an entangled two-qubit quantum state. Over a wide range of unitary transformations, we experimentally showed envariance at  $(99.66 \pm 0.04)\%$  when measured using the fidelity and  $(99.963 \pm 0.005)\%$  using the Bhattacharyya Coefficient. Deviations from perfect envariance are in good agreement

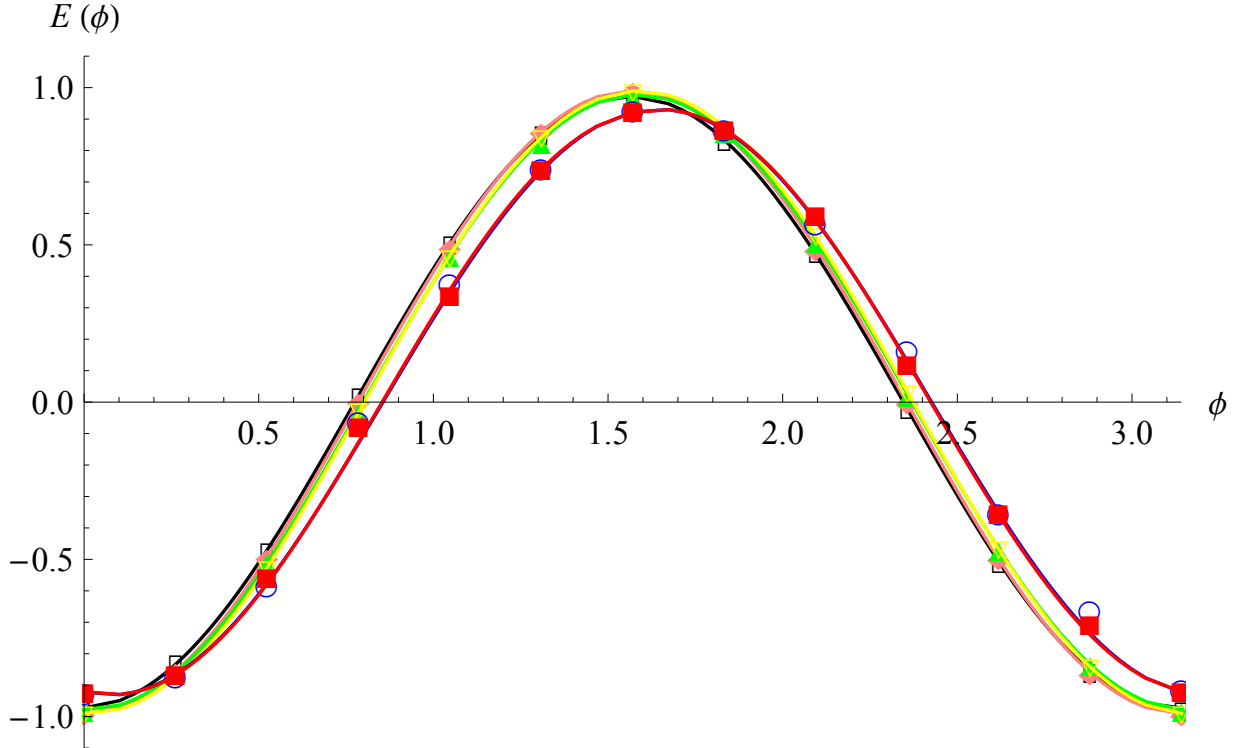


Figure 4.6: Correlation functions versus the rotation angle  $\phi$ . The experimental correlations are extracted from our data for the case where the rotation axis and the measurement basis are given by  $\{[Z,(D,A)], [Z,(R,L)], [Y,(D,A)], [Y,(H,V)], [X,(R,L)], [X,(H,V)]\}$  shown as  $\{\text{red squares, blue circles, green up triangles, yellow down triangles, black empty squares, pink diamonds}\}$  as a function of the rotation angle  $\phi$ . The best fit using Eq. 4.28 for each correlation is shown as a line whose colour matches the corresponding data points. These fits yield estimates for the value of  $n$  of  $\{2.04, 2.01, 2.00, 2.01, 2.01, 2.00\}$ , respectively.

with theory and can be explained by our initial state fidelity and fluctuations in the properties of our state. Fitting our results to a recently published model which does not explicitly assume Born rule yields nevertheless good agreement with it. Our results serve as a benchmark for the property of envariance, as improving the envariance of the state significantly would require substantive improvements in source fidelity and stability. It would be interesting to extend tests of envariance to higher dimensional quantum state and to other physical implementations.

# Chapter 5

## Pure State Tomography using Pauli Observables

### 5.1 Introduction

Quantum state tomography is one of the essential tasks in quantum information. It is very expensive since the required resources grow exponentially with the number of qubits.

What is the task of quantum state tomography? Mathematically, let us consider a  $d$ -dimensional Hilbert space  $\mathcal{H}_d$ , and denote  $D(\mathcal{H}_d)$  the set of density operators acting on  $\mathcal{H}_d$ . We then measure a set of  $m$  linearly independent observables

$$\mathbf{A} = (A_0, A_1, A_2, \dots, A_{m-1}), \quad (5.1)$$

where each  $A_i$  is Hermitian. Without loss of generality, we assume  $A_0 = I$  (i.e. the identity operator on  $\mathcal{H}_d$ ), and  $\text{tr} A_i = 0$  for  $i = 1, 2, \dots, m - 1$ .

For any  $\rho \in D(\mathcal{H}_d)$ , the Born rule tells us that the measurement returns a set of outcomes

$$\boldsymbol{\alpha} = (\text{tr} \rho, \text{tr}(\rho A_1), \text{tr}(\rho A_2), \dots, \text{tr}(\rho A_{m-1})). \quad (5.2)$$

Since  $\rho \in D(\mathcal{H}_d)$ , we should theoretically always have  $\text{tr} \rho = 1$ . However we keep this entry in  $\boldsymbol{\alpha}$  for the reason of experimental calibration [35, 36, 37, 38].

For an arbitrary  $\rho \in D(\mathcal{H}_d)$ , full quantum state tomography requires order  $d^2$  measurement outcomes to determine  $\rho$  [39]. However for a pure state  $|\psi\rangle \in \mathcal{H}_d$ , in general only order  $d$  measurements are needed to determine  $|\psi\rangle$ . It could be by chose any orthonormal

base to expand the pure state  $|\psi\rangle$ , where only  $d$  complex numbers are required to uniquely determine this expansion. By measuring the amplitude of  $|\psi\rangle$  projected onto each basis state and their relative phase, pure state  $|\psi\rangle$  can be determined with  $2(d-1)$  measurements. For a general mixed state, one would need to determine  $\frac{d(d-1)}{2}$  elements of the density matrix to uniquely determine the quantum state. For a pure state, one could use only order  $d$  parameters to describe the state. An ideal protocol should only require order  $d$  measurements.

In literature, people has come up with two slight different ways in interpreting the term ‘determine’, as clarified in a recently paper [40] and could be summarized in the following definition.

**Definition 1.** *A pure state  $|\psi\rangle$  is uniquely determined among pure states (UDP) by measuring  $\mathbf{A}$  if there does not exist any other pure state which has the same measurement results as those of  $|\psi\rangle$  when measuring  $\mathbf{A}$ . A pure state  $|\psi\rangle$  is uniquely determined among all states (UDA) by measuring  $\mathbf{A}$  if there does not exist any other state, pure or mixed, which has the same measurement results as those of  $|\psi\rangle$  when measuring  $\mathbf{A}$ .*

The physical interpretation in this case is clear: it is useful in quantum tomography to have some prior knowledge that the state to be reconstructed is pure or nearly pure. It is known that there exists a family of  $4d-5$  observables such that any  $d$ -dimensional pure state is UDP [41], and  $5d-6$  observables such that any  $d$ -dimensional pure state is UDA [40]. A few other methods for pure-state tomography have also been theorized, and experimentally tested to demonstrate the drop of the number of measurements needed [42, 43, 44, 45, 46, 47, 48, 49]. However, even if there are constructive protocols for the measurement set  $\mathbf{A}$ , in practice these sets may not be easy to measure in an experiment.

One idea of the compressed sensing protocols as discussed in [50, 51] considers measurements of Pauli operators for  $n$ -qubit systems, with Hilbert space dimension  $d = 2^n$ . Since no joint measurements on multiple qubits are needed for Pauli operators, these operators are relatively easy to measure in practice. It is shown that order  $d \log d$  random Pauli measurements are sufficient to UDA almost all pure states [52]. That is, all pure states can be determined, up to a set of states with measure zero (i.e. ‘almost all’ pure states are determined). Experiments also demonstrate the usefulness of this method in pure-state tomography in practice [53]. However, it remains open how many Pauli measurements are needed to determine all pure states (UDP or UDA) of an  $n$ -qubit system.

In this work, we examine the problem of the minimum number of Pauli operators needed to UDA all  $n$ -qubit pure states. For  $n = 1$  the number is known to be 3, i.e. all three Pauli operators  $X, Y, Z$  are needed. We solve the problem for  $n = 2$  and  $n = 3$ , where at least 11

Pauli operators are needed for  $n = 2$  and at least 31 Pauli operators are needed for  $n = 3$ . We then demonstrate that our protocol is robust under depolarizing error with simulated random pure states. We further implement our protocol in our nuclear magnetic resonance (NMR) system and compare our result with other methods. As a direct application of this result, we show that our scheme can also be used to reduce the number of settings needed for pure-state tomography in quantum optical system. My contribution in this work is finding the optimum Pauli set for 2 qubit pure state tomography in section 5.3, proposed test in NMR then process the experimental result and analysis the robustness in section 5.5, and at last generalize the result to optics in section 5.6.

## 5.2 Historical results on UDP and UDA

In this work we consider two different kinds of “unique determinedness” for  $|\psi\rangle$ :

1. We say  $|\psi\rangle$  is *uniquely determined among pure states (UDP) by measuring  $\mathbf{A}$*  if there does not exist any other pure state which has the same measurement results as those of  $|\psi\rangle$  when measuring  $\mathbf{A}$ .
2. We say  $|\psi\rangle$  is *uniquely determined among all states (UDA) by measuring  $\mathbf{A}$*  if there does not exist any other state, pure or mixed, which has the same measurement results as those of  $|\psi\rangle$  when measuring  $\mathbf{A}$ .

It is known that there exists a group of  $4d - 5$  observables, under which any pure state is UDP, in contrast to the  $d^2 - 1$  observables in the standard method of quantum tomography for arbitrary state [41]. Therefore, we can safely say that it is useful for the purpose of quantum state tomography to have the prior knowledge that the state to be reconstructed is pure or nearly pure.

When the state is UDP, to make the result useful, one needs to verify that the state is indeed pure. This is not in general practical. One solution to that would be readily generalize the above mentioned UDP results to low rank states, where the physical constraints (e.g., low temperature, locality of interaction etc.) may ensure that the actual physical state (which ideally supposed to be pure) is indeed low rank. Alternatively, if the state is UDA, however, in terms of tomography one does not need to bother with these physical assumptions, because in the event there is only a unique state compatible with the measurement results, which turns out to be pure (or low rank).

There is also another clear physical intuition for the states that are UDA by measuring observables from  $\mathbf{A}$ . Let us consider a Hamiltonian of the form

$$H_{\mathbf{A}} = \sum_{i=1}^m \alpha_i A_i. \quad (5.3)$$

We observe that any unique ground state  $|\psi\rangle$  of  $H_{\mathbf{A}}$  is UDA by measuring  $\mathbf{A}$ . It is easy to verify: if there is any other state  $\rho$  that gives the same measurement results, then  $\rho$  has the same energy as that of  $|\psi\rangle$ , which is the ground state energy. Therefore, any pure state in the range of  $\rho$  must also be a ground state, which contradicts the fact that  $|\psi\rangle$  is the unique ground state. In other words, UDA is a necessary condition for  $|\psi\rangle$  to be a unique ground state of  $H_{\mathbf{A}}$ . It is in general not sufficient, but the exceptions are likely rare [54, 55].

### 5.3 2 qubit pure state tomography using Paulis measurements

We define the single-qubit Pauli operators by  $\sigma_1 = X, \sigma_2 = Y, \sigma_3 = Z$ , and the identity operator  $\sigma_0 = I$ . For a single qubit, it is straightforward to check that measuring only two of the three operators cannot determine an arbitrary pure state.<sup>1</sup> Therefore all three Pauli operators are needed in the single-qubit case.

For the two-qubit system, there are a total of 16 Pauli operators, including the identity. These are given by the set  $\{\sigma_i \otimes \sigma_j\}$  with  $i, j = 0, 1, 2, 3$ . For simplicity we omit the tensor product symbol by writing, e.g.  $XY$  instead of  $X \otimes Y$ . Of these 16 Pauli operators, there exists a set of 11 Pauli operators  $\mathbf{A}$  such that  $\mathbf{A}$  is UDA for any pure state, as given by the following theorem [56].

**Theorem 3.** *Any two-qubit pure state  $|\phi\rangle$  is UDA by measuring the following set of Pauli operators.*

$$\mathbf{A} = \{II, IX, IY, IZ, XI, YX, YY, YZ, ZX, ZY, ZZ\}, \quad (5.4)$$

---

<sup>1</sup>Some state can still be determined using only two of the three operators. For example, any state  $\frac{1}{2}(I + \alpha X + \beta Y)$ , where  $\alpha^2 + \beta^2 = 1$  could be determined without measuring observable  $Z$

and no set with fewer than 11 Pauli operators can be UDA for all two-qubit pure states. Moreover, any set of Pauli operators which is Clifford equivalent to  $\mathbf{A}$  is UDA for any two-qubit pure states.

This is to say, 11 is the minimum number of Pauli operators needed to UDA any two-qubit pure state, and an example of such a set with 11 Pauli operators is given in Eq. (5.4).

*Proof.* In order for  $\mathbf{A}$  to UDA all two-qubit pure states it is known [40] that any Hermitian operator  $H \in (\mathcal{S}(\mathbf{A}))^\perp$  must have at least two positive and two negative eigenvalues, where  $\mathcal{S}(\mathbf{A})$  means the linear span of  $\mathbf{A}$ .

In this case  $(\mathcal{S}(\mathbf{A}))^\perp = \mathcal{S}(\{XX, XY, XZ, YI, ZI\})$ . Note that the 5 operators which are not measured all mutually anti-commute with each other. It is easy to see that this property is required for if two operators in  $(\mathcal{S}(\mathbf{A}))^\perp$  commuted, then they would be simultaneously diagonalizable and a linear combination would exist which would have at least one 0-eigenvalue. Since two-qubit Pauli operators only have four eigenvalues total, having a single 0 eigenvalue fails the UDA condition.

Furthermore it is easy to show by exhaustive search that there exists no set of more than 5 mutually anti-commuting Pauli operators. So no fewer than 11 Paulis could be measured.

To show that this set of 11 Pauli operators is sufficient to be UDA, we construct a parametrization of all  $H \in (\mathcal{S}(\mathbf{A}))^\perp$ ;

$$H = \alpha_1 XX + \alpha_2 XY + \alpha_3 XZ + \alpha_4 YI + \alpha_5 ZI \quad (5.5)$$

and show that either  $H$  has two positive and two negative eigenvalues or  $H = 0$ . Note that  $H$  then has the following form:

$$\begin{bmatrix} \alpha_5 & 0 & \alpha_3 + \alpha_4 i & \alpha_1 + \alpha_2 i \\ 0 & \alpha_5 & \alpha_1 - \alpha_2 i & -\alpha_3 + \alpha_4 i \\ \alpha_3 - \alpha_4 i & \alpha_1 + \alpha_2 i & -\alpha_5 & 0 \\ \alpha_1 - \alpha_2 i & -\alpha_3 - \alpha_4 i & 0 & -\alpha_5 \end{bmatrix}.$$

The determinant of  $H$  can be calculated and the result is:

$$\begin{aligned} & \alpha_5^4 + \alpha_5^2 |\alpha_3 + \alpha_2 i|^2 + \alpha_5^2 |\alpha_1 + \alpha_2 i|^2 \\ + & |\alpha_3 - \alpha_4 i|^4 + |\alpha_3 - \alpha_4 i|^2 |\alpha_1 + \alpha_2 i|^2 + |\alpha_3 - \alpha_2 i|^2 \alpha_5^2 \\ + & |\alpha_1 - \alpha_2 i|^4 + |\alpha_1 - \alpha_2 i|^2 |\alpha_3 - \alpha_4 i|^2 + |\alpha_1 - \alpha_2 i|^2 \alpha_5^2. \end{aligned}$$

This quantity, being the sum of non-negative terms, is greater than or equal to 0. Equality is reached if and only if all terms in the sum are 0, which only occurs when  $\alpha_1 = \alpha_2 = \alpha_3 = \alpha_4 = \alpha_5 = 0$ . Since  $H$  is a 4-by-4 traceless Hermitian matrix, it can only have positive determinant if and only if it has exactly two positive and two negative eigenvalues.

The same logic follows for any set that is unitarily equivalent to this set. A particular class of unitary operators which maps the set of Pauli operators to itself is called the Clifford group. Thus, the set  $\mathbf{A}$  in Eq. 5.4 and any set which is Clifford equivalent [57] to it are our optimum sets of Pauli measurement operators for two-qubit pure-state tomography.  $\square$

## 5.4 3 qubit pure state tomography using Paulis measurements

The situation for the 3-qubit case is much more complicated [56]. We start by noticing that

$$\begin{aligned} V &= IIZ + IZI + ZII + ZZZ \\ &= 4(|000\rangle\langle 000| - |111\rangle\langle 111|) \end{aligned} \tag{5.6}$$

has one positive and one negative eigenvalue. Therefore, if the set  $\mathbf{F}_1 = \{IIZ, IZI, ZII, ZZZ\}$  is a subset of  $\mathcal{S}(\mathbf{A})^\perp$ , the set  $\mathbf{A}$  cannot UDA all pure states. Similarly any set  $\mathbf{F}_i$  which is Clifford equivalent to  $\mathbf{F}_1$  cannot be a subset of  $\mathcal{S}(\mathbf{A})^\perp$ . Sets such as these we call failing sets.

**Definition 2.** *A failing set  $\mathbf{F}$  is a set of Pauli operators such that there exists a nonzero real combination of elements chosen from  $\mathbf{F}$  such that it has only 1 positive eigenvalue or 1 negative eigenvalue.*

Namely, for an arbitrary pure state  $|\phi\rangle$  to be UDA by measuring operators in a set  $\mathbf{A}$ ,  $\text{span}(\mathbf{F}_i) \not\subset (\text{span}(\mathbf{A}))^\perp$  holds for every set  $\mathbf{F}_i$  that is Clifford equivalent to  $\mathbf{F}_1$ . Thus, for all 945 sets of  $\mathbf{F}_i$ , at least one element in each  $\mathbf{F}_i$  should be included in  $\text{span}(\mathbf{A})$ .

**Theorem 4.** *The following set of 31 Pauli operators are sufficient to UDA any given*

three-qubit pure state  $|\phi\rangle$

$$\begin{aligned} \mathbf{A} = \{ & IIX, I IY, I IZ, I XI, I XX, I XY, I YI, I YX, \\ & I YY, I ZI, X IZ, X XX, X XY, X YX, X YY, \\ & X ZX, X ZY, Y XX, Y XY, Y XZ, Y YX, Y YY, \\ & Y YZ, Y ZI, Z II, Z XZ, Z YZ, Z ZX, Z ZY, \\ & Z ZZ, III\}, \end{aligned} \tag{5.7}$$

and no set with less than 31 Pauli operators can be UDA for all three-qubit pure states. Moreover, any set of Pauli operators which is Clifford equivalent to  $\mathbf{A}$  can be used to UDA for any three-qubit pure states.

Similarly to the two-qubit case this set is obtained by finding the largest set of Pauli operators which do not contain any of the identified failing sets and taking the complement producing the smallest set of measurement operators which could UDA all pure states.

To show that this set  $\mathbf{A}$  will be UDA for any pure state, we look at the traceless Hermitian operator  $H \in (\text{span}(\mathbf{A}))^\perp$ , where

$$\begin{aligned} H = & \alpha_1 I X Z + \alpha_2 I Y Z + \alpha_3 I Z X + \alpha_4 I Z Y + \alpha_5 I Z Z \\ & + \alpha_6 X I I + \alpha_7 X I X + \alpha_8 X I Y + \alpha_9 X X I \\ & + \alpha_{10} X X Z + \alpha_{11} X Y I + \alpha_{12} X Y Z + \alpha_{13} X Z I \\ & + \alpha_{14} X Z Z + \alpha_{15} Y I I + \alpha_{16} Y I X + \alpha_{17} Y I Y \\ & + \alpha_{18} Y I Z + \alpha_{19} Y X I + \alpha_{20} Y Y I + \alpha_{21} Y Z X \\ & + \alpha_{22} Y Z Y + \alpha_{23} Y Z Z + \alpha_{24} Z I X + \alpha_{25} Z I Y \\ & + \alpha_{26} Z I Z + \alpha_{27} Z X I + \alpha_{28} Z X X + \alpha_{29} Z X Y \\ & + \alpha_{30} Z Y I + \alpha_{31} Z Y X + \alpha_{32} Z Y Y + \alpha_{33} Z Z I. \end{aligned}$$

It can be shown that  $H$  either has at least two positive and two negative eigenvalues or  $H = 0$  (see Appendix B for details). Therefore, set  $\mathbf{A}$  in Eq. 5.7 and any set which is Clifford equivalent to it are our optimum Pauli measurement sets for 3-qubit pure-state tomography.

## 5.5 Pure state tomography in NMR system

A nuclear magnetic resonance (NMR) system is an ideal testbed for our protocol. However, the creation of a pure state in NMR requires unrealistic experimental conditions such as extremely low temperatures or high magnetic fields, which makes it impractical for a liquid sample. To overcome this problem, one can prepare a pseudo-pure state (PPS) alternatively

$$\rho_{\text{PPS}} = \frac{1 - \epsilon}{2^N} \mathbb{I} + \epsilon |\phi\rangle\langle\phi|, \quad (5.8)$$

where  $\mathbb{I}$  is the identity matrix,  $N$  is the number of qubits and  $\epsilon \sim 10^{-5}$  represents the polarization. For a traceless Pauli observable  $\sigma$ , only the pure state portion  $\epsilon |\phi\rangle\langle\phi|$  contributes to the measurement result. Therefore, the behavior of a system in the PPS is exactly the same as it would be in the pure state.

To test our protocol, we carried out the experiments in 2- and 3-qubit NMR quantum systems, respectively. The qubits in the 2-qubit system are denoted by the  $^{13}\text{C}$  and  $^1\text{H}$  spins of  $^{13}\text{C}$ -labeled Chloroform diluted in acetone- $d_6$  on a Bruker DRX-500 MHz spectrometer, and in the 3-qubit system by the  $^{13}\text{C}$ ,  $^1\text{H}$  and  $^{19}\text{F}$  spins in Diethyl-fluoromalonate dissolved in  $d$ -chloroform on a Bruker DRX-400 MHz spectrometer. The molecular structures and relevant parameters are shown in Fig. 5.1, and the corresponding natural Hamiltonian for each system can be described as

$$\mathcal{H}_{\text{internal}} = \sum_{i=1} \pi \nu_i \sigma_z^i + \sum_{i < j, =1} \frac{\pi J_{ij}}{2} \sigma_z^i \sigma_z^j, \quad (5.9)$$

where  $\nu_i$  is the resonance frequency of spin  $i$  and  $J_{ij}$  are the scalar coupling constants between spins  $i$  and  $j$ . All parameters are listed in the right table of Fig. 5.1. Note that in experiment we set  $\nu_i = 0$  in the multi-rotating frame for simplicity.

In experiment, the entire tomography process for a PPS becomes: given measurements  $\text{Tr}(\rho \sigma_k) = \epsilon \text{Tr}(\rho_t \sigma_k) = M_k$ , find a density matrix  $\rho_{\text{rec}}$  to best fit the data  $M_k$ . In order to evaluate the performance of our protocol, two comparisons will be made. First, we compare the reconstructed state using the optimum number of Pauli measurements with the one obtained with full tomography. It gives us an idea how good the reconstruction is, and whether the protocol works. Second, we compare our result with the state reconstructed by randomly choosing Pauli measurements. This tells us how different the performance is between selecting the optimum set and a random set of Pauli measurements.

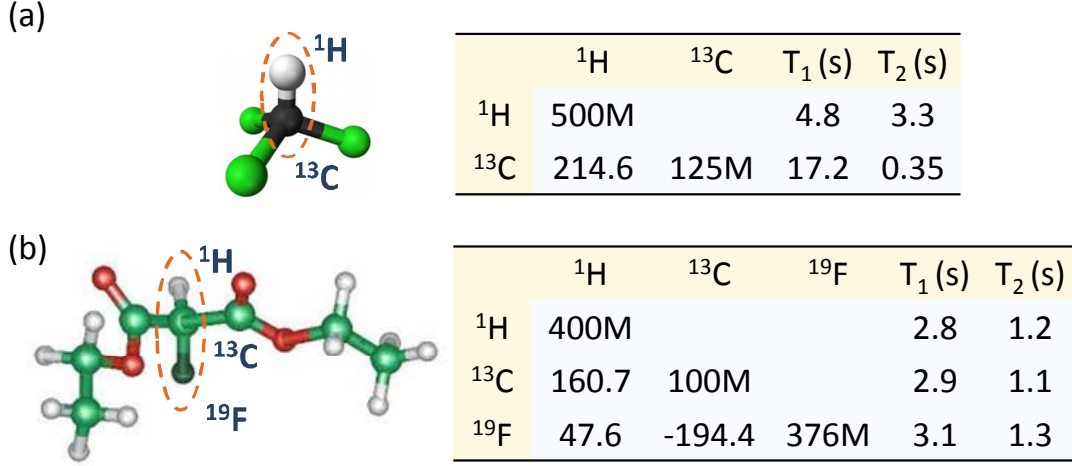


Figure 5.1: Molecular structure of (a) 2-qubit sample <sup>13</sup> C-labeled Chloroform and (b) 3-qubit sample Diethyl-fluoromalonate. The corresponding tables on the right side summarize the relevant NMR parameters at room temperature, including the Larmor frequencies (diagonal, in Hertz, M = 10<sup>6</sup>), the J-coupling constant (off-diagonal, in Hertz) and the relaxation time scales  $T_1$  and  $T_2$ .

### 5.5.1 Pure state tomography for a 2-qubit state

For the 2-qubit protocol, the system is firstly initialized to the PPS

$$\rho_{00} = \frac{1 - \epsilon}{4} \mathbb{I} + \epsilon |00\rangle\langle 00| \quad (5.10)$$

via spatial average technique [58, 59], where  $\mathbb{I}$  is the  $4 \times 4$  identity and  $\epsilon \sim 10^{-5}$  the polarization. The NMR signal of this PPS is used as references for further comparisons with the tomographic results. We then turn on the transversal field with the strength  $\omega_x$  (in terms of radius), so the Hamiltonian includes both internal and external Hamiltonian becomes

$$\mathcal{H} = \frac{\omega_x}{2} (\sigma_x^1 + \sigma_x^2) + \frac{\omega_z}{2} (\sigma_z^1 + \sigma_z^2) + \pi \frac{J_{12}}{2} \sigma_z^1 \sigma_z^2 \quad (5.11)$$

By ignoring the identity in  $\rho_{00}$ , the system should evolve to a time-dependent pure state

$$|\phi\rangle = \alpha(t)|00\rangle + \beta(t)(|01\rangle + |10\rangle)/\sqrt{2} + \gamma(t)|11\rangle, \quad (5.12)$$

where  $t$  is the evolution time and  $\alpha(t), \beta(t), \gamma(t)$  could be calculated using the Hamiltonian in Eq. 5.11. We measured in total 16 different states at a few different time steps using Pauli observables. The measurement result at each time step is used as one instance of the input to our tomography algorithm. We then adopted the maximum likelihood method to reconstruct the states. The reconstructed density matrices for the first and sixteenth experiments are shown in Figs. 5.2. Note that as the time progresses, the relaxation becomes more prominent, where the purity of state  $\text{Tr}(\rho^2)$  drops. Since our protocol is designed for pure-state tomography, the performance of our protocol is expected to drop along with the decrease of purity in a quantum state. The fidelity of different reconstructions compare to the state intended to prepare also drops (See Appendix B for detail), but it is irrelevant for the propose of comparing two tomography methods. In order to further demonstrate the advantages of our protocol, we compare it to a quantum state tomography with Pauli measurements. Using the same number of random Pauli measurements, one could also perform the maximum likelihood method to get a reconstruction of the density matrix. Note that the optimum set of 11 Pauli measurements may be randomly hit in this case, which means the best performance of random Pauli measurement algorithm is the same compared with our protocol. However, in a realistic setting, only one set of random Pauli measurements will be chosen. To show the advantage of our protocol, we only have to outperform the average case of this random algorithm.

We randomly generated 11 distinct 2-qubit Pauli measurements (including identity), and used the maximum likelihood method to get an estimate of our density matrix. If the density matrix given by this set of measurements is not unique, the maximum likelihood method runs multiple times to get an average estimation. For each experiment, 100 sets of random Pauli measurements were chosen. The result is shown in Fig. 5.3. We can see that for high purity, our method significantly outperforms the random Pauli algorithm. The advantage decreases as purity decreases, which indicates our method is more efficient for a state that is close to pure.

### 5.5.2 Pure state tomography for 3-qubit state

For 3-qubit system, we are interested in the GHZ state  $|\text{GHZ}\rangle = (|000\rangle + |111\rangle)/\sqrt{2}$ . The experimental data is from [60], and the GHZ state is prepared via global controls in closed linear Ising spin chains with nearest-neighbor couplings as shown in Fig. 5.4. We measured all 64 Pauli measurements (the measured purity of the prepared state is about 0.89), and only use 31 of them described in Eq. (5.7) for our protocol. As shown in Fig. 5.5, only using less than half of the desired measurements, we reconstructed density matrices for the GHZ state via the maximum likelihood method with 0.96 fidelity. We then compare it

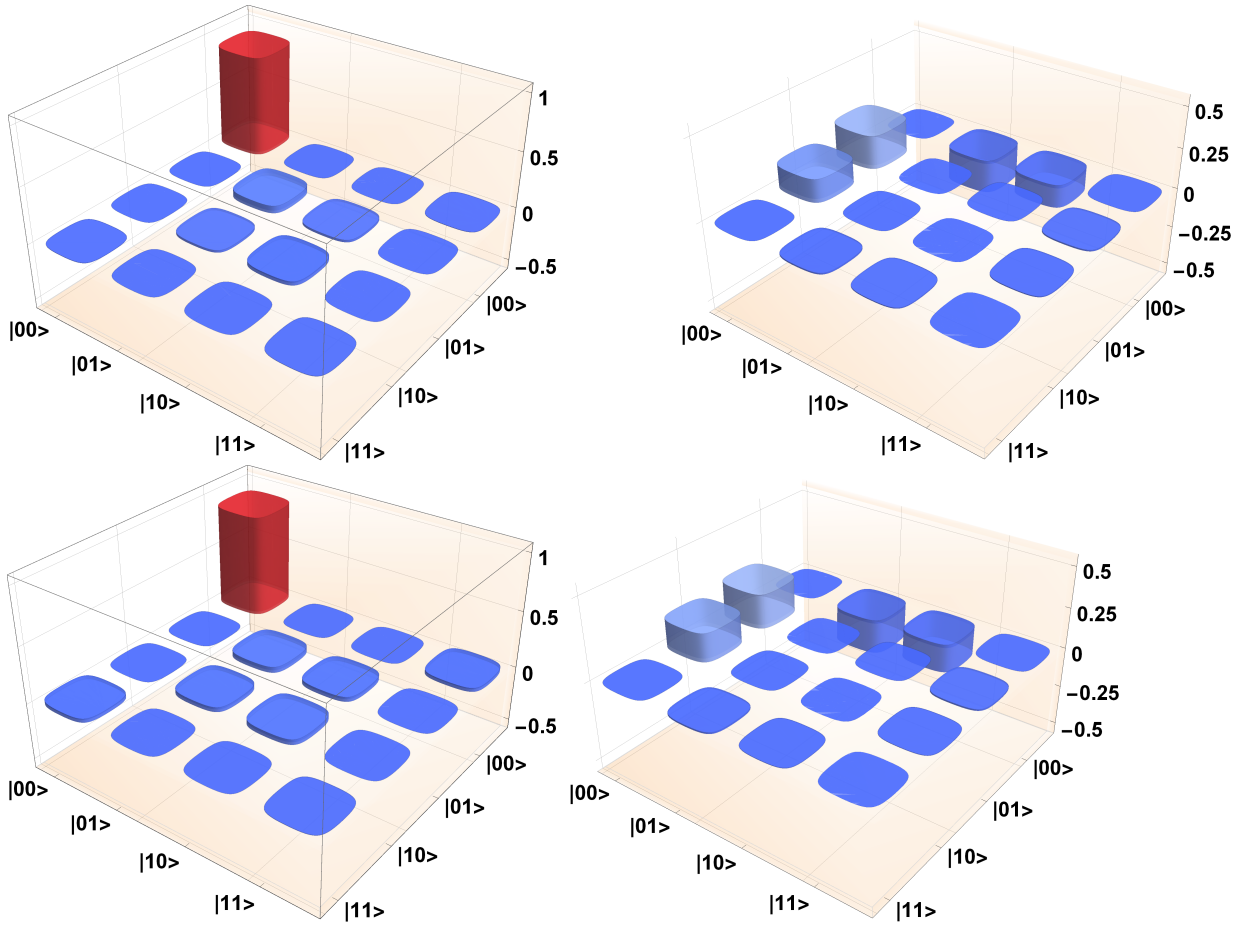


Figure 5.2: The reconstruction of density matrix for state number one. The upper two figures are real and imaginary part of density matrix of state reconstruction using all 16 Pauli measurements. The bottom two figures are real and imaginary part of density matrix of state reconstruction using 11 optimum Pauli measurements described earlier. The fidelity between the two density matrices is 0.992.

to a quantum state tomography algorithm implementing 31 random Pauli measurements (including identity). Since the number of unused Pauli measurements are much more compared to the 2-qubit case, we are less likely to hit the optimum set in this random algorithm. By implementing a similar maximum likelihood reconstruction, we found the average fidelity of this random algorithm to be 0.87 with standard deviation of 0.16. The detailed result is shown in Fig. 5.6, which shows clearly that our protocol has a decent

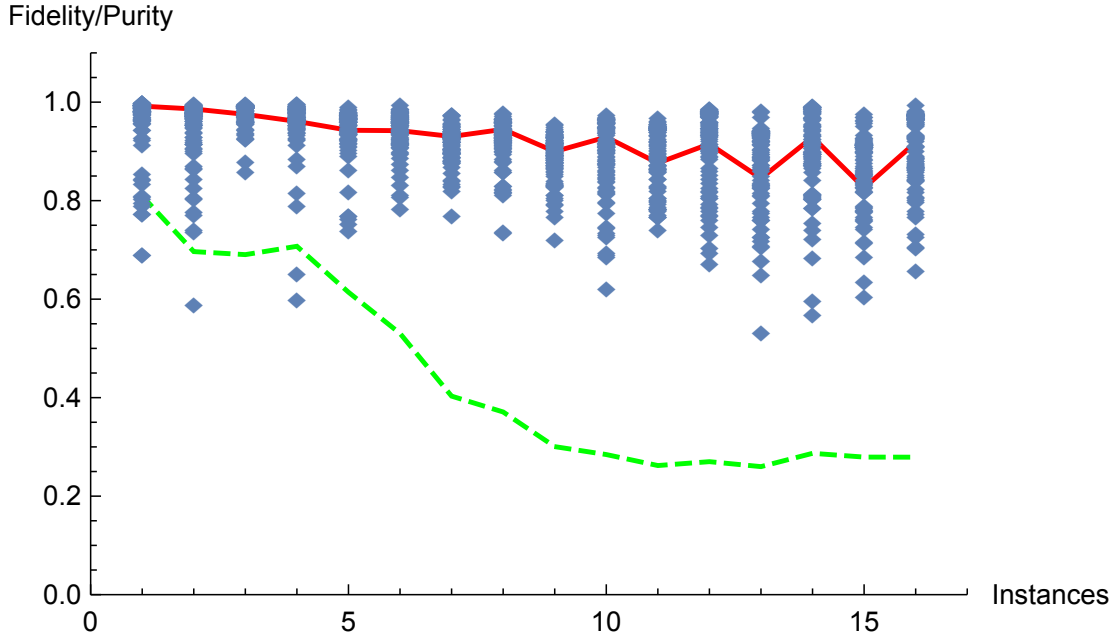


Figure 5.3: Performance of 2-qubit protocol using selected Pauli measurements against randomly Pauli measurements. The blue diamond dots are the fidelity between density matrix reconstructed from all 16 Pauli measurements with density matrix reconstructed from random 11 Pauli measurements. The red line represents fidelity of reconstruction using our protocol, and the green dashed line shows the purity of density matrix reconstructed from all Pauli measurements.

advantage over the average case in the randomized algorithm.

## 5.6 Pure state tomography for polarized photon qubits

Figure 5.7 depicts a typical scheme for measuring a polarization-encoded  $n$ -photon state [61, 62, 63, 64, 65, 66]. Quarter- and half-waveplates in each photon's path are rotated to choose a separable polarization basis. We call the set of angles specifying each waveplate's position the *setting* of the measurement. The  $n$ -photon state is projected onto the basis set by the waveplate angles with  $n$  polarizing beamsplitters. A single-photon detector is present in each of the  $2n$  output ports of the beamsplitters, and  $n$ -fold coincident detections among the  $n$  paths are counted. There are  $2^n$  combinations of  $n$ -fold coincident detection events that correspond to a state with one photon entering each of the  $n$  beamsplitters before

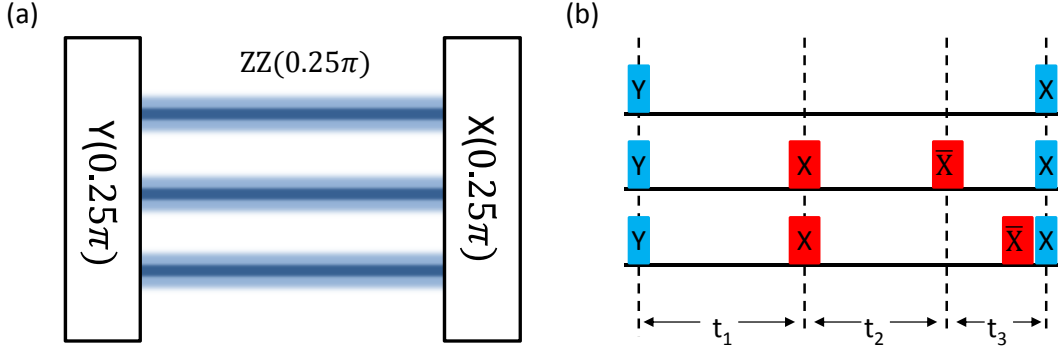


Figure 5.4: (a) General scheme to create the GHZ state via global controls.  $X(\theta)$  and  $Y(\theta)$  are, respectively, the global rotations with  $\theta$  angle along  $x$  and  $y$  directions, and  $ZZ(\tau)$  denotes a free evolution with the  $\tau$  time under the model Ising Hamiltonian. (b) NMR sequence to realize the GHZ state creation from the PPS. Blue and red rectangles represent  $\pi/2$  and  $\pi$  rotations, respectively. The evolution times are  $t_1 = 6.76$  ms,  $t_2 = 6.49$  ms,  $t_3 = 2.84$  ms with our sample.

being detected in one of the two output ports. Summing the total number of  $n$ -fold coincidences over these  $2^n$  combinations gives the total number of copies of the state detected by the measurement.

A minimum of  $3^n$  measurement settings are required for general state tomography using separable projective measurements [36]. We note that, if one performs nonseparable measurements, then general state tomography can be performed with  $2^n + 1$  measurement settings [67]. However, these types of measurements are difficult to perform in practice, so we restrict the discussion here to separable ones.

One can think of each setting as a projective measurement that produces results for multiple Pauli operators simultaneously. For example, consider measuring a 2-photon state with the waveplates set such that a photon in the positive eigenstate of the Pauli  $X$  or  $Y$  operator will be deterministically transmitted at the first or second beamsplitter, respectively. For simplicity we will call this the  $XY$  setting. There are four relevant two-fold coincident detection events, which we denote  $N_{tt}$ ,  $N_{tr}$ ,  $N_{rt}$ , and  $N_{rr}$ , and where the first and second subscripts represent which output port (i.e. transmitted or reflected) the first or second photon was detected, respectively. These counts can be summed in specific ways to find expectation values of different Pauli operators. For example the expectation value of  $\langle XY \rangle$  is given by  $\langle XY \rangle = (N_{tt} - N_{tr} - N_{rt} + N_{rr})/N$ , where the total number of copies  $N$  is given by  $N = N_{tt} + N_{tr} + N_{rt} + N_{rr}$ . Similarly,  $\langle XI \rangle$  can be found with

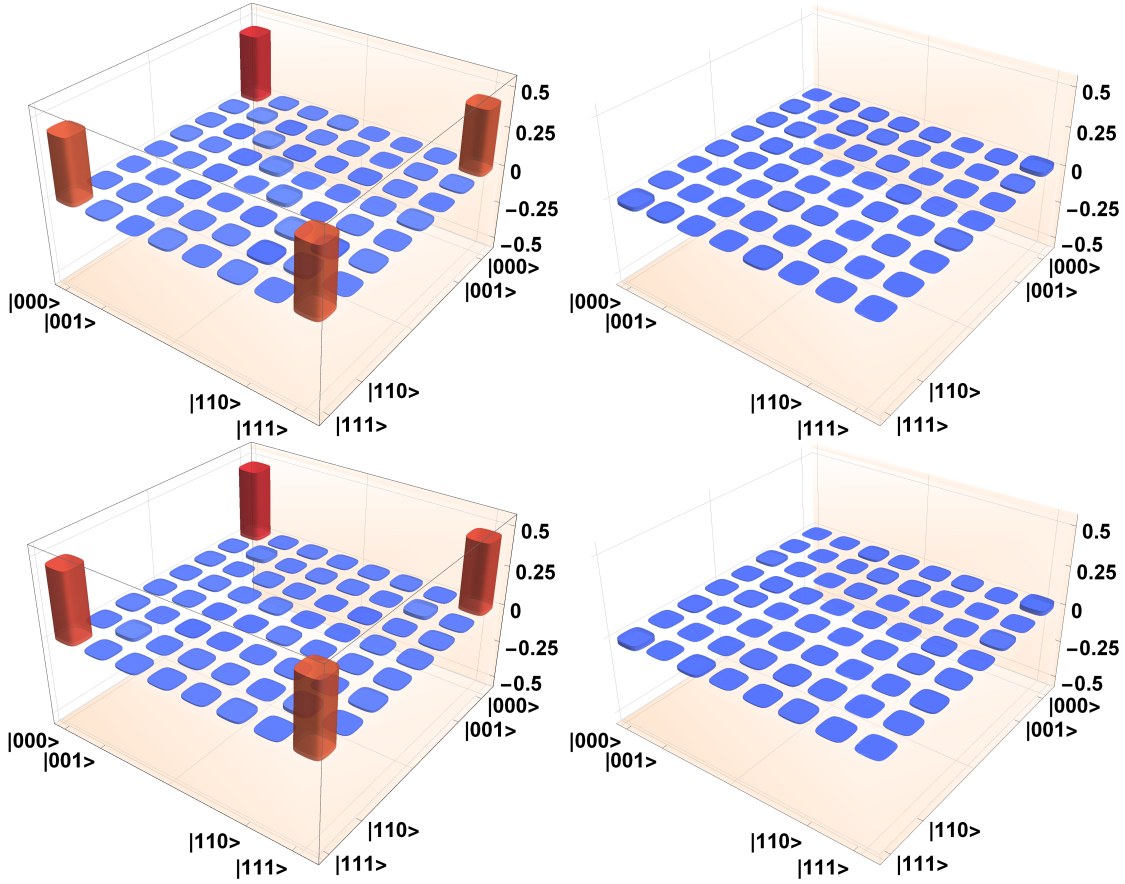


Figure 5.5: The reconstruction of density matrix for GHZ state. The upper two figures are real and imaginary part of density matrix of state reconstruction using all 64 Pauli measurements. The bottom two figures are real and imaginary part of density matrix of state reconstruction using 31 optimum Pauli measurements described in Eq. (5.7). The fidelity between the two density matrices is 0.960.

$\langle XI \rangle = (N_{tt} + N_{tr} - N_{rt} - N_{rr})/N$ . In total, the  $XY$  setting measures the following four Pauli operators:

$$XY, XI, IY, II.$$

Based on this observation, we can use the results of Theorem 3 and Theorem 4 to reduce the number of settings to UDA pure states. For the two-qubit case, recall that the

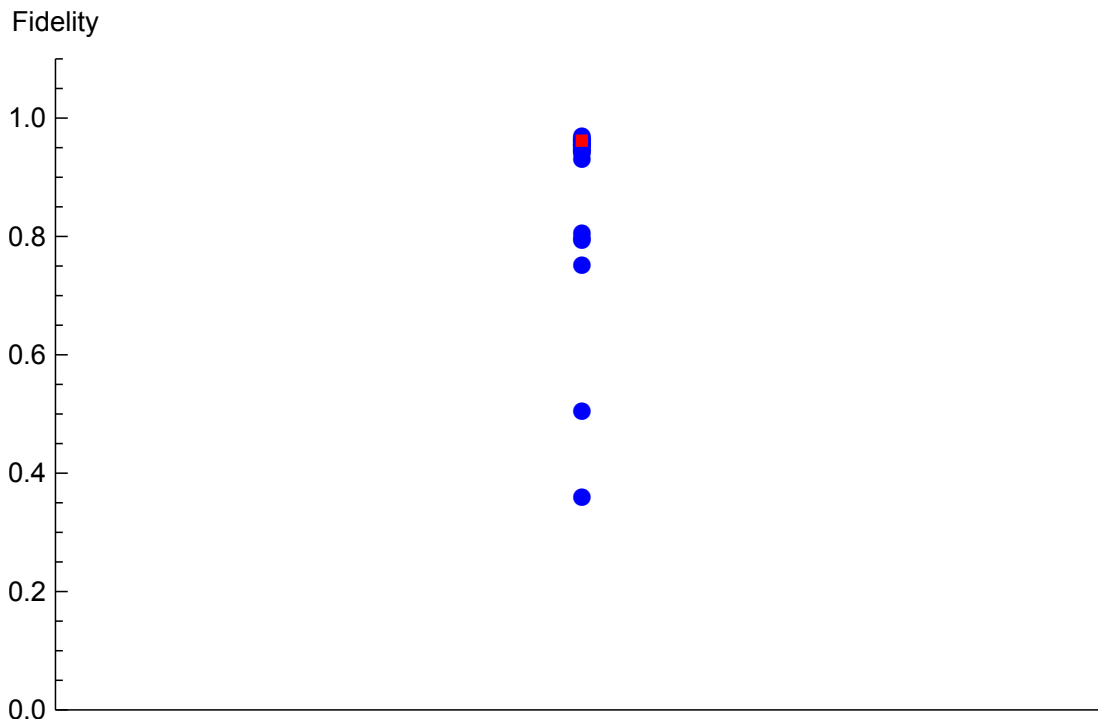


Figure 5.6: Performance of 3-qubit protocol using selected Pauli measurements against randomly Pauli measurements. Blue dots represents fidelity between density matrix reconstructed from all 64 Pauli measurements and density matrix reconstructed from random 31 Pauli measurements. The red square represents fidelity of reconstruction using our protocol.

11 Pauli operators to UDA any pure states are

$$A = \{II, IX, IY, IZ, XI, YX, YY, YZ, ZX, ZY, ZZ\}.$$

Notice that any of the 6 Paulis with no  $I$  component (the two-qubit correlations) only appear in the setting which measures it. However, looking at the remaining 5 Paulis,  $II$  is included in every setting,  $IX$  is included in the  $YX$  setting,  $IY$  in  $YY$ ,  $IZ$  in  $YZ$ . The only operator which does not appear in the settings of the two-qubit correlations is  $XI$ , so for the two qubit case,  $6 + 1 = 7$  settings are required to be sufficient for UDA.

And similar analysis can be done for the three qubit case, with the aid of computer search. That is, we find the minimum number of settings that can produce all the 31 Pauli operators as given in Eq. (5.7). We summarize these results as the corollary below.

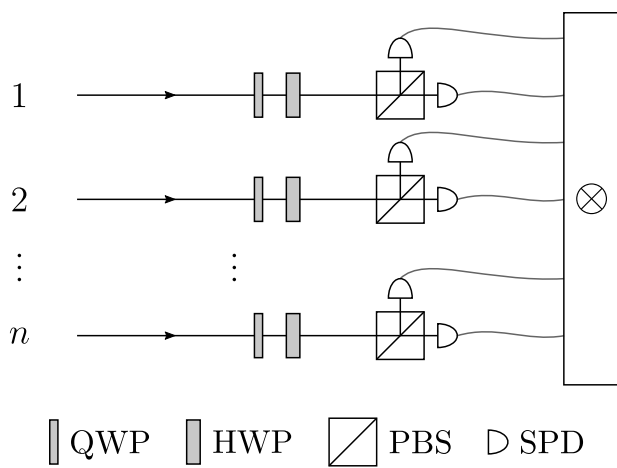


Figure 5.7: Measurement scheme for a polarization-encoded  $n$ -photon state. The  $n$ -qubit state is encoded in the polarizations of the  $n$  photons. Each photon is measured using a quarter-waveplate (QWP), half-waveplate (HWP) and a polarizing beam splitter (PBS) with a single-photon counting detector (SPD) at each of its output ports. The quarter- and half-waveplates are rotated to choose the measurement basis for each photon. Separable projective measurements are performed by counting coincident detection events between all  $n$  photons.

**Corollary 1.** *Only 7 settings*

$$\{XI, YX, YY, YZ, ZX, ZY, ZZ\}.$$

*are needed to UDA any two-qubit pure states, compared with 9 settings needed for general two-qubit state tomography. And only 19 settings*

$$\begin{aligned} &\{XXZ, XYZ, XZX, XZY, XZZ, YXX, \\ &\quad YXY, YYX, YYY, YZX, YZY, YZZ, \\ &\quad ZXX, ZXY, ZXZ, ZYX, ZYY, ZYZ, ZZX\} \end{aligned} \tag{5.13}$$

*are needed to UDA any three-qubit pure states, compared with 27 settings needed for general three-qubit state tomography.*

We remark that Corollary 1 is a direct application of Theorem 3 and Theorem 4. It is possible for even better results to be obtained by including knowledge of settings in the first optimization. However, proving sufficiency becomes more difficult in these cases.

# Chapter 6

## Conclusion

In this thesis, we looked at two separate proposals testing quantum mechanics utilizing tools we found in quantum information. In those proposals, different aspects of quantum mechanics are challenged. In the large scale, where the curvature of spacetime is not negligible, a test was proposed to probe the potential important physics that arises at the intersection of quantum theory and general relativity. The experiment with artificial satellites in Earth orbit proposed in the thesis should be able to refute or be consistent with the alternative quantum optics theory proposed. Many other tests of quantum foundation could be performed using similar setups. Going forward, we could observe and capture naturally occurring events and push the experiment to larger scales with more precise detectors.

In the small scale, we indirectly tested a cornerstone of quantum mechanics, the Born rule, by directly testing a quantum symmetry called envariance. For the later proposal, we put a bound for the Born rule for a generalized quantum mechanics theory. Our experiment demonstrated the quantum symmetry envariance and was able to bound the Born rule. It also gives us a new perspective on the Born rule. Future experiments include testing envariance in a larger system, where the boundary of system and environment could be changed.

In chapter 5, the main question at hand is whether a priori information of state being pure helps us reconstruct the quantum state. The usefulness of such information was proven theoretically for ideal situations, then tested in experiment with noise. We conclude that the knowledge of quantum state being close to a pure state helps us reconstruct the quantum state. With Pauli observables, 2 and 3 qubits pure state could be reconstructed with a minimum of 11 and 31 measurements respectively. The next step would be looking at a larger number of qubits, and what are the optimum sets of observables for state tomography. The result motivates us to look into the structure of quantum states, and

make efficient tomography of a multi-qubit system realizable.

# References

- [1] Wonmin Son. Consistent theory for causal non-locality beyond the borns rule. *Journal of the Korean Physical Society*, 64(4):499–503, 2014.
- [2] David Rideout, Thomas Jennewein, Giovanni Amelino-Camelia, Tommaso F Demarie, Brendon L Higgins, Achim Kempf, Adrian Kent, Raymond Laflamme, Xian Ma, Robert B Mann, et al. Fundamental quantum optics experiments conceivable with satellitesreaching relativistic distances and velocities. *Classical and Quantum Gravity*, 29(22):224011, 2012.
- [3] L Vermeyden, X Ma, J Lavoie, M Bonsma, Urbasi Sinha, R Laflamme, and KJ Resch. Experimental test of environment-assisted invariance. *Physical Review A*, 91(1):012120, 2015.
- [4] Xian Ma, Tyler Jackson, Hui Zhou, Jianxin Chen, Dawei Lu, Michael D Mazurek, Kent AG Fisher, Xinhua Peng, David Kribs, Kevin J Resch, et al. Pure-state tomography with the expectation value of pauli operators. *Physical Review A*, 93(3):032140, 2016.
- [5] Piotr Kolenderski, Wojciech Wasilewski, and Konrad Banaszek. Modeling and optimization of photon pair sources based on spontaneous parametric down-conversion. *Physical Review A*, 80(1):013811, 2009.
- [6] CK Hong and L Mandel. Theory of parametric frequency down conversion of light. *Physical Review A*, 31(4):2409, 1985.
- [7] Harald Weinfurter and Marek Żukowski. Four-photon entanglement from down-conversion. *Physical Review A*, 64(1):010102, 2001.
- [8] James D Franson. Bell inequality for position and time. *Physical Review Letters*, 62(19):2205, 1989.

- [9] Paul G Kwiat, Aephraim M Steinberg, and Raymond Y Chiao. High-visibility interference in a bell-inequality experiment for energy and time. *Physical Review A*, 47(4):R2472, 1993.
- [10] Peter van Loock and Akira Furusawa. Detecting genuine multipartite continuous-variable entanglement. *Physical Review A*, 67(5):052315, 2003.
- [11] Keiichi Edamatsu. Entangled photons: generation, observation, and characterization. *Japanese Journal of Applied Physics*, 46(11R):7175, 2007.
- [12] Emanuel Knill, Raymond Laflamme, and Gerald J Milburn. A scheme for efficient quantum computation with linear optics. *nature*, 409(6816):46–52, 2001.
- [13] Rupert Ursin, F Tiefenbacher, T Schmitt-Manderbach, H Weier, Thomas Scheidl, M Lindenthal, B Blauensteiner, T Jennewein, J Perdigues, P Trojek, et al. Entanglement-based quantum communication over 144 km. *Nature physics*, 3(7):481–486, 2007.
- [14] Nicholas David Birrell and Paul Charles William Davies. *Quantum fields in curved space*. Number 7. Cambridge university press, 1984.
- [15] TC Ralph. Time displaced entanglement and non-linear quantum evolution. *arXiv preprint quant-ph/0510038*, 2005.
- [16] TC Ralph. A model for nonlinear quantum evolution based on time displaced entanglement. In *SPIE Optics+ Photonics*, pages 63050P–63050P. International Society for Optics and Photonics, 2006.
- [17] TC Ralph. Unitary solution to a quantum gravity information paradox. *Physical Review A*, 76(1):012336, 2007.
- [18] TC Ralph, GJ Milburn, and T Downes. Gravitationally induced decoherence of optical entanglement. *arXiv preprint quant-ph/0609139*, 2006.
- [19] Timothy C Ralph, Gerard J Milburn, and T Downes. Quantum connectivity of space-time and gravitationally induced decorrelation of entanglement. *Physical Review A*, 79(2):022121, 2009.
- [20] David Deutsch. Quantum mechanics near closed timelike lines. *Physical Review D*, 44(10):3197, 1991.

- [21] Wojciech Hubert Zurek. Probabilities from entanglement, borns rule  $p_k = |\psi_k|^2$  from envariance. *Physical Review A*, 71(5):052105, 2005.
- [22] Wojciech Hubert Zurek. Environment-assisted invariance, entanglement, and probabilities in quantum physics. *Physical review letters*, 90(12):120404, 2003.
- [23] Wojciech Hubert Zurek. Decoherence, einselection, and the quantum origins of the classical. *Reviews of Modern Physics*, 75(3):715, 2003.
- [24] Wojciech H Zurek. From quantum to classical. *PHYSICS TODAY*, page 37, 1991.
- [25] Maximilian Schlosshauer and Arthur Fine. On zureks derivation of the born rule. *Foundations of Physics*, 35(2):197–213, 2005.
- [26] L Landau. Das dämpfungsproblem in der wellenmechanik. *Zeitschrift für Physik*, 45(5-6):430–441, 1927.
- [27] Michael A Nielsen and Isaac L Chuang. *Quantum computation and quantum information*. Cambridge university press, 2010.
- [28] Max Born. Quantenmechanik der stoßvorgänge. *Zeitschrift für Physik*, 38(11-12):803–827, 1926.
- [29] Taehyun Kim, Marco Fiorentino, and Franco NC Wong. Phase-stable source of polarization-entangled photons using a polarization sagnac interferometer. *Physical Review A*, 73(1):012316, 2006.
- [30] Alessandro Fedrizzi, Thomas Herbst, Andreas Poppe, Thomas Jennewein, and Anton Zeilinger. A wavelength-tunable fiber-coupled source of narrowband entangled photons. *Optics Express*, 15(23):15377–15386, 2007.
- [31] Devon N Biggerstaff, R Kaltenbaek, DR Hamel, G Weihs, T Rudolph, and Kevin J Resch. Cluster-state quantum computing enhanced by high-fidelity generalized measurements. *Physical review letters*, 103(24):240504, 2009.
- [32] Miroslav Ježek, Jaromír Fiurášek, and Zdeněk Hradil. Quantum inference of states and processes. *Physical Review A*, 68(1):012305, 2003.
- [33] Richard Jozsa. Fidelity for mixed quantum states. *Journal of modern optics*, 41(12):2315–2323, 1994.

- [34] Anil Bhattacharyya. On a measure of divergence between two multinomial populations. *Sankhyā: The Indian Journal of Statistics*, pages 401–406, 1946.
- [35] Daniel F. V. James, Paul G. Kwiat, William J. Munro, and Andrew G. White. Measurement of qubits. *Phys. Rev. A*, 64:052312, Oct 2001.
- [36] Mark D. de Burgh, Nathan K. Langford, Andrew C. Doherty, and Alexei Gilchrist. Choice of measurement sets in qubit tomography. *Phys. Rev. A*, 78:052122, Nov 2008.
- [37] Lieven MK Vandersypen and Isaac L Chuang. Nmr techniques for quantum control and computation. *Rev. Mod. Phys.*, 76(4):1037, 2005.
- [38] Ivan Oliveira, Roberto Sarthour Jr, Tito Bonagamba, Eduardo Azevedo, and Jair CC Freitas. *NMR quantum information processing*. Elsevier, 2011.
- [39] M. Nielsen and I. Chuang. *Quantum Computation and Quantum Information*. Cambridge University Press, Cambridge, England, 2000.
- [40] Jianxin Chen, Hillary Dawkins, Zhengfeng Ji, Nathaniel Johnston, David Kribs, Frederic Shultz, and Bei Zeng. Uniqueness of quantum states compatible with given measurement results. *Physical Review A*, 88(1):012109, 2013.
- [41] Teiko Heinosaari, Luca Mazzarella, and Michael M Wolf. Quantum tomography under prior information. *Communications in Mathematical Physics*, 318(2):355–374, 2013.
- [42] S. Weigert. Pauli problem for a spin of arbitrary length: A simple method to determine its wave function. *Phys. Rev. A*, 45:7688–7696, June 1992.
- [43] J.-P. Amiet and S. Weigert. Reconstructing a pure state of a spin  $s$  through three Stern-Gerlach measurements. *J. Phys. A: Math. Gen.*, 32:2777–2784, April 1999.
- [44] J. Finkelstein. Pure-state informationally complete and “really” complete measurements. *Phys. Rev. A*, 70(5):052107, November 2004.
- [45] S. T. Flammia, A. Silberfarb, and C. M. Caves. Minimal Informationally Complete Measurements for Pure States. *Foundations of Physics*, 35:1985–2006, December 2005.
- [46] Nan Li, Christopher Ferrie, and Carlton M Caves. Fisher-symmetric informationally complete measurements for pure states. *arXiv preprint arXiv:1507.06904*, 2015.
- [47] Charles H Baldwin, Ivan H Deutsch, and Amir Kalev. Informational completeness in bounded-rank quantum-state tomography. *arXiv preprint arXiv:1510.02736*, 2015.

- [48] Amir Kalev and Charles H Baldwin. The power of being positive: Robust state estimation made possible by quantum mechanics. *arXiv preprint arXiv:1511.01433*, 2015.
- [49] Carmeli, Claudio, Heinosaari, Teiko, Schultz, Jussi, and Toigo, Alessandro. How many orthonormal bases are needed to distinguish all pure quantum states? *Eur. Phys. J. D*, 69(7):179, 2015.
- [50] D. Gross, Y.-K. Liu, S. T. Flammia, S. Becker, and J. Eisert. Quantum State Tomography via Compressed Sensing. *Phys. Rev. Lett.*, 105(15):150401, October 2010.
- [51] M. Cramer, M. B. Plenio, S. T. Flammia, R. Somma, D. Gross, S. D. Bartlett, O. Landon-Cardinal, D. Poulin, and Y.-K. Liu. Efficient quantum state tomography. *Nat. Commun.*, 1, December 2010.
- [52] Amir Kalev, Robert L Kosut, and Ivan H Deutsch. Quantum tomography protocols with positivity are compressed sensing protocols. *npj Quantum Information*, 1:15018, 2015.
- [53] W.-T. Liu, T. Zhang, J.-Y. Liu, P.-X. Chen, and J.-M. Yuan. Experimental Quantum State Tomography via Compressed Sampling. *Phys. Rev. Lett.*, 108(17):170403, April 2012.
- [54] Jianxin Chen, Zhengfeng Ji, Bei Zeng, and D. L. Zhou. From ground states to local hamiltonians. *Phys. Rev. A*, 86:022339, Aug 2012.
- [55] J. Chen, Z. Ji, M. B. Ruskai, B. Zeng, and D.-L. Zhou. Comment on some results of Erdahl and the convex structure of reduced density matrices. *Journal of Mathematical Physics*, 53(7):072203, July 2012.
- [56] Tyler Jackson. Quantum Tomography with Pauli Operators. Master’s thesis, University of Guelph, Canada, 2013.
- [57] Bei Zeng, Hyeyoun Chung, Andrew W Cross, and Isaac L Chuang. Local unitary versus local clifford equivalence of stabilizer and graph states. *Physical Review A*, 75(3):032325, 2007.
- [58] David G Cory, Amr F Fahmy, and Timothy F Havel. Ensemble quantum computing by nmr spectroscopy. *Proc. Natl. Acad. Sci. USA*, 94(5):1634–1639, 1997.

- [59] Dawei Lu, Aharon Brodutch, Jihyun Park, Hemant Katiyar, Tomas Jochym-O'Connor, and Raymond Laflamme. Nmr quantum information processing. *arXiv preprint arXiv:1501.01353*, 2015.
- [60] Yanxiang Gao, Hui Zhou, Dong Zou, Xinhua Peng, and Jiangfeng Du. Preparation of greenberger-horne-zeilinger and  $w$  states on a one-dimensional ising chain by global control. *Phys. Rev. A*, 87:032335, Mar 2013.
- [61] J. B. Altepeter, E. R. Jeffrey, and P. G. Kwiat. Phase-compensated ultra-bright source of entangled photons. *Opt. Express*, 13(22):8951–8959, Oct 2005.
- [62] Robert Prevedel, Philip Walther, Felix Tiefenbacher, Pascal Bohi, Rainer Kaltenbaek, Thomas Jennewein, and Anton Zeilinger. High-speed linear optics quantum computing using active feed-forward. *Nature*, 445(7123):65–69, Jan 2007.
- [63] Kai Chen, Che-Ming Li, Qiang Zhang, Yu-Ao Chen, Alexander Goebel, Shuai Chen, Alois Mair, and Jian-Wei Pan. Experimental realization of one-way quantum computing with two-photon four-qubit cluster states. *Phys. Rev. Lett.*, 99:120503, Sep 2007.
- [64] Robert Prevedel, Deny R. Hamel, Roger Colbeck, Kent Fisher, and Kevin J. Resch. Experimental investigation of the uncertainty principle in the presence of quantum memory and its application to witnessing entanglement. *Nat. Phys.*, 7(10):757–761, Oct 2011.
- [65] C. Erven, E. Meyer-Scott, K. Fisher, J. Lavoie, B L. Higgins, Z. Yan, C. J. Pugh, J.-P. Bourgoin, R. Prevedel, L. K. Shalm, L. Richards, N. Gigov, R. Laflamme, G. Weihs, T. Jennewein, and K J. Resch. Experimental three-photon quantum nonlocality under strict locality conditions. *Nat. Photon.*, 8(4):292–296, Apr 2014. Letter.
- [66] Deny R. Hamel, Lynden K. Shalm, Hannes Hübel, Aaron J. Miller, Francesco Marsili, Varun B. Verma, Richard P. Mirin, Sae Woo Nam, Kevin J. Resch, and Thomas Jennewein. Direct generation of three-photon polarization entanglement. *Nat. Photon.*, 8(10):801–807, Oct 2014. article.
- [67] R. B. A. Adamson and A. M. Steinberg. Improving quantum state estimation with mutually unbiased bases. *Phys. Rev. Lett.*, 105:030406, Jul 2010.
- [68] Roger A Horn and Charles R Johnson. *Matrix analysis*. Cambridge university press, 2012.

# APPENDICES

# Appendix A

## Testing of envariance to Born rule continued

From Sec 4.2, the derivation of Born rule consists of two parts, which are presented in two theorems. We have tested the first part of derivation, where maximally entangled bipartite is measured, namely the theorem 2. Although this part is undeniable the core of the derivation, it is not exactly Born rule. Combined with the second part of the derivation, where probability of getting a eigenstate is related to the modular square of its eigenvalue, the derivation is complete. The second part of the derivation is called "fine graining" of the state, where the pointer state is expanded to a superposition of eigenstates.

Let's begin with looking at what is the minimum number of qubits needed for this test. The most simplified example it to show that the state  $|\Phi\rangle = \frac{1}{\sqrt{3}}|0\rangle|0\rangle + \frac{\sqrt{2}}{\sqrt{3}}|1\rangle|1\rangle$  satisfies Born rule. one just have to show that the probability of measuring the first qubit in  $|0\rangle$  is  $\frac{2}{3}$  and the probability of measuring it in  $|1\rangle$  is  $\frac{1}{3}$ . We call the first qubit system A, and the second qubit system B. If system B is large enough, say at least an 6 dimension Hilbertspace, we could add an additional qutrit to system B. The state becomes

$$\begin{aligned} |\Phi_0\rangle &= \left( \frac{1}{\sqrt{3}}|0\rangle|0\rangle + \frac{\sqrt{2}}{\sqrt{3}}|1\rangle|1\rangle \right) |0\rangle \\ &= \frac{1}{\sqrt{3}}|0\rangle_A|00\rangle_B + \frac{\sqrt{2}}{\sqrt{3}}|1\rangle_A|10\rangle_B \end{aligned} \tag{A.1}$$

Find a transformation acting on system B alone which maps  $|00\rangle_B$  to  $|00\rangle_B$  and  $|10\rangle_B$  to  $\frac{1}{\sqrt{2}}(|11\rangle_B + |02\rangle_B)$ . The state after this transformation becomes

$$\begin{aligned}
|\Phi'\rangle &= \frac{1}{\sqrt{3}}|0\rangle_A|00\rangle_B + \frac{1}{\sqrt{3}}|1\rangle_A|11\rangle_B + \frac{1}{\sqrt{3}}|1\rangle_A|02\rangle_B \\
&= \frac{1}{\sqrt{3}}|0\rangle_A|0\rangle_{B_1}|0\rangle_{B_2} + \frac{1}{\sqrt{3}}|1\rangle_A|1\rangle_{B_1}|1\rangle_{B_2} + \frac{1}{\sqrt{3}}|1\rangle_A|0\rangle_{B_1}|2\rangle_{B_2} \quad (\text{A.2})
\end{aligned}$$

We could use the envariance property of  $|\Phi'\rangle$  to show that the probability of getting  $|0\rangle_A|0\rangle_{B_1}$ ,  $|1\rangle_A|1\rangle_{B_1}$  and  $|1\rangle_A|0\rangle_{B_1}$  from measuring  $|\Phi'\rangle$  in computational basis are the same.

We denote the probability of getting  $|0\rangle_A|0\rangle_{B_1}$ ,  $P_{|\Phi'\rangle}(|0\rangle_A|0\rangle_{B_1})$ , and the probability of getting  $|1\rangle_A|1\rangle_{B_1}$ ,  $P_{|\Phi'\rangle}(|1\rangle_A|1\rangle_{B_1})$ . If we swap the state  $|0\rangle_A|0\rangle_{B_1}$  and  $|1\rangle_A|1\rangle_{B_1}$  on system  $A$  and system  $B_1$ , we get a updated state

$$|\Phi'\rangle_{\text{Swap}} = \frac{1}{\sqrt{3}}|0\rangle_A|0\rangle_{B_1}|1\rangle_{B_2} + \frac{1}{\sqrt{3}}|1\rangle_A|1\rangle_{B_1}|0\rangle_{B_2} + \frac{1}{\sqrt{3}}|1\rangle_A|0\rangle_{B_1}|2\rangle_{B_2}$$

Note that the swap operation could be done by swapping the measurement outcome  $|1\rangle_A|1\rangle_{B_1}$  and  $|0\rangle_A|0\rangle_{B_1}$ . Thus,  $P_{|\Phi'\rangle}(|1\rangle_A|1\rangle_{B_1}) = P_{|\Phi'\rangle_{\text{Swap}}}(|0\rangle_A|0\rangle_{B_1})$  and  $P_{|\Phi'\rangle}(|0\rangle_A|0\rangle_{B_1}) = P_{|\Phi'\rangle_{\text{Swap}}}(|1\rangle_A|1\rangle_{B_1})$ . From the envariance property of  $|\Phi'\rangle$ , we know that the swap  $|0\rangle_A|0\rangle_{B_1}$  and  $|1\rangle_A|1\rangle_{B_1}$  on system  $A$  and system  $B_1$  could be undone by a swap  $|1\rangle_{B_2}$  and  $|0\rangle_{B_2}$  on system  $B_2$ . The operation on system  $B_2$  should not affect the probabilities we got in system  $A$  and system  $B_1$ . Thus,  $P_{|\Phi'\rangle}(|1\rangle_A|1\rangle_{B_1}) = P_{|\Phi'\rangle_{\text{Swap}}}(|1\rangle_A|1\rangle_{B_1})$  and  $P_{|\Phi'\rangle}(|0\rangle_A|0\rangle_{B_1}) = P_{|\Phi'\rangle_{\text{Swap}}}(|0\rangle_A|0\rangle_{B_1})$ . In sum, we should have  $P_{|\Phi'\rangle}(|0\rangle_A|0\rangle_{B_1}) = P_{|\Phi'\rangle}(|1\rangle_A|1\rangle_{B_1})$ .

Similarly, we could derive  $P_{|\Phi'\rangle}(|1\rangle_A|0\rangle_{B_1}) = P_{|\Phi'\rangle}(|1\rangle_A|1\rangle_{B_1})$ . Thus,  $P_{|\Phi'\rangle}(|0\rangle_A|0\rangle_{B_1}) = P_{|\Phi'\rangle}(|1\rangle_A|0\rangle_{B_1}) = P_{|\Phi'\rangle}(|1\rangle_A|1\rangle_{B_1})$ , the probability of getting  $|0\rangle_A|0\rangle_{B_1}$ ,  $|1\rangle_A|1\rangle_{B_1}$  and  $|1\rangle_A|0\rangle_{B_1}$  from measuring  $|\Phi'\rangle$  in computational basis are the same.

Assumes Alice have access to the first and the second qubit of  $|\Phi'\rangle$  and Bob have access to the first qubit only. Alice should be measuring  $|00\rangle$ ,  $|10\rangle$  and  $|11\rangle$  with same probability from the argument above. The measurement result from Bob can't be conflict with the one from Alice, so he should be getting  $|1\rangle$  twice as much as  $|0\rangle$ . Thus, the probability of measuring  $|1\rangle$  is  $\frac{2}{3}$  while the probability of measuring  $|0\rangle$  is  $\frac{1}{3}$  for the first qubit.

By running experiments on envariance testing, we would like to put bounds on the Born rule.

In the previous experiment, we tested envariance for the state  $|\Phi^+\rangle = \frac{1}{\sqrt{2}}(|00\rangle + |11\rangle)$ . Ideally for state  $|\Phi^+\rangle$ , any unitary  $U_S$  on the first qubit could be undone by an unitary  $U_{\mathcal{E}}$  on the second qubit. Define  $U_S = \begin{pmatrix} 1 & 0 \\ 0 & e^{i\theta} \end{pmatrix}$ , we could get the corresponding recover unitary  $U_{\mathcal{E}} = \begin{pmatrix} 1 & 0 \\ 0 & e^{-i\theta} \end{pmatrix}$ . Note that  $U_S \otimes \mathbf{1} |\Phi^+\rangle = \frac{1}{\sqrt{2}}(|00\rangle + e^{i\theta} |11\rangle)$ , which gives a relative phase  $e^{i\theta}$ . This could be undone by operation on the second qubit, which should not affect any probability distribution we can get from the first qubit. We could conclude that probability of measuring  $|0\rangle$  or  $|1\rangle$  for the first qubit is independent of the phase  $e^{i\theta}$ . Moreover, using the argument in section 1.2, we could also conclude that the probability of getting  $|0\rangle$  or  $|1\rangle$  is  $\frac{1}{2}$ . The experimental result indicates that after operation  $U_S \otimes U_{\mathcal{E}}$  we could recover  $|\Phi^+\rangle$  with high fidelity. We can't conclude  $|\Phi^+\rangle$  is envariant under  $U_S$  since we can't get fidelity 1. However, we can try to put bounds on Born rule for state like  $|\Phi^+\rangle$  once we could get bounds on the experimental errors. (on going)

One might want to consider a more general state  $|\psi_{S\mathcal{E}}\rangle = \sum_{k=1}^N \alpha_k |\sigma_k\rangle |\epsilon_k\rangle$ , where  $|\alpha_i|^2 \neq \frac{1}{N}$ . To provide evidence or put bound on Born rule for this type of states, additional experiments are required.

The goal is to perform an experiment to transform the state from  $|\Phi_0\rangle = \frac{1}{\sqrt{3}}|000\rangle + \frac{\sqrt{2}}{\sqrt{3}}|111\rangle$  to  $|\Phi'\rangle = \frac{1}{\sqrt{3}}|000\rangle + \frac{1}{\sqrt{3}}|111\rangle + \frac{1}{\sqrt{3}}|102\rangle$  followed by an experiment to test the envariance property of the state  $|\Phi'\rangle$ . Since qubit is more accessible than qutrit in the lab, we could replace the qutrit with two qubits and use  $|00\rangle$ ,  $|11\rangle$  and  $|10\rangle$  as our three level system.

We could summarize the task as followed:

1) Construct state  $|\Phi_0\rangle = \frac{1}{\sqrt{3}}|0000\rangle + \frac{\sqrt{2}}{\sqrt{3}}|1111\rangle$ , and find a transformation without touching the first qubit to map  $|\Phi_0\rangle$  to  $|\Phi'\rangle = \frac{1}{\sqrt{3}}|0000\rangle + \frac{1}{\sqrt{3}}|1111\rangle + \frac{1}{\sqrt{3}}|1010\rangle$

2) Test the state  $|\Phi'\rangle = \frac{1}{\sqrt{3}}|0000\rangle + \frac{1}{\sqrt{3}}|1111\rangle + \frac{1}{\sqrt{3}}|1010\rangle$  is envariant under swap operations on the first two qubits. For example, the swap between  $|00\rangle$  and  $|11\rangle$  on the first and second qubit could be undone by the same operation on the third and fourth qubit.

Here we propose a experiment with linear optics. We use polarization of photons as our qubits, where  $|1\rangle = |V\rangle$  and  $|0\rangle = |H\rangle$ . Figure A.1 shows a circuit which outputs  $|\Phi'\rangle = \frac{1}{\sqrt{3}}|0000\rangle + \frac{1}{\sqrt{3}}|1111\rangle + \frac{1}{\sqrt{3}}|1010\rangle$  if we in put  $|\Phi\rangle = \frac{1}{\sqrt{3}}|0\rangle|0\rangle + \frac{\sqrt{2}}{\sqrt{3}}|1\rangle|1\rangle$  at node A and B.

To understand what does the circuit in Figure A.1 does, first we take a closer look at what the elements in the blue dash line box do A.1. If the detector 1 detects a photon

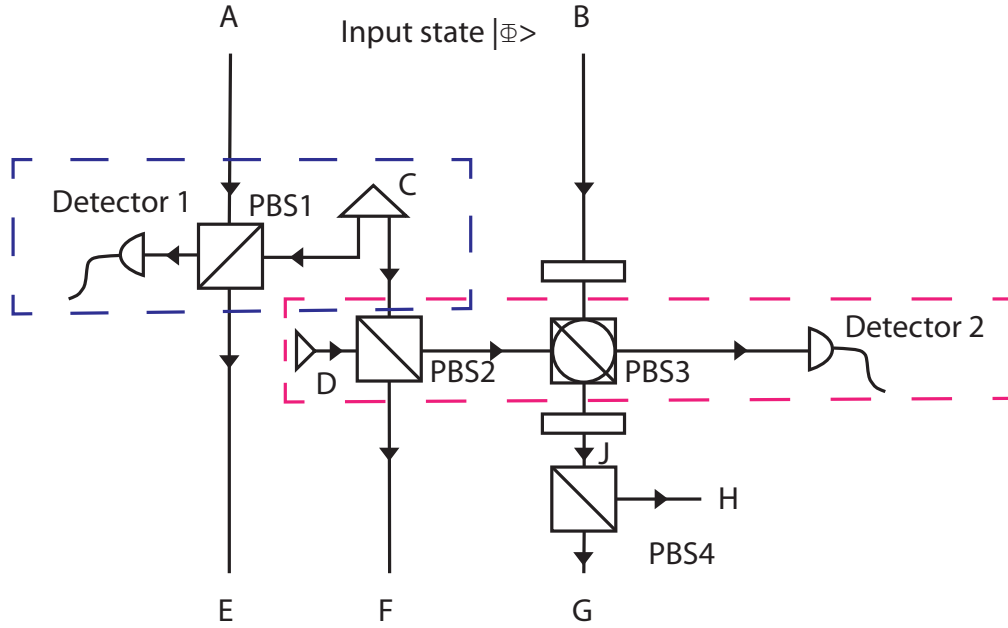


Figure A.1: Testing “Fine graining”. The input state at A and B is  $|\Phi\rangle = \frac{1}{\sqrt{3}} |0\rangle |0\rangle + \frac{\sqrt{2}}{\sqrt{3}} |1\rangle |1\rangle$ , where  $|0\rangle = |H\rangle$  represents horizontal polarization  $|1\rangle = |V\rangle$  represents vertical polarization. Node C prepares a pair of photons in the state  $\frac{1}{\sqrt{2}} |0\rangle |0\rangle + \frac{1}{\sqrt{2}} |1\rangle |1\rangle$ , while Node D emits a single photon with random polarization. Upon detect exactly one photon at detector 1 and detector 2, The state coming out from E,F,G,H could be  $|\Phi'\rangle = \frac{1}{\sqrt{3}} |0000\rangle + \frac{1}{\sqrt{3}} |1100\rangle + \frac{1}{\sqrt{3}} |1111\rangle$

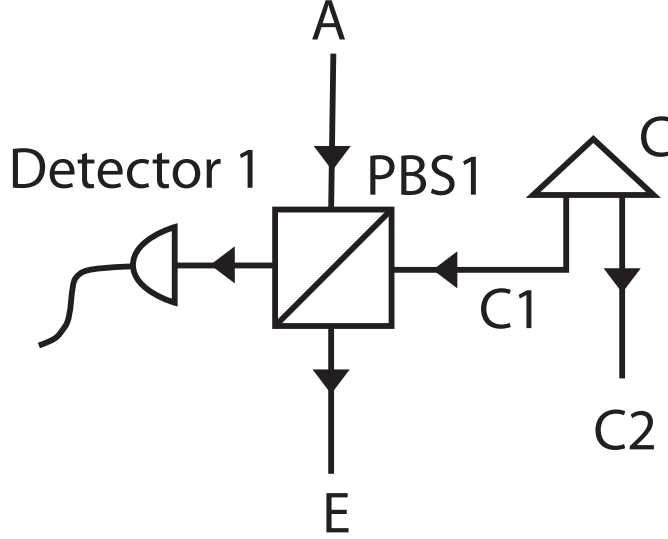


Figure A.2: Preparation of entangled state  $\alpha|00\rangle + \beta|11\rangle$

in horizontal polarization, that photon must coming from C1. The photon in C2 should be in horizontal polarization as well since we prepared  $\frac{1}{\sqrt{2}}|0\rangle|0\rangle + \frac{1}{\sqrt{2}}|1\rangle|1\rangle$  at node C. Moreover, the photon from A should be in horizontal polarization since it went through the PBS. Thus, the photon in C2 and E are both in  $|0\rangle$ . Similarly, if detector 1 detect a photon in vertical polarization, the photon in C2 and B are both in  $|1\rangle$ . Upon post select exactly one photon detected at detector 1, we know that the state in B and C2 should have the form  $\alpha|0\rangle|0\rangle + \beta|1\rangle|1\rangle$ .

The elements in the red dash line box is a C-NOT gate upon detect one photon at detector 2. We could conjugate the C-NOT gate with two  $\frac{\pi}{4} - Z$  gate to get a controlled-Hadamard gate.

Thus, if we input  $|\Phi\rangle = \frac{1}{\sqrt{3}}|0\rangle_A|0\rangle_B + \frac{\sqrt{2}}{\sqrt{3}}|1\rangle_A|1\rangle_B$ , the elements in the blue box will transform the state into  $\frac{1}{\sqrt{3}}|0\rangle_E|0\rangle_F|0\rangle_B + \frac{\sqrt{2}}{\sqrt{3}}|1\rangle_E|1\rangle_F|1\rangle_B$ . The controlled-Hadamard gate will further transform the state into  $\frac{1}{\sqrt{3}}|0\rangle_E|0\rangle_F|0\rangle_B + \frac{1}{\sqrt{3}}|1\rangle_E|1\rangle_F|0\rangle_{B'} + \frac{1}{\sqrt{3}}|1\rangle_E|1\rangle_F|1\rangle_{B'}$ . We consider the spatial degree of freedom for the photon through PBS4 as our fourth qubit. Thus, we get the state coming out from E,F,G,H could be  $|\Phi'\rangle = \frac{1}{\sqrt{3}}|0000\rangle + \frac{1}{\sqrt{3}}|1100\rangle +$

$\frac{1}{\sqrt{3}} |1111\rangle$ .

Once we have prepared state  $|\Phi'\rangle = \frac{1}{\sqrt{3}} |0000\rangle + \frac{1}{\sqrt{3}} |1010\rangle + \frac{1}{\sqrt{3}} |1111\rangle$ , we could proceed to test the invariance operation for state  $|\Phi'\rangle$ . We would like to swap  $|00\rangle$  and  $|10\rangle$  for the first two qubits, and see if the same swap operation for the last two qubits recovers  $|\Phi'\rangle$ . We propose the two possible tests as followed:

1) Perform a state tomography experiment, and get the  $16 \times 16$  density matrix  $\rho$  for the output state  $|\Phi'\rangle$ . The swap operations could be done by rearrange the rows and columns of  $\rho$ . Ideally, after swapping  $|00\rangle$  and  $|10\rangle$  for the first two qubits and the last two qubits, we should get the same  $\rho$ . The possible deviation from  $\rho$  could come from either experimental error or the failure of invariance theory.

2) Pick a random orthonormal basis  $\{B_i\}$  and measure  $|\Phi'\rangle$  with this basis. After large number of trials, we could estimate the probability  $P_i$  of getting outcome  $B_i$ . Then we swap  $|00\rangle$  and  $|10\rangle$  for the first two qubits and same for the last two qubits for all  $B_i$ , and we could get another orthonormal basis  $\{B'_i\}$ . Measure  $|\Phi'\rangle$  with  $\{B'_i\}$ , and estimate the probability  $P'_i$  of getting outcome  $B_i$ . We will have two arrays at the end of experiment,  $\{P_i\}$  and  $\{P'_i\}$ . Ideally they should be the same. Any difference should come from either experimental error or the failure of invariance theory.

# Appendix B

## Proof of UDA using selected Paulis for 3 qubits

In order to prove Theorem 4, it suffices to prove the following result.

**Theorem 5.** *Any Hermitian operator perpendicular to*

$$\begin{aligned} & \{IIX, ILY, IIZ, IXI, IXX, IXY, IYI, IYX, IYY, IZI, \\ & XIZ, XXX, XXY, XYX, XYY, XZX, XZY, YXX, \\ & YXY, YXZ, YYX, YYY, YYZ, YZI, ZII, ZXZ, ZYZ, \\ & ZZX, ZZY, ZZZ\} \end{aligned} \tag{B.1}$$

*must have at least two positive and two negative eigenvalues.*

*Proof.* The proof proceeds as follows. First construct an 8-by-8 traceless Hermitian matrix  $H$  which is orthogonal to all the above Pauli operators. This will be a real linear combination of every Pauli operator that is not being measured. This  $H$  is then a general description of any Hermitian matrix in the complement of the span of all measured operators. We will show through a case by case analysis that if we assume  $H$  only has one positive eigenvalue, then it follows that  $H$  must be the zero matrix. A similar argument holds for having only one negative eigenvalue therefore  $H$  must have at least two positive and two negative eigenvalues.

Let us begin by constructing  $H$  which is a real linear combination of the 33 Pauli operators not being measured (excluding the identity).  $H$  is then:

$$\begin{aligned}
H = & x_1IXZ + x_2IYZ + x_3IZZ + x_4IZY \\
& + x_5IZZ + x_6XII + x_7XIX + x_8XIY \\
& + x_9XXI + x_{10}XXZ + x_{11}XYI + x_{12}XYZ \\
& + x_{13}XZI + x_{14}XZZ + x_{15}YII + x_{16}YIX \\
& + x_{17}YIY + x_{18}YIZ + x_{19}YXI + x_{20}YYI \\
& + x_{21}YZX + x_{22}YZY + x_{23}YZZ + x_{24}ZIX \\
& + x_{25}ZII + x_{26}ZIZ + x_{27}ZXI + x_{28}ZXX \\
& + x_{29}ZXY + x_{30}ZYI + x_{31}ZYG + x_{32}ZYY \\
& + x_{33}ZZI.
\end{aligned}$$

Writing  $H$  in matrix form will give the form:

$$\begin{bmatrix}
c_{11} & c_{12} & c_{13} & c_{14} & c_{15} & c_{16} & c_{17} & 0 \\
c_{12}^* & c_{22} & c_{23} & c_{24} & c_{25} & c_{26} & 0 & c_{28} \\
c_{13}^* & c_{23}^* & c_{33} & c_{34} & c_{35} & 0 & c_{37} & c_{38} \\
c_{14}^* & c_{24}^* & c_{34}^* & c_{44} & 0 & c_{46} & c_{47} & c_{48} \\
c_{15}^* & c_{25}^* & c_{35}^* & 0 & c_{55} & c_{56} & c_{57} & c_{58} \\
c_{16}^* & c_{26}^* & 0 & c_{46}^* & c_{56}^* & c_{66} & c_{67} & c_{68} \\
c_{17}^* & 0 & c_{37}^* & c_{47}^* & c_{57}^* & c_{67}^* & c_{77} & c_{78} \\
0 & c_{28}^* & c_{38}^* & c_{48}^* & c_{58}^* & c_{68}^* & c_{78}^* & c_{88}
\end{bmatrix} \tag{B.2}$$

where

$$\begin{aligned}
c_{11} &= x_5 + x_{26} + x_{33}; \\
c_{22} &= -x_5 - x_{26} + x_{33}; \\
c_{33} &= -x_5 + x_{26} - x_{33}; \\
c_{44} &= x_5 - x_{26} - x_{33}; \\
c_{55} &= x_5 - x_{26} - x_{33} = c_{44}; \\
c_{66} &= -x_5 + x_{26} - x_{33} = c_{33}; \\
c_{77} &= -x_5 - x_{26} + x_{33} = c_{22}; \\
c_{88} &= x_5 + x_{26} + x_{33} = c_{11}; \\
c_{12} &= x_3 + x_{24} - i(x_4 + x_{25}); \\
c_{34} &= -x_3 + x_{24} + i(x_4 - x_{25}); \\
c_{56} &= x_3 - x_{24} - i(x_4 - x_{25}) = -c_{34}; \\
c_{78} &= -x_3 - x_{24} + i(x_4 + x_{25}) = -c_{12}; \\
c_{13} &= x_1 + x_{27} - i(x_2 + x_{30}); \\
c_{24} &= -x_1 + x_{27} + i(x_2 - x_{30}); \\
c_{57} &= x_1 - x_{27} - i(x_2 - x_{30}) = -c_{24}; \\
c_{68} &= -x_1 - x_{27} + i(x_2 + x_{30}) = -c_{13}; \\
c_{14} &= x_{28} - x_{32} - i(x_{29} + x_{31}); \\
c_{23} &= x_{28} + x_{32} + i(x_{29} - x_{31}); \\
c_{58} &= -x_{28} + x_{32} + i(x_{29} + x_{31}) = -c_{14}; \\
c_{67} &= -x_{28} - x_{32} - i(x_{29} - x_{31}) = -c_{23}; \\
c_{15} &= x_6 + x_{13} + x_{14} - i(x_{15} + x_{18} + x_{23}); \\
c_{26} &= x_6 + x_{13} - x_{14} - i(x_{15} - x_{18} - x_{23}); \\
c_{37} &= x_6 - x_{13} - x_{14} - i(x_{15} + x_{18} - x_{23}); \\
c_{48} &= x_6 - x_{13} + x_{14} - i(x_{15} - x_{18} + x_{23}) \\
&= c_{15} - c_{26}^* + c_{37}^*; \\
c_{16} &= x_7 - x_{17} - x_{22} - i(x_8 + x_{16} + x_{21}); \\
c_{25} &= x_7 + x_{17} + x_{22} + i(x_8 - x_{16} - x_{21}); \\
c_{38} &= x_7 - x_{17} + x_{22} - i(x_8 + x_{16} - x_{21}); \\
c_{47} &= x_7 + x_{17} - x_{22} + i(x_8 - x_{16} + x_{21}) \\
&= c_{16}^* + c_{25} - c_{38}^*;
\end{aligned}$$

$$\begin{aligned}
c_{17} &= x_9 + x_{10} - x_{20} - i(x_{11} + x_{12} + x_{19}); \\
c_{28} &= x_9 - x_{10} - x_{20} - i(x_{11} - x_{12} + x_{19}); \\
c_{35} &= x_9 + x_{10} + x_{20} + i(x_{11} + x_{12} - x_{19}); \\
c_{46} &= x_9 - x_{10} + x_{20} + i(x_{11} - x_{12} - x_{19}) \\
&= c_{28}^* + c_{35} - c_{17}^*;
\end{aligned}$$

Note that the anti-diagonal terms are all zeros. This was by design, since any set of Pauli operators Clifford equivalent to the result from the hyper-graph dualization program is also a solution, we had the freedom to choose a set which would make the proof simpler. Choosing the set of operators which contained all Pauli operators constructed by tensoring only  $X$  operators and  $Y$  operators meant  $H$  would have zero main anti-diagonal. The only reason for choosing this set is it makes this proof a little simpler.

Here we assume  $H$  is a Hermitian matrix with only one positive eigenvalue. We first show all diagonal entries of  $H$  must be zero. Observe that  $c_{55} = c_{44}$ ,  $c_{66} = c_{33}$ ,  $c_{77} = c_{22}$ ,  $c_{88} = c_{11}$ . In order for the traceless condition on  $H$  to hold, it is then clear that  $c_{11} + c_{22} + c_{33} + c_{44} = 0$ . If  $H$  has some nonzero diagonal entry, then at least one of  $c_{11}, c_{22}, c_{33}$  and  $c_{44}$  will be positive. Without loss of generality, let  $c_{11} > 0$ , then the submatrix of  $H$  formed by the rows (1, 8) and columns (1, 8), which will be of the form  $c_{11} * I$ , will have two positive eigenvalues.

**Lemma 1.** *Cauchy's Interlacing Theorem states[68]:*

*Let:*

$$A = \begin{bmatrix} B & C \\ C^\dagger & D \end{bmatrix}$$

*be an  $n$ -by- $n$  Hermitian matrix, where  $B$  has size  $m$ -by- $m$  ( $m < n$ ). If the eigenvalues of  $A$  and  $B$  are  $\alpha_1 \leq \dots \leq \alpha_n$  and  $\beta_1 \leq \dots \leq \beta_m$  respectively. Then:*

$$\alpha_k \leq \beta_k \leq \alpha_{k+n-m}, k = 1, \dots, m.$$

It follows from Cauchy's interlacing property that if a principle submatrix of  $H$  has 2 positive eigenvalues then  $H$  also has at least two positive eigenvalues.

Hence,  $H$  must be in the following form:

$$H = \begin{bmatrix} 0 & c_{12} & c_{13} & c_{14} & c_{15} & c_{16} & c_{17} & 0 \\ c_{12}^* & 0 & c_{23} & c_{24} & c_{25} & c_{26} & 0 & c_{28} \\ c_{13}^* & c_{23}^* & 0 & c_{34} & c_{35} & 0 & c_{37} & c_{38} \\ c_{14}^* & c_{24}^* & c_{34}^* & 0 & 0 & c_{28}^* + c_{35} - c_{17}^* & c_{16}^* + c_{25} - c_{38}^* & c_{15} - c_{26}^* + c_{37}^* \\ c_{15}^* & c_{25}^* & c_{35}^* & 0 & 0 & -c_{34} & -c_{24} & -c_{14} \\ c_{16}^* & c_{26}^* & 0 & c_{28} + c_{35}^* - c_{17} & -c_{34}^* & 0 & -c_{23} & -c_{13} \\ c_{17}^* & 0 & c_{37}^* & c_{16} + c_{25}^* - c_{38} & -c_{24}^* & -c_{23}^* & 0 & -c_{12} \\ 0 & c_{28}^* & c_{38}^* & c_{15} - c_{26} + c_{37} & -c_{14}^* & -c_{13}^* & -c_{12}^* & 0 \end{bmatrix}.$$

In fact, under the assumption that  $H$  has only 1 positive eigenvalue, it follows from Cauchy's interlacing theorem that any principle submatrix of  $H$  cannot have more than one positive eigenvalue. Otherwise, we will have a contradiction.

Let us look at the submatrix formed by rows 1, 2, 4, 5 and the same columns. It is a traceless Hermitian matrix with determinant  $|c_{14}c_{25} - c_{15}c_{24}|^2$ . Again, if the submatrix has positive determinant, then it must have exactly two positive eigenvalues. Once again by applying Cauchy's interlacing property,  $H$  will have at least two positive eigenvalues. This immediately contradicts our assumption. The above argument implies that, under our assumption  $H$  has only 1 positive eigenvalue, we have  $|c_{14}c_{25} - c_{15}c_{24}|^2 \leq 0$ . It is not surprising that the inequality holds if and only if the equality holds. Then we have  $c_{14}c_{25} - c_{15}c_{24} = 0$ .

Similarly, by considering other 4-by-4 submatrices constructed from the rows and

columns  $a, b, 4, 5$  where  $a, b$  are any two of the remain six rows, we can show that:

$$\begin{aligned}
c_{14}c_{35} - c_{15}c_{34} &= 0; \\
-c_{14}c_{34}^* - c_{15}(c_{28} + c_{35}^* - c_{17}) &= 0; \\
-c_{14}c_{24}^* - c_{15}(c_{16} + c_{25}^* - c_{38}) &= 0; \\
-c_{14}c_{14}^* - c_{15}(c_{15}^* - c_{26} + c_{37}) &= 0; \\
c_{24}c_{35} - c_{25}c_{34} &= 0; \\
-c_{24}c_{34}^* - c_{25}(c_{28} + c_{35}^* - c_{17}) &= 0; \\
-c_{24}c_{24}^* - c_{25}(c_{16} + c_{25}^* - c_{38}) &= 0; \\
-c_{24}c_{14}^* - c_{25}(c_{15}^* - c_{26} + c_{37}) &= 0; \\
-c_{34}c_{34}^* - c_{35}(c_{28} + c_{35}^* - c_{17}) &= 0; \\
-c_{34}c_{24}^* - c_{35}(c_{16} + c_{25}^* - c_{38}) &= 0; \\
-c_{34}c_{14}^* - c_{35}(c_{15}^* - c_{26} + c_{37}) &= 0; \\
-c_{24}^*(c_{28} + c_{35}^* - c_{17}) + c_{34}^*(c_{16} + c_{25}^* - c_{38}) &= 0; \\
-c_{14}^*(c_{28} + c_{35}^* - c_{17}) + c_{34}^*(c_{15}^* - c_{26} + c_{37}) &= 0; \\
-c_{14}^*(c_{16} + c_{25}^* - c_{38}) + c_{24}^*(c_{15}^* - c_{26} + c_{37}) &= 0.
\end{aligned}$$

The above equations will imply that the 8-by-2 submatrix formed by the 4-th and 5-th columns has rank at most 1.

The same argument can be used to prove that the 8-by-2 submatrices formed by columns (1, 8), (2, 7) or (3, 6) also have rank at most 1.

As a straightforward consequence,  $H$  has rank no more than 4.

In other words, the  $k$ -th column and the  $(9-k)$ -th column are linearly dependent. This means that there exist  $\lambda_1, \lambda_2, \lambda_3, \lambda_4$  such that the following equations hold:

$$\lambda_1 \vec{C}_1 + (1 - \lambda_1) \vec{C}_8 = \lambda_2 \vec{C}_2 + (1 - \lambda_2) \vec{C}_7 = 0 \quad (\text{B.3})$$

$$\lambda_3 \vec{C}_3 + (1 - \lambda_3) \vec{C}_6 = \lambda_4 \vec{C}_4 + (1 - \lambda_4) \vec{C}_5 = 0 \quad (\text{B.4})$$

Here we have used  $\vec{C}_k$  to represent the  $k$ -th column of the matrix (B.3).

Let us start with a special case. Let  $\lambda_1 = 0$ . Then  $c_{12} = c_{13} = c_{14} = c_{28} = c_{38} = 0$  and  $c_{15} = c_{26}^* - c_{37}^*$ .  $H$  can be simplified as the following:

$$H = \begin{bmatrix} 0 & 0 & 0 & 0 & c_{26}^* - c_{37}^* & c_{16} & c_{17} & 0 \\ 0 & 0 & c_{23} & c_{24} & c_{25} & c_{26} & 0 & 0 \\ 0 & c_{23}^* & 0 & c_{34} & c_{35} & 0 & c_{37} & 0 \\ 0 & c_{24}^* & c_{34}^* & 0 & 0 & c_{35} - c_{17}^* & c_{16}^* + c_{25} & 0 \\ c_{26} - c_{37} & c_{25}^* & c_{35}^* & 0 & 0 & -c_{34} & -c_{24} & 0 \\ c_{16}^* & c_{26}^* & 0 & c_{35}^* - c_{17} & -c_{34}^* & 0 & -c_{23} & 0 \\ c_{17}^* & 0 & c_{37}^* & c_{16} + c_{25}^* & -c_{24}^* & -c_{23}^* & 0 & 0 \\ 0 & 0 & 0 & 0 & 0 & 0 & 0 & 0 \end{bmatrix}.$$

If we set  $c_{23} = c_{24} = c_{34} = 0$ , then the top-left 4-by-4 submatrix is zero. In this case, the characteristic polynomial of  $H$  contains only even powers. Thus  $H$  has only one positive eigenvalue implies  $H$  has only one negative eigenvalue too. As a consequence, the top-right 4-by-4 submatrix of  $H$  has rank exactly 1.

As a result, any 2-by-2 submatrix of the top-right submatrix must have determinant zero. From suitable choices of submatrices we can obtain the following equations:

$$c_{26}c_{37} = 0; \quad (\text{B.5})$$

$$c_{26}(c_{26}^* - c_{37}^*) = c_{16}c_{25}; \quad (\text{B.6})$$

$$c_{37}(c_{26}^* - c_{37}^*) = c_{17}c_{35}; \quad (\text{B.7})$$

$$c_{16}(c_{16}^* + c_{25}) + c_{17}(c_{17}^* - c_{35}) = 0. \quad (\text{B.8})$$

Using the above equations we can obtain:

$$\begin{aligned} 0 &= c_{16}(c_{16}^* + c_{25}) + c_{17}(c_{17}^* - c_{35}) \\ &= c_{16}c_{25} - c_{17}c_{35} + |c_{17}|^2 + |c_{16}|^2 \\ &= c_{26}(c_{26}^* - c_{37}^*) - c_{37}(c_{26}^* - c_{37}^*) + |c_{17}|^2 + |c_{16}|^2 \\ &= |c_{26} - c_{37}|^2 + |c_{17}|^2 + |c_{16}|^2 \end{aligned} \quad (\text{B.9})$$

This implies  $c_{16} = c_{17} = 0$  and  $c_{26} = c_{37}$ . Also since  $c_{26}c_{37} = 0$  we know that  $c_{26} = c_{37} = 0$ . Furthermore  $c_{25}(c_{16}^* + c_{25}) = 0$  and  $c_{35}(c_{35} - c_{17}^*) = 0$  will guarantee  $c_{25} = c_{35} = 0$ . Therefore  $H$  is once again the zero matrix.

We must then assume at least one of  $c_{23}, c_{24}, c_{34}$  must be nonzero. If  $c_{23} \neq 0$ , then by considering submatrices formed by rows/columns  $(1, 2, 3, k)$  ( $5 \leq k \leq 8$ ), we have

$c_{16} = c_{17} = 0$  and  $c_{26} = c_{37}$ . For the case that  $c_{24} = 0$  or  $c_{34} = 0$ , we will also have  $c_{16} = c_{17} = 0$  and  $c_{26} = c_{37}$  by considering appropriately chosen submatrices.

We are then left with  $H$  in the form:

$$H = \begin{bmatrix} 0 & 0 & 0 & 0 & 0 & 0 & 0 & 0 \\ 0 & 0 & c_{23} & c_{24} & c_{25} & c_{26} & 0 & 0 \\ 0 & c_{23}^* & 0 & c_{34} & c_{35} & 0 & c_{26} & 0 \\ 0 & c_{24}^* & c_{34}^* & 0 & 0 & c_{35} & c_{25} & 0 \\ 0 & c_{25}^* & c_{35}^* & 0 & 0 & -c_{34} & -c_{24} & 0 \\ 0 & c_{26}^* & 0 & c_{35}^* & -c_{34}^* & 0 & -c_{23} & 0 \\ 0 & 0 & c_{26}^* & c_{25}^* & -c_{24}^* & -c_{23}^* & 0 & 0 \\ 0 & 0 & 0 & 0 & 0 & 0 & 0 & 0 \end{bmatrix}.$$

Now, recall the fact that the submatrices formed by the  $k$ -th and the  $(9-k)$ -th columns will always have rank 1. From this it can be shown we will have  $H$  is a zero matrix.

Take the submatrix formed by the second and seventh columns for example. Since they are linearly dependent, the determinant of any 2-by-2 submatrix must be zero. From this we can get that  $|c_{23}|^2 + |c_{26}|^2 = 0$ . Therefore  $c_{23} = c_{26} = 0$ . By similar arguments on various submatrices,  $H$  can be shown to be the zero matrix.

Thus, under our assumption that  $H$  has exactly one positive eigenvalue,  $\lambda_1 \neq 0$ . Similarly, we can also prove that  $\lambda_1 \neq 1, \lambda_2, \lambda_3, \lambda_4 \neq 0, 1$ . We can then assume from now on that  $H$  has no zero columns or rows.

Hence, there exists certain  $\lambda_1, \lambda_2, \lambda_3$  and  $\lambda_4 \neq 0, 1$  which satisfies equation [B.3](#).

Let us use  $\Re$  and  $\Im$  to denote the real part and imaginary part of a complex number. Then the above equations can be rewritten as linear equations of real numbers.

Let us use  $M(\lambda_1, \lambda_2, \lambda_3, \lambda_4)$  to denote the 48-by-30 coefficient matrix. If we can prove that the coefficient matrix always has rank 30 for any  $\lambda_1, \lambda_2, \lambda_3$  and  $\lambda_4$ , then it will imply that all  $c_{ij}$ 's are zeros which will immediately contradict our assumption.

Unfortunately, we are not that lucky.  $M(\lambda_1, \lambda_2, \lambda_3, \lambda_4)$  will be degenerate under certain assignment of variables  $(\lambda_1, \lambda_2, \lambda_3, \lambda_4)$ . For example,  $rank(M(\frac{1+i}{2}, \frac{1+i}{2}, \frac{1+i}{2}, \frac{1+i}{2})) = 27 < 30$ . However, we can still show that  $M(\lambda_1, \lambda_2, \lambda_3, \lambda_4)$  will have rank 30 except for some

degenerate cases which will be dealt with separately . The top-left 2-by-2 submatrix has rank 2 if and only if  $\lambda_1 \neq 0$

At least one of the following situations must happen:

1.  $\begin{bmatrix} -C_1 & A_1 \\ B_2 & C_2 \end{bmatrix}$  has full rank. This implies  $c_{12} = c_{17} = 0$ .
2.  $\begin{bmatrix} A_1 & C_1 \\ -D_2 & A_2 \end{bmatrix}$  has full rank. This implies  $c_{12} = c_{28} = 0$ .
3.  $\begin{bmatrix} B_3 & C_3 \\ -C_1 & A_1 \end{bmatrix}$  has full rank. This implies  $c_{13} = c_{16} = 0$ .
4.  $\begin{bmatrix} A_1 & C_1 \\ -D_3 & A_3 \end{bmatrix}$  has full rank. This implies  $c_{13} = c_{38} = 0$ .
5.  $\begin{bmatrix} -C_1 & A_1 \\ B_4 & C_4 \end{bmatrix}$  has full rank. This implies  $c_{14} = c_{15} = 0$ .
6.  $\begin{bmatrix} -C_2 & A_2 \\ B_3 & C_3 \end{bmatrix}$  has full rank. This implies  $c_{23} = c_{26} = 0$ .
7.  $\begin{bmatrix} A_2 & C_2 \\ -D_3 & A_3 \end{bmatrix}$  has full rank. This implies  $c_{23} = c_{37} = 0$ .
8.  $\begin{bmatrix} -C_2 & A_2 \\ B_4 & C_4 \end{bmatrix}$  has full rank. This implies  $c_{24} = c_{25} = 0$ .
9.  $\begin{bmatrix} -C_3 & A_3 \\ B_4 & C_4 \end{bmatrix}$  has full rank. This implies  $c_{34} = c_{35} = 0$ .

10.

$$\begin{aligned}
& \det \left( \begin{bmatrix} -C_1 & A_1 \\ B_2 & C_2 \end{bmatrix} \right) = \det \left( \begin{bmatrix} A_1 & C_1 \\ -D_2 & A_2 \end{bmatrix} \right) \\
& = \det \left( \begin{bmatrix} B_3 & C_3 \\ -C_1 & A_1 \end{bmatrix} \right) = \det \left( \begin{bmatrix} A_1 & C_1 \\ -D_3 & A_3 \end{bmatrix} \right) \\
& = \det \left( \begin{bmatrix} -C_1 & A_1 \\ B_4 & C_4 \end{bmatrix} \right) = \det \left( \begin{bmatrix} -C_2 & A_2 \\ B_3 & C_3 \end{bmatrix} \right) \\
& = \det \left( \begin{bmatrix} A_2 & C_2 \\ -D_3 & A_3 \end{bmatrix} \right) = \det \left( \begin{bmatrix} -C_2 & A_2 \\ B_4 & C_4 \end{bmatrix} \right) \\
& = \det \left( \begin{bmatrix} -C_3 & A_3 \\ B_4 & C_4 \end{bmatrix} \right) = 0.
\end{aligned}$$

With assistance of symbolic computation package like Mathematica, we find that the only solution to the above equations is  $\Re\lambda_1 = \Re\lambda_2 = \Re\lambda_3 = \Re\lambda_4 = \frac{1}{2}$ .

Here we will prove that there is no Hermitian matrix in the form ( B.3) with only one positive eigenvalue for every situations:

1.  $c_{12} = c_{17} = 0$ . Any  $H$  with only one positive eigenvalue must be in the following form:

$$H = \begin{bmatrix} 0 & 0 & c_{13} & c_{14} & c_{15} & c_{16} & 0 & 0 \\ 0 & 0 & c_{23} & c_{24} & c_{25} & c_{26} & 0 & c_{28} \\ c_{13}^* & c_{23}^* & 0 & c_{34} & c_{35} & 0 & c_{37} & c_{38} \\ c_{14}^* & c_{24}^* & c_{34}^* & 0 & 0 & c_{28}^* + c_{35} & c_{16}^* + c_{25} - c_{38}^* & c_{15} - c_{26}^* + c_{37}^* \\ c_{15}^* & c_{25}^* & c_{35}^* & 0 & 0 & -c_{34} & -c_{24} & -c_{14} \\ c_{16}^* & c_{26}^* & 0 & c_{28} + c_{35}^* & -c_{34}^* & 0 & -c_{23} & -c_{13} \\ 0 & 0 & c_{37}^* & c_{16} + c_{25}^* - c_{38} & -c_{24}^* & -c_{23}^* & 0 & 0 \\ 0 & c_{28}^* & c_{38}^* & c_{15}^* - c_{26} + c_{37} & -c_{14}^* & -c_{13}^* & 0 & 0 \end{bmatrix}.$$

By considering submatrices formed by row/columns  $(1, 2, p, q)$  where  $3 \leq p < q \leq 8$ , we have that the first two rows are linearly dependent. Under our assumption that there is no row of  $H$  containing only zero entries, we have  $c_{28} = 0$ .

Recall that the 4-th and 5-th rows are linearly dependent, thus  $c_{34}(-c_{34}^*) = c_{35}(c_{28} + c_{35}^*)$  which now can be simplified as  $|c_{34}|^2 + |c_{35}|^2 = 0$ . Hence  $c_{34} = c_{35} = 0$ . Then

$$H = \begin{bmatrix} 0 & 0 & c_{13} & c_{14} & c_{15} & c_{16} & 0 & 0 \\ 0 & 0 & c_{23} & c_{24} & c_{25} & c_{26} & 0 & 0 \\ c_{13}^* & c_{23}^* & 0 & 0 & 0 & 0 & c_{37} & c_{38} \\ c_{14}^* & c_{24}^* & 0 & 0 & 0 & 0 & c_{16}^* + c_{25} - c_{38}^* & c_{15} - c_{26}^* + c_{37}^* \\ c_{15}^* & c_{25}^* & 0 & 0 & 0 & 0 & -c_{24} & -c_{14} \\ c_{16}^* & c_{26}^* & 0 & 0 & 0 & 0 & -c_{23} & -c_{13} \\ 0 & 0 & c_{37}^* & c_{16} + c_{25}^* - c_{38} & -c_{24}^* & -c_{23}^* & 0 & 0 \\ 0 & 0 & c_{38}^* & c_{15}^* - c_{26} + c_{37} & -c_{14}^* & -c_{13}^* & 0 & 0 \end{bmatrix}.$$

Again, by applying our submatrix argument, we have the submatrix formed by (3, 4, 5, 6) columns must has rank 1.

If there is a zero element in the submatrix formed by rows (1, 2, 7, 8) and columns (3, 4, 5, 6), then there must be a row or a column containing only zero elements in  $H$ . So, here we assume the submatrix formed by rows (1, 2, 7, 8) and columns (3, 4, 5, 6) does not contain any zero element.

Then  $\frac{c_{15}}{c_{25}} = \frac{c_{13}}{c_{23}} = \frac{c_{38}}{c_{37}}$  which implies  $c_{38}c_{25} = c_{37}c_{15}$ .

Follows from the rank 1 condition, we have

$$\begin{aligned} c_{15}(c_{15}^* - c_{26} + c_{37}) &= -|c_{14}|^2, \\ c_{25}(c_{16} + c_{25}^* - c_{38}) &= -|c_{24}|^2. \end{aligned}$$

By substituting  $c_{38}c_{25} = c_{37}c_{15}$  and  $c_{15}c_{26} = c_{25}c_{16}$  into the above two equations, we have

$$\begin{aligned} |c_{15}|^2 + |c_{14}|^2 &= c_{15}c_{26} - c_{15}c_{37} \\ &= c_{25}c_{16} - c_{25}c_{38} \\ &= -|c_{24}|^2 - |c_{25}|^2 \end{aligned}$$

which implies  $c_{15} = c_{14} = c_{24} = c_{25} = 0$ . However, it contradicts our assumption that there is no zero element in the submatrix formed by (1, 2, 7, 8) rows and (3, 4, 5, 6) columns.

Similarly, we can also prove that there is no Hermitian matrix in the form [B.3](#) with only one positive eigenvalue if any of the following conditions apply.

2.  $c_{12} = c_{28} = 0$ .

3.  $c_{13} = c_{16} = 0.$

4.  $c_{13} = c_{38} = 0.$

5.  $c_{14} = c_{15} = 0.$

6.  $c_{23} = c_{26} = 0.$

7.  $c_{23} = c_{37} = 0.$

8.  $c_{24} = c_{25} = 0.$

9.  $c_{34} = c_{35} = 0.$

Now, the only case we left is the following:

10.  $\Re\lambda_1 = \Re\lambda_2 = \Re\lambda_3 = \Re\lambda_4 = \frac{1}{2}.$  In this case,  $rank\left(\begin{bmatrix} -C_1 & A_1 \\ B_2 & C_2 \end{bmatrix}\right) = 3.$  Hence

$(\Re c_{12}, \Im c_{12}, \Re c_{17}, \Im c_{17})$  lies in the nullspace of  $\begin{bmatrix} -C_1 & A_1 \\ B_2 & C_2 \end{bmatrix} = \begin{bmatrix} -\frac{1}{2} & -b_1 & \frac{1}{2} & b_1 \\ b_1 & -\frac{1}{2} & b_1 & -\frac{1}{2} \\ \frac{1}{2} & -b_2 & \frac{1}{2} & b_2 \\ b_2 & \frac{1}{2} & -b_2 & \frac{1}{2} \end{bmatrix}.$

Thus

$$\begin{aligned} & [c_{12} : c_{17}] \\ = & [2(b_2 - b_1) + (1 + 4b_1b_2)i : 2(b_1 + b_2) + (4b_1b_2 - 1)i]. \end{aligned}$$

Similarly, we will have

$$\begin{aligned}
& [c_{12} : c_{17} : c_{28}] \\
= & [2(b_2 - b_1) + (1 + 4b_1b_2)i : \\
& 2(b_1 + b_2) + (4b_1b_2 - 1)i : -2(b_1 + b_2) - (4b_1b_2 - 1)i]; \\
& [c_{13} : c_{16} : c_{38}] \\
= & [2(b_1 - b_3) - (1 + 4b_1b_3)i : \\
& -2(b_1 + b_3) - (4b_1b_3 - 1)i : 2(b_1 + b_3) + (4b_1b_3 - 1)i]; \\
& [c_{23} : c_{26} : c_{37}] \\
= & [2(b_3 - b_2) + (4b_2b_3 + 1)i : \\
& 2(b_2 + b_3) + (4b_2b_3 - 1)i : -2(b_2 + b_3) - (4b_2b_3 - 1)i]; \\
& [c_{14} : c_{15}] \\
= & [2(b_4 - b_1) - (4b_1b_4 + 1)i : \\
& 2(b_1 + b_4) + (4b_1b_4 - 1)i]; \\
& [c_{24} : c_{25}] \\
= & [2(b_4 - b_2) + (4b_2b_4 + 1)i : \\
& 2(b_2 + b_4) + (4b_2b_4 - 1)i]; \\
& [c_{34} : c_{35}] \\
= & [2(b_4 - b_3) + (4b_3b_4 + 1)i : \\
& 2(b_3 + b_4) + (4b_3b_4 - 1)i].
\end{aligned}$$

Here  $[q_1 : q_2 : \dots : q_m] = [r_1 + s_1i : r_2 + s_2i : \dots : r_m + s_mi]$  means there exists some  $\mu \in \mathbb{R}$  such that  $q_i = \mu(r_i + s_i i)$  for any  $1 \leq i \leq m$ .

Observe that  $c_{28} = -c_{17}$ ,  $c_{38} = -c_{16}$ ,  $c_{37} = -c_{26}$ , we thus simplify the matrix form of  $H$  as the following:

$$H = \begin{bmatrix} 0 & c_{12} & c_{13} & c_{14} & c_{15} & c_{16} & c_{17} & 0 \\ c_{12}^* & 0 & c_{23} & c_{24} & c_{25} & c_{26} & 0 & -c_{17} \\ c_{13}^* & c_{23}^* & 0 & c_{34} & c_{35} & 0 & -c_{26} & -c_{16} \\ c_{14}^* & c_{24}^* & c_{34}^* & 0 & 0 & c_{35} - 2c_{17}^* & c_{25} + 2c_{16}^* & c_{15} - 2c_{26}^* \\ c_{15}^* & c_{25}^* & c_{35}^* & 0 & 0 & -c_{34} & -c_{24} & -c_{14} \\ c_{16}^* & c_{26}^* & 0 & c_{35}^* - 2c_{17} & -c_{34}^* & 0 & -c_{23} & -c_{13} \\ c_{17}^* & 0 & -c_{26}^* & c_{25}^* + 2c_{16} & -c_{24}^* & -c_{23}^* & 0 & -c_{12} \\ 0 & -c_{17}^* & -c_{16}^* & c_{15}^* - 2c_{26} & -c_{14}^* & -c_{13}^* & -c_{12}^* & 0 \end{bmatrix}.$$

It follows from the fact that the submatrix formed by 4-th and 5-th columns has rank exactly 1, we have  $c_{14}(-c_{14}^*) = c_{15}(c_{15}^* - 2c_{26})$ . Thus at least one of the following cases must happen:

(10.1)  $c_{14} = c_{15} = 0$ . We can still assume there is no column containing only zero elements as this is the case that we have already discussed. Thus  $c_{26} = 0$  which would also lead to  $c_{23} = 0$ .

(10.2)  $c_{26} = c_{15}^*$ .

Similarly, at least one of the following conditions:

(10.I)  $c_{24} = c_{25} = c_{16} = c_{13} = 0$ ; or

(10.II)  $c_{16} = -c_{25}^*$

and one of the following conditions:

(10.A)  $c_{34} = c_{35} = c_{17} = c_{12} = 0$ ; or

(10.B)  $c_{17} = c_{35}^*$

must apply.

We have already discussed the cases that  $c_{12} = c_{17} = 0$ ,  $c_{13} = c_{16} = 0$  or  $c_{23} = c_{26} = 0$  previously. Hence the only remaining case is  $c_{26} = c_{15}^*$ ,  $c_{16} = -c_{25}^*$ ,  $c_{17} = c_{35}^*$ . Thus

$$H = \begin{bmatrix} 0 & c_{12} & c_{13} & c_{14} & c_{15} & -c_{25}^* & c_{35}^* & 0 \\ c_{12}^* & 0 & c_{23} & c_{24} & c_{25} & c_{15}^* & 0 & -c_{35}^* \\ c_{13}^* & c_{23}^* & 0 & c_{34} & c_{35} & 0 & -c_{15}^* & c_{25}^* \\ c_{14}^* & c_{24}^* & c_{34}^* & 0 & 0 & -c_{35} & -c_{25} & -c_{15} \\ c_{15}^* & c_{25}^* & c_{35}^* & 0 & 0 & -c_{34} & -c_{24} & -c_{14} \\ -c_{25} & c_{15} & 0 & -c_{35}^* & -c_{34}^* & 0 & -c_{23} & -c_{13} \\ c_{35} & 0 & -c_{15} & -c_{25}^* & -c_{24}^* & -c_{23}^* & 0 & -c_{12} \\ 0 & -c_{35} & c_{25} & -c_{15}^* & -c_{14}^* & -c_{13}^* & -c_{12}^* & 0 \end{bmatrix}.$$

According to  $c_{26} = c_{15}^*$ , we have  $2(b_2 + b_3)(1 - 4b_1b_4) = (4b_2b_3 - 1)(2b_1 + 2b_4)$  which implies  $4(b_1b_2b_3 + b_1b_2b_4 + b_1b_3b_4 + b_2b_3b_4) = b_1 + b_2 + b_3 + b_4$ .

1.  $4b_1b_2 + 4b_1b_3 + 4b_2b_3 = 1$ . Thus  $b_1 + b_2 + b_3 = 4b_1b_2b_3$ . However, one can easily verify that there do not exist three real numbers  $b_1, b_2, b_3$  satisfying these two equations.

2.  $4b_1b_2 + 4b_1b_3 + 4b_2b_3 \neq 1$ . Hence  $b_4 = \frac{b_1+b_2+b_3-4b_1b_2b_3}{4b_1b_2+4b_1b_3+4b_2b_3-1}$ . By substituting the

assignment of  $b_4$  into Equation B.10, we have

$$\begin{aligned}
c_{14} &= p \cdot \left( \frac{2(1 - 4b_1^2)(b_2 + b_3) + 4b_1(1 - 4b_2b_3)}{4b_1b_2 + 4b_1b_3 + 4b_2b_3 - 1} \right. \\
&\quad \left. + \frac{-8b_1(b_2 + b_3) + (1 - 4b_1^2)(1 - 4b_2b_3)}{4b_1b_2 + 4b_1b_3 + 4b_2b_3 - 1} i \right); \\
c_{15} &= p \cdot \left( \frac{2(1 + 4b_1^2)(b_2 + b_3)}{4b_1b_2 + 4b_1b_3 + 4b_2b_3 - 1} \right. \\
&\quad \left. + \frac{(1 + 4b_1^2)(1 - 4b_2b_3)}{4b_1b_2 + 4b_1b_3 + 4b_2b_3 - 1} i \right); \\
c_{23} &= p \cdot \left( \frac{2(1 + 4b_1^2)(b_3 - b_2)}{4b_1b_2 + 4b_1b_3 + 4b_2b_3 - 1} \right. \\
&\quad \left. + \frac{(1 + 4b_1^2)(1 + 4b_2b_3)}{4b_1b_2 + 4b_1b_3 + 4b_2b_3 - 1} i \right); \\
c_{24} &= q \cdot \left( \frac{2(1 - 4b_2^2)(b_1 + b_3) + 4b_2(1 - 4b_1b_3)}{4b_1b_2 + 4b_1b_3 + 4b_2b_3 - 1} \right. \\
&\quad \left. + \frac{8b_2(b_1 + b_3) - (1 - 4b_2^2)(1 - 4b_1b_3)}{4b_1b_2 + 4b_1b_3 + 4b_2b_3 - 1} i \right); \\
c_{25} &= q \cdot \left( \frac{2(1 + 4b_2^2)(b_1 + b_3)}{4b_1b_2 + 4b_1b_3 + 4b_2b_3 - 1} \right. \\
&\quad \left. + \frac{(1 + 4b_2^2)(1 - 4b_1b_3)}{4b_1b_2 + 4b_1b_3 + 4b_2b_3 - 1} i \right); \\
c_{13} &= q \cdot \left( \frac{2(1 + 4b_2^2)(b_1 - b_3)}{4b_1b_2 + 4b_1b_3 + 4b_2b_3 - 1} \right. \\
&\quad \left. - \frac{(1 + 4b_2^2)(1 + 4b_1b_3)}{4b_1b_2 + 4b_1b_3 + 4b_2b_3 - 1} i \right); \\
c_{34} &= r \cdot \left( \frac{2(1 - 4b_3^2)(b_1 + b_2) + 4b_3(1 - 4b_1b_2)}{4b_1b_2 + 4b_1b_3 + 4b_2b_3 - 1} \right. \\
&\quad \left. + \frac{8b_3(b_1 + b_2) - (1 - 4b_3^2)(1 - 4b_1b_2)}{4b_1b_2 + 4b_1b_3 + 4b_2b_3 - 1} i \right); \\
c_{35} &= r \cdot \left( \frac{2(1 + 4b_3^2)(b_1 + b_2)}{4b_1b_2 + 4b_1b_3 + 4b_2b_3 - 1} \right. \\
&\quad \left. + \frac{(1 + 4b_3^2)(1 - 4b_1b_2)}{4b_1b_2 + 4b_1b_3 + 4b_2b_3 - 1} i \right); \\
c_{12} &= r \cdot \left( \frac{2(1 + 4b_3^2)(b_2 - b_1)}{4b_1b_2 + 4b_1b_3 + 4b_2b_3 - 1} \right. \\
&\quad \left. + \frac{(1 + 4b_3^2)(1 + 4b_1b_2)}{4b_1b_2 + 4b_1b_3 + 4b_2b_3 - 1} i \right).
\end{aligned}$$

Again, with assistance of symbolic computation package like Mathematica, we can verify that the characteristic polynomial of  $H$  contains only even powers. This implies  $H$  has nonzero eigenvalue  $\lambda$  if and only if it also has eigenvalue  $-\lambda$ . Therefore, under our assumption that  $H$  has only 1 positive eigenvalue,  $H$  also has only 1 negative eigenvalue.

However, let us consider the 3-by-3 submatrix of  $H$  formed by (5, 7, 8)-th rows and (1, 2, 3)-th columns . Its determinant is  $(-i + 2b_1)(i + 2b_1)^2(1 + 2ib_2)(i + 2b_2)^2(i - 2b_3)^2(i + 2b_3)^2r((1 + 4b_1^2)p^2 + (1 + 4b_2^2)q^2 + (1 + 4b_3^2)r^2)$ . It is always nonzero unless  $p = q = r$  or  $r = 0$ . If  $r = 0$  this implies that  $c_{12} = c_{34} = c_{35} = 0$ . This case has already been covered, Thus  $H$  has rank at least 3 which contradicts our previous conclusion that  $H$  has only one positive eigenvalue and only one negative eigenvalue.

To summarize, under our assumption that  $H$  has only one positive eigenvalue, a contradiction always exist in every situation we studied. Hence,  $H$  must has at least 2 positive eigenvalues and at least 2 negative eigenvalues. This completes our proof.  $\square$